PHYSICO-CHEMICAL PROCESSES BEHIND SHOCK FRONTS

Thesis by

Frederick Clay Harshbarger

In Partial Fulfillment of the Requirements

for the Degree of

Doctor of Philosophy

California Institute of Technology

Pasadena, California

1957

ACKNOWLEDGEMENTS

The author is indebted to Dr. S. S. Penner for his continued interest, support, and advice during the progress of the research. The investigations on the production of hydrazine from ammonia were carried out at the suggestion of Dr. H. S. Tsien. The author is grateful to Dr. A. T. Ellis, Major E. N. Bennett, and Messrs. D. Weber and W. Hooker for their assistance with some of the experimental studies. He wishes to acknowledge helpful suggestions from Dr. L. Lees concerning some of the computations.

Support for the experimental and theoretical studies, through the Daniel and Florence Guggenheim Foundation, Olin Industries Fellowship grant, the U. S. Navy Office of Naval Research under Contract Nonr-220(03), NR 015 401, and the U. S. Air Force under Contract AF 18(603)-2, is gratefully acknowledged.

ABSTRACT

PART I: INTRODUCTION TO THE STUDY OF PHYSICO-CHEMICAL PHENOMENA BY THE USE OF SHOCK TUBES

The use of the shock tube for the determination of physico-chemical parameters at elevated temperatures is surveyed. We first describe the principles and performance of various shock-tube designs. Next the use of a number of measuring techniques suitable for shock-tube studies is discussed. This section is followed by a summary of representative determinations of physico-chemical parameters behind incident and reflected shock waves.

PART II: EXPERIMENTAL STUDIES OF REACTIONS BEHIND SHOCKS

The original experimental research involved the study of two chemical reactions. First we describe an unsuccessful attempt to produce hydrazine from ammonia. Second, carbon formation from acetylene is considered theoretically and experimentally. In the calculations, the state of the gas is determined behind the incident and reflected shocks, preceding chemical reaction. Estimates are made for the minimum times spent by the gas in a uniform state at the elevated temperatures behind reflected shocks. The experimental studies led to a new method for making simultaneous light emission and absorption measurements. A kinetic interpretation is given to the induction time necessary to form carbon after the passage of the reflected shock. Spectroscopic studies are presented which indicate that the emitted radiation associated with carbon formation follows a blackbody distribution law. A two-color method has been developed

for the determination of temperature as a function of time behind carbon-forming shocks.

TABLE OF CONTENTS

LIST OF SYMBOLS

a	local velocity of sound
A	area
A	prism angle
B	frequency factor
B	Kerr constant
c_2	second radiation constant
c_p	specific heat capacity at constant pressure
d	grating constant
D	deflection angle
E	electric field strength
E'	effective molar activation energy
G	gain factor
h	specific enthalpy
i	angle of incidence to the prism
i'	angle of incidence to the grating
k	Boltzmann's constant
$\overline{l}$	average mean free path
m'	magnification of the telescope
M	Mach number
M_s	Mach number of the incident shock, u_s/a_1
M_{sr}	Mach number of the reflected shock relative to a_1, u_{sr}/a_1
n	index of refraction
n	order of the chemical reaction
p	pressure
r	angle of reflection from the grating
R	universal gas constant

R_g	specific gas constant
S_λ	spectrometer spectral response
t	time
t_o	time before the reflected shock wave passes the observation window, measured from the time at which the diaphragm is ruptured
t_c	time before the reflected shock wave intersects the constact surface, measured from the time at which the diaphragm is ruptured
t_e	time before the initial shock wave reflects from the end of the shock tube, measured from the time at which the diaphragm is ruptured
t_r	time before the first reflected rarefaction wave would intercept the contact surface in a shock tube with an infinite downstream section, measured from the time at which the diaphragm is ruptured
T	temperature
T_{br}	brightness temperature
T_c	color temperature
u	gas velocity
v	gas velocity relative to a shock front
W	molecular weight
x	distance
x_e	distance from the diaphragm to the low-pressure end of the shock tube
x_c	distance from the diaphragm to the position of interaction between the reflected shock wave and the contact surface
x_ℓ	distance from the diaphragm to the high-pressure end of the shock tube
x_o	distance from the diaphragm to the position where the observation is made
γ	specific heat ratio
δ	shock wave thickness
λ	wavelength of light
ϱ	density

Subscripts

$(\ )_1$	initial conditions of low-pressure gas
$(\ )_2$	flow properties between the incident shock and the contact surface
$(\ )_3$	flow properties behind the contact surface
$(\ )_4$	initial conditions of the high-pressure gas
$(\ )_5$	flow properties behind the reflected shock

I. INTRODUCTION

The shock tube was first used by Vieille,[1] and later by Payman and Shepherd, who investigated the flow after the bursting of the diaphragm.[2] In recent years a great many experimental and theoretical studies concerning the shock tube have been published in which its use is described for gas-dynamic studies as well as its versatility as a research tool for obtaining physico-chemical data under unusual conditions.

Part I of this thesis is concerned with a qualitative survey of the principles and methods useful for understanding the application of the shock tube as a research tool for high-temperature investigations (Section II), a survey of measurement techniques suitable for determining the state of the gas behind incident and reflected shocks (Section III), and a survey of representative experiments which may be used to determine physico-chemical data (Section IV). The survey in Part I is not meant to be exhaustive. Particular emphasis is given to less commonly used methods of approach.

In Part II we summarize the original experimental investigations which represent the first step in a larger research program for the study of physico-chemical phenomena behind shock waves. Section V deals with an unsuccessful attempt to produce hydrazine from ammonia in a shock tube. In Section VI theoretical and experimental results of carbon-forming experiments are discussed.

PART I

INTRODUCTION TO THE STUDY OF PHYSICO-CHEMICAL PHENOMENA BY THE USE OF SHOCK TUBES

II. SURVEY OF SHOCK-TUBE TECHNOLOGY*

A. Introduction

A shock tube consists of two chambers separated by a diaphragm (fig. 1). Initially one chamber contains gas at (high) pressure p_4 ("driver" gas) while the other chamber is filled with gas at (low) pressure p_1 ("driven" gas) where $p_4 > p_1$. In general, the two gases differ in temperature and in chemical composition. The diaphragm is made from a material which, when properly stressed, has the property of rupturing rapidly (in a time of about 100 μsec) and completely when a small hole is punctured through its surface. When the diaphragm is broken, a shock wave is propagated into the low-pressure gas and a rarefaction wave into the high-pressure gas.

A shock wave is characterized by steep pressure, density, and temperature gradients (fig. 2). The change from the initial to the final state occurs in a distance corresponding to a few molecular collisions. Thus the effective width of the shock wave (δ) is of the order of several mean free paths.

The rarefaction wave lowers the pressure, density, and temperature of the gas through which it passes. It is characterized by smaller gradients than the shock wave and, furthermore, it broadens

---

* The material presented in Section II to IV follows the paper "Use of the Shock Tube for the Determination of Physico-Chemical Parameters" by S. S. Penner, F. Harshbarger, and V. Vali, Combustion Researches and Reviews 1956, Butterworths Scientific Publications, London (in press).

as it advances. The rate of change of temperature with time across a rarefaction wave is of the order of 10^6 °K/sec.

B. One-Dimensional Continuous Wave Motion in a Perfect Gas with Constant Specific Heat

The one-dimensional theory of shock waves, for the case of an ideal gas with constant specific heats at constant pressure (c_p),[3-8] relates the initial pressure ratio across the diaphragm (p_4/p_1) to the flow in the two chambers after rupture of the diaphragm. Experiments carried out with shock tubes of constant area, using gases with constant specific heats (e.g., gas 4 = helium and gas 1 = argon), for pressure ratios which are sufficiently low to prevent measurable electronic excitation or ionization, yield observable results which differ only slightly from theoretical predictions. For large pressure ratios, deviations are obtained which may be ascribed partly to non-ideal characteristics of shock-tube flow (for example, the flow in the region behind the contact surface is not steady but has a noticeable turbulence level, as shown by schlieren studies).[4, 6, 7] In cases where the constant specific heat assumption is not valid (e.g., very strong shocks in monatomic gases, moderate to strong shocks in polyatomic gases, or shock waves of arbitrary strength in reactive gases), a real-gas calculation allowing for variable specific heats and/or mixture composition must be made before wave propagation in the shock tube can be predicted from the initial pressure ratio across the diaphragm (p_4/p_1). It is customary in the theoretical studies to assume that the shock and rarefaction waves are estab-

lished immediately after diaphragm rupture. However, actually the shock does not become fully developed until it has traveled some ten diameters down the length of the shock tube.

The flow in a shock tube is most easily pictured by use of a distance-time (x-t) diagram. In figure 3 is shown an x-t diagram for the initial shock-tube flow prior to reflection from the walls. The conditions behind the incident shock are identified by the subscript 2 and behind the incident rarefaction wave by the subscript 3.

(1) The Contact Surface

The contact surface (C) is the interface between the gases which were initially at pressures p_1 and p_4, respectively. When the diaphragm is broken, it advances into the region which was initially at pressure p_1 (fig. 3). The gas velocities on either side of the contact surface must be equal. There is no mechanism for supporting a pressure difference across the contact surface; therefore also $p_3 = p_2$. In the elementary studies it is assumed that the contact surface represents a discontinuity in chemical composition, entropy, and temperature. Actually, gradual mixing by diffusion occurs across the contact surface.

(2) The Incident and Reflected Shock Waves

The incident shock wave propagates with constant velocity u_s (i.e., with constant Mach number $M_s = u_s/a_1$),* accelerates the gas behind the shock to the velocity u_2 ($M_2 = u_2/a_2$), raises it to a

---

* Here a denotes the local sound velocity.

temperature $T_2 (T_2 > T_1)$ and to a pressure $p_2 (p_2 > p_1)$. The flow behind the shock is assumed to be uniform and isentropic.

The pressure ratio across the diaphragm, the chemical composition (molecular weight and c_p) of gases 1 and 4, and the temperatures T_1 and T_4, determine the properties of rarefaction and shock waves uniquely. In this connection it is of interest to note[8] that, even for infinite pressure ratios across the diaphragm, the shock Mach number (M_s) is limited by the relation:

$$(M_s) = \frac{\gamma_1 + 1}{\gamma_4 - 1} \frac{a_4}{a_1} \quad . \tag{1}$$

For physico-chemical studies, we are most interested in the temperature and pressure behind the shock. The temperature ratio T_2/T_4 and the pressure ratio p_2/p_1 are unique functions of the Mach number. For gases with constant heat capacity ratios γ_1 and γ_4, the limiting values of T_2/T_4 and p_2/p_1 are

$$\left(\frac{T_2}{T_4}\right)_{max} \simeq \frac{\gamma_4(\gamma_1 - 1)}{2\gamma_1} \left(\frac{\gamma_1 + 1}{\gamma_4 - 1}\right)^2 \frac{W_1}{W_4} \tag{2}$$

and

$$\left(\frac{p_2}{p_1}\right)_{max} \simeq \frac{2\gamma_1(\gamma_1 + 1)}{(\gamma_4 - 1)^2} \left(\frac{a_4}{a_1}\right)^2 \quad . \tag{3}$$

It is apparent that $(T_2/T_4)_{max}$ can be increased, all other things being equal, by using the largest possible molecular weight

ratio W_1/W_4; the limiting pressure ratio across the incident shock, p_2/p_1, is increased by increasing the sound velocity ratio a_4/a_1, which can be accomplished, for example, by increasing the temperature ratio T_4/T_1.

When the shock wave arrives at the right-hand end of the tube (i.e., the "wall"), it is reflected. The conditions across the shock wave after reflection are determined by the boundary conditions at the wall and by the Mach number of the incident shock. At the wall the gas particles must have zero velocity. Applying this condition to the shock equations, the properties of the reflected shock are determined uniquely. The variables in the region of gas flow behind the reflected shock are denoted by the subscript 5 (fig. 4).

(3) The Rarefaction Wave

The rarefaction wave is, in good approximation, an isentropic wave and travels at the local speed of sound with respect to the gas. Thus the head (or front) of the rarefaction wave, F, moves with the local velocity of sound (a_4) with respect to the tube toward the high-pressure end of the shock tube. The rear end, R, of the rarefaction wave travels with velocity a_3 ($a_3 < a_4$) with respect to the (expanded) gas. The rarefaction wave accelerates the gas, which was initially in state 4, to a constant velocity u_3, expands it to a pressure p_3 ($p_3 < p_4$), and cools it to a temperature T_3 ($T_3 < T_4$).

When the rarefaction wave arrives at the high-pressure end of the tube it is reflected. The velocity of the gas particles next to this wall must also be zero. This boundary condition determines the

the manner in which the rarefaction wave is reflected. We can illustrate what happens by considering the reflection of the leading edge or the head (F) of the rarefaction wave (fig. 4). After reflection the head of the rarefaction wave travels with increasing velocity as it traverses the remainder of the incident rarefaction wave, until it reaches the uniform flow conditions in region 3. In region 3 the velocity of the head of the rarefaction wave will be $u_3 + a_3$. Explicit relations for the position of the head of the rarefaction wave as a function of time are easily obtained. The method of characteristics can be used to describe other regions of the rarefaction flow.

(4) Interactions Between Shock and Rarefaction Waves

The rarefaction wave will ultimately catch and interact with the shock wave. We may consider four distinct cases, which are represented schematically in figures 5a to 5d. In figures 5a to 5d only the length of the downstream chamber changes while the initial conditions across the diaphragm (i.e., the states of gases 4 and 1) remain the same. In figure 5a the rarefaction wave interacts with the shock wave after the shock wave has been reflected from the wall and after it has passed through the contact surface. In figure 5b the shock and the rarefaction waves arrive at the contact surface simultaneously. In figure 5c the rarefaction wave interacts with the contact surface before interacting with the reflected shock. In figure 5d the head of the rarefaction wave (F) not only interacts with the contact surface (C) before the arrival of the reflected shock, but it also

arrives at the incident shock before the shock reaches the end of the tube.

It should be noted that the rarefaction wave will always overtake the shock wave. The velocity of the shock wave relative to the particle velocity behind the shock wave $(u_s - u_2)$ is less than the local sound velocity behind the shock (a_2). The head of the rarefaction wave travels in region 2 with the velocity $(u_2 + a_2) > a_2 > (u_s - u_2)$.

Interaction of the reflected rarefaction wave with the incident shock, as shown in figure 5d, decreases the pressure p_2 behind the shock and, hence, decreases the pressure ratio p_2/p_1 which supports the shock velocity. As p_2/p_1 is decreased, the velocity of the shock (M_s) is decreased. This attenuation of shock velocity is represented by a curved line in the x-t diagram (fig. 5d).

The x-t diagram is a useful guide for the design of shock tube experiments. The method of characteristics is valuable in determining the general character of the flow following complicated interactions.[3,5,9,10] However, after a complicated interaction between a contact surface and a shock wave, between a shock wave and a rarefaction wave, or after several reflections within the shock tube, the method of characteristics cannot be depended upon to give an accurate detailed picture of the flow.

(5) Temperature- and Pressure-Time Histories in Shock-Tube Experiments

For physico-chemical studies it is important to determine the

temperature and pressure of a given mass of gas as a function of time. This can be done conveniently by following the particle paths in the x-t diagram. Representative particle paths are shown by dotted lines in figure 6. For the regions of uniform flow we have $u_1 = 0$, $u_2 = u_3$ = a function of M_s, $u_4 = 0$, and $u_5 \simeq 0$. Particle velocities in regions of non-uniform flow are again determined by use of the method of characteristics.

Consider the three particles x', y, and z,* which are initially located in different parts of the shock tube (fig. 6). Particle x' remains at rest in the high-pressure region until the head of the rarefaction wave passes its location and accelerates it to the right while it is cooled. Ultimately particle x' traverses the rear of the rarefaction wave at the uniform velocity $u_3 = u_2$; the local sound velocity is a_3 ($a_3 < a_4$). Particle y is initially close to the diaphragm in the low-pressure section of the tube. Shortly after the diaphragm breaks, the shock wave passes particle y and it is (almost) instantaneously accelerated to the right; it acquires the velocity $u_2 = u_3$ and is heated to the temperature T_2 ($T_2 > T_1$) with a corresponding sound velocity a_2 ($a_2 > a_1$). Particle y continues in this uniform state until some time after the shock has been reflected from the wall; when the reflected shock passes particle y, it acquires a constant velocity $u_5 \simeq 0$ and an even higher temperature T_5 ($T_5 > T_2 > T_1$) at the local velocity of sound a_5 ($a_5 > a_2 > a_1$). Particle z is situated

---

* Particle x' means a small volume element of gas initially located at position x'; etc.

near the end of the tube; the shock does not pass this station until some time after it has passed the initial station of particle y. Particle z is in the uniform region 2 ($u = u_2$ and $a = a_2$) for a very short time only before the reflected shock passes and changes the velocity of particle z to $u_5 \simeq 0$ and the local velocity of sound to a_5. When the rarefaction wave arrives in region 5, it cools particle y before particle z. The rate of cooling of the rarefaction wave $-dT/dt$ decreases with time so that particle y is cooled at a more rapid rate than is particle z.

The temperature (pressure) versus time histories for particles x', y, and z are represented schematically in figure 7a for the flow specified in the x-t diagrams of figures 5b and 6. The temperature (pressure) versus time histories for these three particles, under the flow conditions described by the x-t diagram in figure 5d, are shown schematically in figure 7b.

From the preceding results it is evident that all particles (i.e., gas molecules identified by their initial positions) undergo different temperature- (pressure-) time histories. However, two particles initially located very close to one another will have nearly the same temperature- (pressure-) time histories.

The uniform cross-section shock tube may be used to apply a wide variety of temperatures (pressures) to the gas originally located at a fixed distance from the diaphragm. High temperatures (pressures) are obtained behind the incident and the reflected shocks by using large pressure ratios across the diaphragm, high-pressure

gas of relatively low molecular weight, and low-pressure gas of relatively high molecular weight. The rate of cooling of the gas is increased by using a short high-pressure chamber and is greatest for the gas closest to the diaphragm. The length of time during which the gas is at the uniform temperature T_2 behind the incident shock is longest for gas located close to the diaphragm. The length of time during which gas is under the uniform conditions and high temperature behind the reflected shock is longest for gas close to the end of the tube. By increasing the lengths of the high- and low-pressure chambers proportionately, all the times may be increased by the same factor. Quantitative results are obtained by using the method of characteristics. Typical times at the temperatures T_2 and T_5 are of the order of a millisecond for weak shocks ($T_5 \approx 3000^{\circ}K$) in shock tubes of conventional design and length.

C. Uses for Shock Tubes with Non-Uniform Cross-Section[11-14]

For many experiments, the uniform cross-section shock tube does not offer sufficient flexibility for producing desired temperature or pressure versus time profiles. By modifying the cross-sectional area of the shock tube it is possible to overcome some of the limitations.

(1) Downstream Expansion Chamber for Prevention of Shock Reflection

A useful method for minimizing the strength of reflected shocks is to place a large expansion chamber at the downstream end of the shock tube. When the shock wave enters this large chamber it is rapidly attenuated. Baffles are sometimes used to prevent wave

reflection.

The downstream expansion chamber need not be filled with low-pressure gas if a very weak diaphragm is placed at the end of the constant cross-section part of the tube. If this secondary diaphragm is stressed so that a small additional pressure rise is sufficient to produce rupture, then it will offer little resistance to the incident shock and the shock will pass directly into the expansion chamber. The hot gas behind the shock is cooled and accelerated as it expands. When this gas is slowed down again, the kinetic energy will be reconverted to thermal energy. The downstream expansion chamber can be used to cool a gas sample rapidly (cooling rates of the order of 10^6 ^oK/sec are easily attainable) if the subsequent reheating can be tolerated.

(2) Upstream Expansion Chamber for Prevention of Shock Reflection[14]

In figure 8 a second use for an expansion chamber is illustrated; this time the chamber is located upstream of the compression chamber. Diaphragm (a) is broken first and a shock passes down the tube. At some later time, which is usually made equal to x_o/a_4 (where x_o is the distance between the two diaphragms), the second diaphragm (b) is broken, thereby producing a very strong rarefaction wave which travels down the tube and catches the shock. This rarefaction wave originates from a large vacuum reservoir and may be made sufficiently strong (if the downstream tube is long enough) to annihilate the shock before it is reflected. This method of minimizing the reflected shock has the advantage of bringing the gas

to rest (or at least slowing it down) as it cools.

The rupturing of two diaphragms at accurately spaced time intervals requires special instrumentation (see Section V D(1)).

(3) Upstream Expansion Chamber Used to Produce Rapid Cooling Behind the Reflected Shock[14]

The strong rarefaction wave formed at the interface between the vacuum chamber and diaphragm (b) may be used also to produce very rapid cooling behind the reflected shock (fig. 8). The desired result is obtained by suitable selection of section lengths in the shock tube. The gas particles behind the reflected shock are (nearly) at rest. If an observation window is placed at the downstream portion of the tube, analysis can be made of gas particles at rest after they are heated by the reflected shock, before and during cooling by the rarefaction wave.

A modification of the design shown in figure 8 has been referred to as the "chemical shock tube" (see Section IIIA(1)).

D. Methods for Producing Strong Shock Waves

For sufficiently large pressure ratios p_4/p_1 across the diaphragm, equations 2 and 3 may be used to determine upper limits for the pressure and temperature, respectively, behind the incident shock. If the specific heat at constant pressure were constant, then the temperature T_5 behind the reflected shock would be nearly equal to $2T_2$ whereas p_5 may be larger than p_2 by factors of 10 to 20. However, for real gases the specific heats increase rapidly with temperature and, therefore, the ultimate limit of the temperature T_5

is greatly reduced. Many techniques are available for increasing the strengths of shock waves. Some of these are described in the following paragraphs.

(1) Selection of Gas Mixtures and Heating of the Gas in the High-Pressure Chamber

For a given pressure ratio across the diaphragm, and for a fixed gas composition downstream, the strength of the shock wave can be increased by increasing the temperature T_4 and by decreasing the molecular weight W_4 of the high-pressure gas. Low-molecular weight gases, which are relatively inexpensive and readily available, are nitrogen, helium, and hydrogen, in order of increasing desirability. The particular experimental program will dictate which of these gases should be used.

Hydrogen, which has the lowest molecular weight, may not be suitable for experiments on air in which the uniform region behind the reflected shock is used for observations since the hydrogen-oxygen mixture at the contact surface is easily detonated when the reflected shock passes this region. Also, if a chemical analysis is to be made of the downstream gas after the experiment, some hydrogen may diffuse into the sample before the sample can be drawn from the tube. For experiments, in which it is essential to avoid contamination with a reactive gas, helium is commonly used as the driver gas.

Several investigators have suggested atomic hydrogen as a driver gas. However, no successful experiments utilizing this

technique have been described in the published literature.

(2) Explosive or Combustible Gas in the Compression Chamber

Explosive and/or combustible gases may be used to create high pressures and high temperatures in the high-pressure chamber before the diaphragm ruptures. One of the more widely used combinations is a mixture of oxygen and hydrogen containing excess hydrogen, which can be detonated with a high-energy spark discharge. The incomplete information available concerning the use of this technique suggests that the shock velocity is high but that it is often not uniform. If combustion is not completed prior to the rupture of the diaphragm, the additional heat release behind the propagating incident shock could be responsible for non-uniformity of the shocks.

(3) High-Voltage Discharge[15]

The high-voltage discharge is another method which is being explored as a tool for increasing the internal energy and decreasing the average molecular weight of the high-pressure gas. Preliminary results suggest that it may be possible to control the initial conditions with a high-voltage discharge more closely than with explosion or combustion techniques. Few results describing the use of this method have, however, been published.

(4) Excitation of the Downstream Gas

Very strong shocks may produce electronic excitation and dissociation of the gases. Preliminary calculations indicate that for very strong shocks the ultimate limit for the temperature behind the incident shock (T_2) can be raised by exciting the downstream gas

molecules before the shock arrives. A method for accomplishing this result involves the use of an energetic electromagnetic field inside a pyrex tube.

(5) Non-Uniform Tube Sections

The use of non-uniform shock tube sections to get stronger shocks for the same pressure ratio has been discussed and applied successfully by several investigators.[8, 11, 13] In a uniform shock tube the gas in the compression chamber is expanded to a velocity u_3 through an unsteady expansion (the rarefaction wave). If the high-pressure section is made with a larger cross-sectional area than the downstream section (fig. 10), then the acceleration will take place partly through steady expansion and partly through an unsteady expansion. A steady expansion is relatively more efficient in accelerating the gas and stronger shocks can be attained for the same initial pressure ratio (p_4/p_1).

If the area ratio is fixed and the pressure ratio is increased, then the gas velocity in the "throat" (the diaphragm section) will ultimately equal the sound velocity. As the pressure ratio p_4/p_1 is raised beyond this point, no further gain in velocity at the diaphragm is reached. A "gain factor" G for the non-uniform shock tube has been defined by the relation

$$G = (p_{4_u}/p_{4_n})_{p_1} \tag{4}$$

in such a way that the same shock strength is attained, for a given

downstream pressure p_1, if the compression chamber pressure for the uniform shock tube is p_{4_u} compared with p_{4_n} for the non-uniform shock tube.[10] The gain factor G is plotted as a function of p_{4_u}/p_1 for A_4/A_1 equal to 2.80 in figure 11.

(6) The Double-Diaphragm Technique

As the pressure ratio across the diaphragm is raised, the strength of the shock wave approaches an asymptotic limiting value. For this reason, it is advantageous, for sufficiently large pressure ratios, to increase the temperature ratio of the two gases across the diaphragm rather than to raise p_4/p_1 to a higher value. Some representative results, showing the dependence of M_s on p_4/p_1 for various values of T_4/T_1, are given in figure 12.

An effective increase in the temperature ratio T_4/T_1 can be achieved by use of the double-diaphragm technique. The calculated results for He - He - air, He - air - air, and air - air - air gas combinations in the three chambers, assuming these gases have constant specific heats, have been given by Yoler.[11] The times at which the two diaphragms should be broken are determined by the relative lengths of the three chambers and by the desired duration of uniform flow in the test section before the reflected waves arrive.

Two modifications of the double-diaphragm technique are shown in figures 13a and 13b. The shock tube shown in figure 13a combines the advantages of the double-diaphragm technique and of a steady expansion. The shock tube sketched in figure 13b also has

two diaphragms, but the second diaphragm is broken by the impact of the incident shock and, consequently, requires no differential timing mechanism.

III. SURVEY OF MEASUREMENT TECHNIQUES USED IN SHOCK TUBES

Physico-chemical experiments in shock tubes are limited by the available measurement techniques. As we have seen in Section II, the duration of uniform flow conditions behind shock fronts is at most a few milliseconds. For this reason specialized techniques have been developed with a time resolution appreciably greater than 10^{-4} seconds.

This section includes a brief outline of well-known methods of shock tube instrumentation to determine pressure, density, extent of ionization, electrical conductivity, and temperature. Also included is a discussion of special optical techniques, many of which are in the state of development, which seem to be particularly well suited for detailed studies behind shock fronts. The development of some of these specialized optical techniques is the subject of much of the original research reported in this thesis.

A. Pressure Measurements

Reliable pressure measurements at the wall of a shock tube are possible for $M_s < 3$. Three readily available transducers which can be used to measure pressure in a shock tube are strain gauges, barium titanate and quartz piezoelectric crystals.

Barium titanate pressure gauges are easily constructed (and are commercially available*). A simple pressure pick-up consists

---

* For example, Endevco Corp., 689 S. Fair Oaks Ave., Pasadena, California.

of a barium titanate crystal compressed against a thin diaphragm (about .050 inch thick) which is flush with the inside of the shock tube. To act as a pressure pick-up, the barium titanate crystal must be correctly terminated in a cathode follower. A barium titanate gauge cannot be calibrated statically. This is not a serious problem because calibration can be made from the pressure rise across weak shocks (M_s less than 1.5) which is accurately predicted from the shock velocity and ideal shock theory at high pressure levels.

Recently a pressure pick-up using a quartz crystal as a transducer has become commercially available (the SLM gauge*) which has, perhaps, more isolation designed into it than other commercially available pressure pick-ups. This gauge can be supplied with a very high impedance cathode follower so that static calibration is possible.

A strain gauge can be used as a pressure transducer when it is mounted on a thin diaphragm which is flush with the inside of the shock tube. The strain gauge signal, however, requires much more amplification than either the barium titanate or the quartz gauge. A strain gauge pressure pick-up can be calibrated statically; however, a good direct current amplifier is necessary.

All three pressure pick-ups are sensitive to tube ringing which is associated with either the diaphragm rupture or with the passage of the shock. Without careful isolation, the ringing noise is a large

---

* The SLM gauge representative in the U. S. is Kistler Instrument Co., 15 Webster St., Tonawanda, N. Y.

fraction of the pressure signal for weak to moderate strength shocks. For shocks of Mach numbers of five or greater (and a downstream initial pressure less than one cm of Hg) the noise is often one hundred percent of the pressure signal.

Both the barium titanate and strain gauge transducers have excellent rise-time characteristics* and can be used as triggers for shock velocity measurements if they are suitably isolated from the tube ringing associated with the rupture of the diaphragm. The SLM gauge has a rise-time of the order of fifty microseconds and is not useful as an accurate trigger for shock velocity measurements.

B. Density Measurements

Interferometric, X-ray absorption and schlieren techniques only will be discussed here.

(1) Interferometric Techniques[16-19]

The local change of density behind shock fronts can be observed if the gas velocity is not too much smaller than the local velocity of sound.[17] A change of density, under otherwise uniform conditions, produces a change in index of refraction. Since the geometrical path in a shock tube remains constant, the change in index of refraction produces a change in optical pathlength at constant geometric pathlength. The change in optical pathlength, in turn, produces a fringe shift in an interferometer which can be measured with a very high degree of accuracy. In this manner the change in

---

* Their rise-time is limited essentially to the time it takes the shock to traverse their length.

density may be determined as a function of time.

For practical applications the Mach-Zender interferometer[17] is perhaps most suitable. It allows wide separation of mirrors, the beam passes through the region of interest only once, thereby making the interpretation of results relatively simple, and it is possible to locate the fringes at any desired position. A schematic diagram of the interferometer arrangement is shown in figure 14. Light from a source L is split at the beam splitter BS into two components of equal intensity, one of which passes through the shock tube S while the other traverses a compensator C. The two beams are superimposed behind the second beam splitter BS after having traversed nearly equal optical paths. A schematic diagram of the interference fringes is sketched in figure 15. The shock front SF corresponds to a region in which the density changes very rapidly with distance and is easily identified by the discontinuities in the interferogram. For properly designed experiments, the density change in region 2 behind the incident shock corresponds to vibrational relaxation of the gases. The rate of change of density with time behind the shock front may be used to determine the vibrational relaxation time (see Section IV C) by noting that the measured lengths x and shock velocities u_s determine the time according to the relation

$$t = \frac{x}{u_s} \quad \frac{\rho_2}{\rho_1} \quad , \tag{5}$$

where the factor ρ_2 / ρ_1 corrects for the motion of the gas in the direction of propagation of the shock front.

Since exposure times of less than one microsecond are required, and since the interferograms are recorded photographically, a very intense light source, such as a condensor spark discharge, must be used. Fringe shifts on the interferograms are observable only if the density change exceeds a well-defined lower limit. For example, for $\lambda = 5460$ Å and a 10 cm geometric pathlength in the shock tube, a density change of 2.5×10^{-6} g/cm^3 produces a fringe shift equal to one tenth of the distance between fringes.

(2) X-Ray Absorption Techniques[20]

The absorption of X-rays is proportional to the density of the medium through which they travel. Kistiakowsky has used soft X-rays to study the density change through detonation reaction zones.[20] A 2 to 4 mm wide X-ray beam was directed through the shock tube onto a terphenyl scintillation crystal backed by a 1P21 photomultiplier tube. A thin aluminum film was used to prevent light penetration to the scintillation crystal. The photon flux was sufficient to maintain a photomultiplier output which varied by only one or two percent from the mean value. Experimentally it seems difficult to obtain both fast response and accuracy of measurement by using this technique.

(3) Schlieren Techniques[21-23]

Schlieren techniques, in conjunction with rotating drum cameras or photoelectric receivers, may be used for the study of shock front propagation, reflection, propagation of rarefaction waves, etc. The schlieren effect is, in first approximation, pro-

portional to the first derivative of the density with respect to distance and is, therefore, most useful for qualitative studies concerning the location of sharp density gradients.

A suitable arrangement for the determination of shock velocities is shown schematically in figure 16. Light from the source L passes normal to the shock tube axis (fig. 16) after a narrow beam has been defined by suitably arranged slits S. The knife edge K blocks the light path to the multiplier phototube P before the shock passes. When the shock passes the observation station, the light beam is deflected and the corresponding phototube output marks passage of the shock front. The rise-time of the schlieren signal is about one microsecond. In addition, a schlieren trigger is insensitive to tube vibration if the system is mechanically isolated from the shock tube and if the windows W in the shock tube have no surface undulations which are apparent to the naked eye. In practice only shocks exceeding a minimum strength (and leading to corresponding, well defined, density gradients) are observable with a given experimental arrangement.

The schlieren effect can be made quantitative, in principle, and can be used for actual density measurements by replacing the knife edge by a coarse grid or a suitable filter. In practice, quantitative interpretation of results is, however, very difficult.

From the foregoing discussion it is clear that the flow density can be measured more accurately than the flow pressure. Experimentally it is easier to isolate the density measurement from

superfluous tube noise. Furthermore, the pressure is measured at the wall while the density measurement is made by integrating electromagnetic radiation over the entire diameter of the shock tube, thus minimizing the wall effects.

C. Ionization Density and Conductivity Measurements

The most commonly applied techniques for the determination of ion density and conductivity in high-temperature gases, namely the Langmuir single- and double-probe methods,[24-26] have been found to be unreliable for shock-tube investigations because the surface resistance of the electrodes is apparently too large.[26] Kantrowitz and his collaborators[26] found that better results could be obtained by measuring the change of the magnetic field as the shock front passes.

A schematic diagram of the experimental arrangement is shown in figure 17. The coil M is used to produce a stationary magnetic field whose change is measured by use of the pick-up coil P. The system may be calibrated by measuring the change in the magnetic field intensity when a cylindrical piece of aluminum of known conductivity and velocity is shot through the tube. The induced emf in the pick-up coil P may be compared directly with the corresponding emf produced by ionized gas behind a shock front which is propagated with known velocity.

Optical methods for the determination of ion densities depend on the use of Stark broadening of spectral lines or on spectral line shifts.[26-28]

An experiment by Schuler and Weber[29] suggests the use of microwaves to directly determine ion densities behind shock fronts. In this experiment[29] a microwave bridge operating slightly off balance was used to determine electron densities in premixed flames down to about 5×10^8 electrons per cm^3. The presence of free electrons introduces conductivity and affects the dielectric constant of the region occupied by the flame. Perhaps a modification of this technique could be utilized in shock tube research.

D. Temperature Measurements

Temperature measurements can be made on the wall of the shock tube by using resistance gauges and in the flow itself by using optical techniques.

(1) Thin Metallic Film Technique[30, 31]

Thin metallic films are used as resistance thermometers to measure transient surface temperatures and heat transfer rates. The gauge developed at the Guggenheim Aeronautical Laboratory, California Institute of Technology,[31] is made of a thin layer of platinum (about 10^{-6} cm thick) sputtered over an insulating backing plate. The gauge has a response time of less than 1 μ-sec when the platinum film (of rectangular shape and roughly 1 mm by 20 mm) is mounted in the shock tube with the long dimension perpendicular to the tube axis. The temperature gauge has a linear output of about 1.5 - 2.5 mv/^{o}C. This gauge has durability, repeatability, and a very small resistance change over a large number of tests.

The resistance gauge offers the best general purpose shock

velocity trigger. The metallic film is not sensitive to mechanical vibration and has a fast rise-time. Adequate signals are obtained for shock strengths above a Mach number of 2.

(2) Optical Techniques

In principle, almost any optical technique[32-37] (e.g., line reversal measurements; rotational, vibrational, and electronic populational temperatures from line profiles; etc.) can be adapted for shock tube observations. In practice, these studies are, however, very difficult to perform with adequate time resolution and no results of actual measurements have been described. The principal practical problems for the use of most optical methods are associated with the lack of intensity and absence of suitable calibration methods.

For carbon-forming shocks (e.g., shocks in various hydrocarbons) a modified two-color method has been used with very good success behind reflected shocks, after conditions have become substantially uniform and the emitted radiation has acquired a greybody spectral distribution (see Section VI G(3)). A schematic diagram of the experimental arrangement is shown in figure 18. The blackbody (or greybody) character of the emitted radiation has to be verified by independent spectroscopic measurements. The system described in figure 18 can be calibrated conveniently by using a greybody (or blackbody) source at the shock-tube window for the actual optical system, mirror, wavelength filters, and phototubes used. The light intensity ratio R(T) measured by P_1 and P_2 is a unique function of the greybody or blackbody temperature. For

suitably selected filters R(T) can be made a very sensitive function of T. The time resolution attainable is better than 10^{-6} sec.

The scheme outlined above for carbon-forming shocks can probably be adapted also to various aerodynamic applications in which a small amount of carbon-producing material (such as acetylene) is added to the air. Presumably the flow characteristics will not be affected by a suitably selected temperature indicator of this type.

E. Light Absorption and Emission Measurements at Selected Wavelength Regions

The use of photomultipliers and/or photographic methods for recording the light intensity in absorption or emission for a fixed wavelength region presents few unusual features for shock-tube applications. The light beam must be well collimated in order to minimize total reflection and schlieren effects at the shock front; it should enter in the plane of the shock front. Either filters or monochromators may be used to isolate the desired wavelength region. For absorption studies it may be difficult to obtain extraneous light sources of sufficient intensity. The use of photographic recording techniques may be impeded by the lack of adequate light intensity in emission for easy observation. Finally, absorption measurements using steady light sources may be complicated by relatively intense emission behind the shock front.

Simultaneous light emission and absorption measurements can be made by the judicious use of Kerr cells (see Section VI E). With a Kerr cell it is possible to obtain chopping rates of sufficiently high

frequencies (up to 10 megacycles) to permit light modulation even during the short periods of time in which the gas is in a uniform state behind incident and reflected shocks.

Interpretation of quantitative light absorption and emission measurements in terms of absolute concentrations involves the usual analytical and experimental difficulties. However, compared with sources such as flames, the uniform regions behind shock fronts have the important advantage of being at uniform temperature in the line of sight for properly aligned optical instruments. Both temperature and pressure can be predicted with fair accuracy on the basis of one-dimensional shock tube theory unless relaxation effects and/or chemical reactions are taking place. Finally, the pressures as a function of time may be measured for moderate strength shocks with piezoelectric gauges whereas shock velocity determinations yield independent estimates for the effective specific heat ratio across shock fronts. Thus the quantitative conversion of observed light absorption and emission data to concentrations, although difficult without independent calibration, appears to be far simpler for shock tube studies than for flames.

F. Spectroscopic Measurements

Simultaneous observations at different wavelengths of the light absorbed or emitted behind incident and reflected shocks requires special instrumentation. Four essentially different methods of approach have been used or are under development for shock-tube applications. A brief description of each of these methods is presented in the following paragraphs. In a final paragraph we summarize

the characteristics of transducers which are suitable for infrared spectroscopy in shock tubes.

(1) Rotating-Drum Cameras[38, 39]

Rotating-drum cameras have been used in conventional spectrographic arrangements for the determination of spectra in which the time scale is determined through the position of the spectrum. The use of this type of instrument is severely limited by the low intensity of the emitted radiation in many shock-tube experiments. However, rotating drum cameras have been used successfully for very strong shocks.

A schematic diagram illustrating the optical arrangement of the rotating-drum-camera-spectrograph is shown in figure 19. The emitted light is reflected from a concave grating G and photographed on a strip of paper located on the inside of the rotating drum D. The drum may be driven with an electric motor or a turbine. The light emission from the shock tube should last a period of time which is shorter than the time for one complete revolution in order to obviate the necessity for synchronization between the shock front and recording of the spectrograph. Resolving times up to about one microsecond are easily obtained by use of the arrangement sketched in figure 19. For very high scanning speeds the plane mirror M may be replaced with a rotating triangular mirror, which sweeps the image across the film (streak camera).[40] For a drum camera driven with a helium turbine at 5500 rps, a time dispersion of 8 mm/μsec. and a time resolution of 2.5×10^{-8} sec. have been

obtained.*

(2) Spectrographs Utilizing a Bank of Photomultipliers

Perhaps the simplest method for recording simultaneously the light intensity as a function of time at several wavelengths involves the use of a spectrograph with a number of photomultipliers, each of which covers a well defined wavelength region. This arrangement is, however, cumbersome and expensive to instrument effectively.

The required number of photomultipliers can be reduced by modulating some of the wavelengths through a Kerr cell, as in the method described in Section VI E for the simultaneous determination of absorbed and emitted radiation at a fixed wavelength.

(3) Image Converters Used in Conjunction with Rotating-Drum Cameras

Image intensifier tubes provide a powerful method for the detection of weak signals over wide wavelength regions. Two of the tubes, which are still under development, deserve special attention for application in shock-tube spectroscopy.

A tube built at Westinghouse[41] consists of a photoemitting layer followed by a number of dynodes (i.e., thin films permeable to electrons) parallel to the light-sensitive layer. These films are covered on the exit side with secondary emitting layers. The other end of the tube is made up of a phosphorescent screen. The accelerating voltage between dynodes and between the photolayer and the

---

* "Specifications for Model 194 Continuous-Writing Streak Camera", Beckman and Whitley, Inc., San Carlos, California.

first dynode is a few kilovolts, which is sufficient for electrons to penetrate the film and produce secondary electrons. The voltage between the last dynode and the output phosphor depends on the phosphor used. To get clearer images, a focusing magnetic field may be employed. In the spectrograph, the intensified image on the phosphor could then be recorded on a rotating-drum camera.

Another tube, the Lumicon, has been developed by the Bendix Aviation Company and operates on a different principle from that of the Westinghouse tube.* Unfortunately, relatively small image amplification is obtained with the Lumicon. It is only about 35 times more sensitive than a photographic emulsion, whereas the Westinghouse tube should provide image amplification factors much greater than this.

(4) Scanning Spectrograph**

A Kerr cell (arranged as a prism) may be useful as a beam deviator, in conjunction with a spectrograph, to provide sufficiently high scanning speeds for shock-tube studies over a limited wavelength range.

For substances which exhibit birefringence under the influence of an electric field, the index of refraction is related to the field strength E (in esu) through the expression

$$n_e - n_o = \lambda B E^2 = \Delta n \qquad (6)$$

---

* This tube is essentially a television receiver tube.

** The scanning spectrograph described in this section was suggested by Dr. S. S. Penner and first analysed by Dr. V. Vali of the Lockheed Missile Systems Division, Van Nuys, Calif.

where n_e and n_o represent, respectively, the indices of refraction with and without the field, λ is the wavelength (in cm), and B is an empirically determined constant (the Kerr constant) for the material used in the Kerr cell. For $\lambda = 5 \times 10^{-5}$ cm, $B = 2.2 \times 10^{-5}$ (the value for nitrobenzene at room temperature), and E = 50,000 volts/cm,*

$$\Delta n = 3 \times 10^{-5} .$$

This small change in index of refraction is sufficient for use in a scanning spectrograph if the Kerr cell is employed only as a beam deviator in a prism.

The deflection angle D of a light beam passing through a prism is

$$D = i - A + \sin^{-1} \left\{ n \sin \left[A - \sin^{-1} \left(\frac{\sin i}{n} \right) \right] \right\} \quad (7)$$

where i is the angle of incidence, A equals the prism angle and r is the index of refraction of the prism with respect to the surrounding medium (in this case, a container of nitrobenzene). In order to find the maximum change in the deflection angle D as the index of refraction, prism angle A, and the angle of incidence i are changed, the derivative of D with respect to n, i.e.,

$$\frac{dD}{dn} = \frac{1}{\cos (D+A-i)} \left\{ \sin \left[A - \sin^{-1} \left(\frac{\sin i}{n} \right) \right] + \frac{\sin i}{\sqrt{n^2 - \sin^2 i}} \cos \left[A - \sin^{-1} \left(\frac{\sin i}{n} \right) \right] \right\} \quad (8)$$

---

* This field strength is below the dielectric breakdown of nitrobenzene.

must be maximized. The function dD/dn has a singularity at n = sin i corresponding to the angle of total reflection on the front surface of the prism. Since the second term in the square brackets is large compared to the first one, it is obvious that the optimum value of A is close to $\pi/2$. In figure 20 the deflection angle is plotted against the index of refraction for different values of sin i.* It is seen that, even two or three degrees from the angle of total reflection, there is an appreciable change of the deflection angle.

The change in the deflection angle may be magnified by the use of a telescope, as shown in figure 21. After emerging from the telescope T, the light beam is reflected from a concave grating G and the intensity recorded at the Rowland circle behind a fixed slit on the photomultiplier P. Since the angle of reflection r from the grating is fixed, the following relations hold as the angle of incidence i' to the grating changes:

$$\lambda = d\,(\sin i' + \sin r) \qquad (9)$$

and

$$\Delta\lambda = d \cos i'\ \Delta i' \qquad (10)$$

where d is the grating constant.

Assuming a magnification of the telescope m' = 10, $d = 1/2000\ \text{cm}^{-1}$, and $i' \simeq 90^{\circ}$, we find

$$\Delta\lambda \simeq d\ \Delta i'$$

or

$$\Delta\lambda \simeq d\ m'\ \Delta D = 500\ \text{Å}\ .$$

---

* The data shown in figure 20 are taken from the studies of Dr. V. Vali.

Here $\Delta D = 3.6$ minutes of arc represents the change in the angle of deviation of the beam emerging from the prism when the angle of incidence differs from the angle of total reflection by about two degrees (fig. 20). Actually the intensity losses are very great close to the angle of total reflection so that, in practice, the attainable value of ΔD will be smaller than 3.6 minutes.

The prism-Kerr-cell-spectrograph combination will probably be most useful for studies of narrow spectral regions covering wavelength intervals of only a few angstroms.

(5) Photoconductive Cells

Photoconducting cells are effective as transducers in the infrared spectrum region. Most of the pertinent information on these cells is classified.

Dr. Windsor collected available samples of PbS, PbTe, and PbSe photoconducting cells and used a high speed mechanical light chopper to determine their rise-time and output characteristics. The results of his investigation are listed in table I.

Reference to table 1 indicates that rise-times of the order of 5 - 10 μ secs are available, but at a greatly reduced signal output.

G. Light Reflection Measurements

The equations developed for reflection of a light beam from a one-dimensional non-uniform layer of gas show that the coefficient of reflectivity is dependent on the density profile. This fact can be utilized to investigate the structure of the shock front. The rotational relaxation times may then be inferred by comparing shock front thick-

nesses for monatomic and diatomic gases (see Section III G)

The light reflected from a shock front is of very low intensity and short duration. In order to obtain adequate signal detection, the response time of the receiver must be of the order of microseconds and care must be taken to reduce the background of scattered light. For practical purposes it is also desirable to make the system sufficiently flexible to allow changes in the angle of incidence of the light beam.

A schematic diagram of the experimental arrangement is shown in figure 22.[42] Light from the source L is used to form a parallel beam and is reflected from the shock front SF after passing through the filter F and the slit C. The reflected light is focused on the photomultiplier P where it is detected. Measurement of the light intensity as a function of the angle of incidence, wavelength, and other physical properties may then be used to calculate the density profile through the shock front as well as rotational relaxation times (see Section III G). In this connection it is of interest to note that it is generally not possible to use interferometric methods for the measurement of rotational relaxation times because the resolving power of the interferometer is usually not sufficient for this work. Thus the shock reflection method and interferometric studies may be regarded as complementary techniques for measuring rotational and vibrational relaxation times, respectively.

IV. USE OF THE SHOCK TUBE FOR THE DETERMINATION OF PHYSICO-CHEMICAL PARAMETERS

In this section are described some representative applications of the shock tube for the determination of physico-chemical parameters. The following topics will be considered:

A. Reaction rate measurements for homogeneous gas reactions.

B. Study of ionization rates.

C. Measurements of vibrational relaxation times.

D. Gas emissivities at elevated temperatures.

E. Measurements of heats of dissociation.

F. Determination of transport properties.

G. Thickness of shock fronts and rotational heat capacity lags.

H. Initiation of detonation with shock waves and thickness of detonation fronts.

A. Reaction Rate Measurements for Homogeneous Gas Reactions

In the survey on the aerodynamics of shock-tube theory and applications described in Section II, the versatility of the shock tube was stressed as a research tool for producing temperature vs. time and pressure vs. time pulses of almost any desired magnitude. This property of the shock tube is of unique importance in permitting the preparation of reacting samples of known chemical composition at the conditions which are of interest for investigations of chemical reaction rates.

The principal difficulty encountered in the use of the shock

tube for rate measurements is associated with the short duration of the uniform state of the gas behind incident and reflected shocks. For tubes of conventional dimensions (i.e., overall lengths of 10 to 50 ft.), it is generally not possible to study reaction rates with a half-life much longer than about a millisecond. On the other hand, the available optical methods for following composition changes (see Section III) are characterized by response times between 10^{-8} and 10^{-5} sec. Thus the shock tube is generally useful only for chemical changes with half lives between about 10^{-3} and 10^{-6} sec. In practice this restriction is not a serious one because (a) many atomic and free radical reactions can presumably be studied and (b) for chemical reactions with sizable activation energies we may select T_2 and p_2 or T_5 and p_5 in such a way as to obtain reaction rates of the desired order of magnitude.

Two essentially distinct techniques have been used for the study of reaction rates behind shock fronts. These will now be described.

(1) The "Chemical Shock Tube"

The chemical shock tube is designed to yield essentially a single, well defined, temperature pulse. The desired result may be obtained by use of the double-diaphragm technique with upstream expansion chamber described in Section IIC(3). When properly used, chemical reactions before reheating by the reflected shock may be neglected and the cooling rate afforded by the rarefaction wave is sufficient to "freeze" the gas composition in the state reached at

the uniform conditions behind the reflected shock. The shape of the temperature pulse is controlled through the length ratio of the driver section to the driven section, the time delay between breaking of the two diaphragms, and the absolute length of the driven section. The absolute magnitude of the temperature pulse depends on the strength of the incident shock wave, i.e., on the pressure ratio across the diaphragm separating the driver and driven gases.

The performance of the chemical shock tube is well illustrated by experiments on nitric oxide formation carried out on air. In figure 23 the percentage yield of NO is plotted as a function of temperature. Calculated equilibrium values, as well as experimental data obtained by analysis of the gas composition after passage of the shock, are shown. The data plotted in figure 23 may be understood by noting that below 2500°K there was insufficient time at the peak temperature to reach chemical equilibrium; between 2500 and 2900°K, the observed values of the NO concentration are in fair agreement with the equilibrium values; above 2900°K, inadequate cooling rates were obtained to prevent some decomposition of the NO formed at the highest temperature. The experimental data below 2500°K have been used[42] to obtain a crude estimate for the rate of NO formation on the assumption that the reaction proceeds according to the bimolecular mechanism

$$N_2 + O_2 \rightleftharpoons 2NO \ .$$

For the determination of reaction rates at elevated temperatures, the use of the chemical shock tube can be refined by con-

trolling the duration of the peak temperature and determining the composition as a function of time under conditions where quenching is completely effective. However, this method of approach does not seem to be usable for atomic and free radical reactions with small activation energies. Nevertheless, the method is interesting particularly because (crude) rate data can be obtained without the necessity of following the composition change as a function of time during the extremely short times available under uniform conditions behind the reflected shock.

(2) Determination of Chemical Reaction Rates from Optical Measurements Behind Incident and Reflected Shocks[44-46]

Chemical reaction rates under the uniform conditions existing behind incident and reflected shocks have been studied by several investigators. Some of the reactions which have been investigated are the following:

$$N_2O_4 \rightleftharpoons 2NO_2, \quad (44)$$

$$M + I_2 \rightleftharpoons 2I + M, \quad (45)$$

and the overall process

$$H_2 + Br_2 \rightleftharpoons 2HBr. \quad (45)$$

Chemical changes behind incident and reflected shocks have been studied by following the composition with a suitable optical technique depending, in the published studies, on ultraviolet absorption measurements.[44-46] The quantitative interpretation of

experimental rate data involves the assumption that the relaxation times for the internal degrees of freedom are short compared with the times during which measurable chemical changes occur. For details concerning the experimental work, particularly proper calibration and conversion of the observed dependence of absorption on time, reference should be made to the published literature. For observations behind the incident shock, it is necessary to allow for the finite gas velocity and to convert apparent observed times to proper times spent by the gas behind the shock. Since the gas should be (nearly) at rest behind the reflected shock, observed and true times are practically equivalent in this region.

B. Study of Ionization Rates[26]

The published studies of ionization rates have been restricted to measurements on argon behind strong shocks (up to Mach number 20). The electrical conductivity of the gas was measured[26] by observing the deflection of a magnetic field produced by the motion of the conducting gas through the field coil (see Section IIIC); the measured conductivities were found to be in fair accord with predictions based on theoretical estimates for electron mobility. The electron density was measured directly[38] by determining the shift of spectral lines and correlating the results with calculated values for these line shifts. Finally, the absolute intensity of radiation in the visible region of the spectrum was estimated and found to constitute an important energy loss for the gas behind the shock. The theory for the rate of approach to equilibrium ionization behind strong shock waves has been studied

extensively by Petschek.[47]

C. Measurement of Vibrational Relaxation Times

As mentioned in Section IIIB(1), an interferometer may be used to study the change in density behind shock fronts. Passage of the shock is followed by very rapid adjustment of the translational degrees of freedom to produce a Maxwellian random velocity distribution; the rotational degrees of freedom adjust somewhat more slowly and their relaxation time can be estimated from shock reflection studies of the type discussed in Section IIIG. The adjustment of the vibrational degrees of freedom occurs much more slowly, requiring generally some 10^4 molecular collisions. As energy is transferred from the translational (and rotational) degrees of freedom to the vibrational degrees of freedom, the translational temperature decreases and the density increases. This density increase may be determined, by use of an interferometer, with a high degree of accuracy.

For observations behind incident shocks, it is again necessary to introduce a suitable correction for the motion of the compressed gas in the direction of the shock front. Determinations of vibrational relaxation times, based on experimental measurements of the density profile, have been carried out, for example, for O_2 at temperatures between 800 and 3000°K and for N_2 at temperatures between 3500 and 5500°K.[17-19] In general, the observed results have been found to be in good agreement with theoretical predictions.[48,49]

Of particular interest for many practical applications is an ingenious use of vibrational relaxation time measurements made by Herzfeld.[50] This author infers that the Lennard-Jones interaction potential, for some collisions between specified chemical species, applies up to very high temperatures because the parts of the interaction potential curve, used for successful correlation of vibrational relaxation times with theoretical studies, correspond to very high temperatures ($\sim 10,000^{\circ}K$) for the calculation of transport coefficients.

D. Gas Emissivities at Elevated Temperatures

Gas emissivities are required for quantitative computations of radiant energy transfer in combustion devices. Experimental data are available at temperatures up to about $1500^{\circ}K$ for several stable molecules (e.g., CO, H_2O, CO_2) which make perhaps the most important contributions to the radiant flux.[51]

The theoretical calculation of gas emissivities from spectroscopic considerations has progressed to the point where reasonable estimates can be made for diatomic molecules[52] for the entire temperature range which is of interest (up to about $3500^{\circ}K$). However, for polyatomic molecules the theoretical computations become exceedingly laborious at elevated temperatures[53] and, furthermore, cannot be carried out because the required basic spectroscopic parameters have not been measured. It therefore appears to be highly desirable to investigate the potential utility of the shock tube

for gas emissivity studies at elevated temperatures.*

Successful emissivity determinations behind shock fronts are complicated by the lack of satisfactory radiation receivers which combine high response speed and uniform sensitivity to all wavelengths, i.e., fast black receivers are not available. Furthermore, gas emissivity measurements require the greatest care in eliminating the impurities which are encountered in normal shock tube operation. The direct measurement of gas emissivities at temperatures above 1500°K is an important fundamental problem which should be difficult but not impossible to perform in the laboratory.

E. Measurements of Heats of Dissociation[54, 55]

The effective equation of state for a gas at elevated temperatures can be determined if the actual particle velocity is measured simultaneously with the shock velocity. Application of the equations for conservation of mass and momentum then gives the corresponding values for the pressure (p_2/p_1) and density (ρ_2/ρ_1) ratios across the shock front. Thus

$$\frac{\rho_2}{\rho_1} = \frac{u_s}{u_s - u_2} \tag{11}$$

and

$$\frac{p_2}{p_1} = \frac{1}{R_g T_1} u_s u_2 + 1 \tag{12}$$

---

* An extensive experimental program, designed to yield gas emissivities at elevated temperatures, is currently in progress at the California Institute of Technology (S.S. Penner, D. Weber, and others).

where u_s and u_2 denote the shock and particle velocities, respectively, R_g is the gas constant per gram, T denotes the initial temperature, and the subscripts 1 and 2 define, respectively, the conditions before and behind the shock front.

In practice, the shocks were generated[54] with a plate driven by a high-explosive charge. The shock and plate (particle) velocities were then recorded by using a suitable photographic system and markers.[54]

A comparison between the calculated and observed Hugoniot curves for argon showed satisfactory agreement for pressure ratios between 200 and 1146 with $T_1 \simeq 300^{\circ}K$, $p_1 \simeq 60$ cm. of Hg.[54] After the feasibility of the method had been established by the tests in argon, measurements were made in nitrogen.[55] For sufficiently strong shocks, N_2 will dissociate appreciably; the extent of dissociation, in turn, will influence the observed results. By comparing calculated and "observed" values of ρ_2/ρ_1 as a function of p_2/p_1 it should be possible to estimate the correct value for the dissociation energy of N_2 provided equilibrium excitation of internal degrees of freedom is obtained. The "observed" values of pressure and density ratios were computed from the shock and particle velocities according to equations 11 and 12. The calculated values of the ratios were derived from straightforward equilibrium computations for two heats of dissociation of N_2(7.385 ev and 9.764 ev) using the ideal gas equation of state and the Hugoniot equation. Comparison of calculated and observed data showed better agreement if the higher value was

assumed for the heat of dissociation of N_2(9.764 ev), thus providing support for the validity of this estimate.

The simultaneous experimental determination of shock and particle velocities appears to be a useful tool for approximate heat of dissociation measurements for molecules other than nitrogen.

F. Determination of Transport Properties

No successful direct determination of any of the transport coefficients, using shock tube techniques, have come to the author's attention (see, however, the last paragraph in Section IV G).

The most promising line of approach seems to involve the use of heat transfer gauges for measuring the total energy transfer to a flat plate mounted in a shock tube (see Section IIID(1)). By carrying out carefully controlled experiments, it should be possible to obtain estimates for the thermal conductivity of non-dissociating gases, at least at temperatures where radiant energy transfer may be neglected. The aerodynamics of stagnation point heat transfer is relatively well understood. The more interesting and vital information on transport properties in dissociated gases will require ingenious interpretive work on carefully planned experiments. Thus it may be possible to disentangle the composite energy transport associated with thermal conduction and surface recombination of atoms by performing experiments with systematic changes in pressure, since diffusion coefficients vary inversely with pressure whereas thermal conductivities are insensitive to pressure. The direct determination of viscosity coefficients at elevated temperatures, using shock-tube

techniques, may be very difficult.

G. Thickness of Shock Fronts and Rotational Heat Capacity Lags

Theoretical studies of the effective thickness and structure of shock fronts have been carried out by a number of authors.[56-60] Thomas, using Becker's hydrodynamic theory,[59] made approximate allowance for the temperature dependence of the viscosity and thermal conductivity by using a hard-sphere model in the kinetic theory of gases.[60] More recently theoretical studies have been carried out by Wang Chang,[61] Mott-Smith,[62] and Zoller.[63]

A few years ago Hornig[64] suggested a procedure for the direct experimental determination of shock front thickness in gases, which was utilized effectively in subsequent investigations by Hornig and his collaborators.[42,65,66] The method has been applied also to studies of the shock front in liquids.[67]

Hornig's method utilizes the fact that the wavelength of visible light is of the same order of magnitude as the estimated thickness of the shock front in a gas for ordinary conditions of temperature and pressure. Therefore, the optical properties of the shock front should be sensitive functions of the thickness and, in particular, the reflectivity of the shock front can be used for making experimental estimates. Measurements have been performed for N_2,[42,65,66] A,[65,66] H_2,[66] and O_2.[66]

In order to interpret the experimental data it is necessary to make an estimate for the dependence of index of refraction on distance, n(x). Five models for n(x) have been used. Of these, one

("model II") is that obtained theoretically by Mott-Smith [62] and is the limiting expression for weak shocks in Becker's theory, [59] and is very close to Thomas' estimate [60] for all shock strengths. The shock thickness was defined as the ratio of the total change in index of refraction divided by the maximum value of dn/dx. Since systematic transmission errors do not affect the rate of change of the logarithm of (a reduced) reflectivity with the logarithm of the wavelength, the measured data for this parameter are most easily used to obtain estimates for the shock front thickness δ. Less satisfactory results have been derived from the change of reflectivity with pressure. [42] In effect, both the shock thickness and an overall sensitivity for the apparatus are obtained by comparing calculated and theoretical results. Although the differences in the calculated data for different models of n(x) are only barely beyond the limits of observed experimental scatter, the measured values favor the model II for n(x) defined previously.

A comparison of calculated and observed results for $\bar{\ell} / \delta$ in argon, as a function of shock Mach number, is shown in figure 24, where $\bar{\ell}$ represents the mean free path. [66] Reference to figure 24 shows that the observed results are in fair agreement with the theories of Wang Chang, [61] Mott-Smith, [62] and Zoller [63] for weak shocks (Mach number $\leq$ 1.4) and seem to follow roughly Zoller's calculations for larger Mach numbers. After considerable refinement of experimental technique, Hornig and his colleagues suggest the possibility that the remaining principal sources of error in the

experimental measurements are associated with very small fluctuations in the angle between the shock front and the tube axis.

For diatomic gases such as H_2, N_2, and O_2 it is not valid to assume that the rotational degrees of freedom are in equilibrium with the translational degrees of freedom. For H_2, equilibration of the rotational degrees of freedom occurs so slowly at shock Mach number 1.4 that it may be neglected immediately behind the shock, the corresponding density profile therefore being indistinguishable from that for a monatomic gas.[66] In nitrogen the rotational energy is rapidly equilibrated, as shown by the change of the shock front with time; furthermore, at least two relaxation times are required to describe the process.[66] Oxygen behaves like nitrogen but has slightly longer relaxation times.[66]

A very interesting new application of the shock reflection technique has been described recently.[68] The thickness of the shock front was measured in carbon dioxide and nitrous oxide gases. The observed shock front thicknesses were then compared with theoretical predictions allowing only for heat conduction and shear viscosity and assuming that the molecular vibrations were not excited at the shock front. Since calculated and observed results were found to be in agreement, it was inferred that the bulk viscosity, which is a manifestation of rotational excitation processes, must be very small.[68]

H. Initiation of Detonation with Shock Waves and Thickness of Detonation Fronts

Shock initiation of detonations[69] has been studied by a number of investigators using such reactive mixtures as methane-oxygen,[70] ethylene-oxygen,[70], hydrogen-oxygen,[71, 72] etc. Kistiakowsky and his collaborators[73] initiated detonation in various gaseous systems by the use of shocks formed from the decay of a detonation wave originating in a different mixture. A similar arrangement was used also by Mooradian and Gordon.[74]

The results of studies on shock initiation of detonation emphasize the care which must be used in shock tube experiments. Fay[71] reported minimum "ignition" temperatures, computed from simple shock wave theory, which were well below those normally associated with the mixtures under study. Later Hooker,[75] using the identical shock tube, discovered that the discrepancy in results was caused by a small hole in the shock tube end-plate. The small amount of gas in the hole was subjected to a stronger shock (due to the area contraction) than the surrounding gas. This small amount of gas actually reached the adiabatic ignition temperature, detonated, and then triggered the detonation of the surrounding gas. Hooker[75] found no discrepancy* with the adiabatic ignition temperature when using end-plate holes smaller than 1/32 inch in diameter or shorter than one hole diameter length.

Extensive studies on the density profile for detonation in mixtures of O_2, C_2H_2, and methyl bromide, as well as in stoichiometric mixtures of H_2 and O_2, have been carried out by Kistiakowsky and his collaborators,[20] who have used X-ray

* This conclusion is in agreement also with the results of unpublished observations made at Gottingen by Professor W. Jost and his collaborators.

measurements for the system $2H_2 - O_2$ (with X_e added to increase X-ray absorption) at initial pressures between 20 and 85 mm, Kistiakowsky found essentially no induction period; the duration of the reaction zones (identified as zones of high initial density) for steady detonation waves varied from about 2 to 20 μsec, changing roughly as the inverse square of the pressure. Gilkerson and Davidson[72] observed that the light output of the detonations was coincident with the shock front, within their instrumental rise time of 2 to 3 μsec. These results seem to be in rough agreement with Kistiakowsky's observations if suitable corrections are made for the difference in experimental conditions. The estimated upper limit for the thickness of the detonation front corresponds to completion of reaction in 10^3 to 10^4 collisions.

It seems unlikely that detailed studies of shock initiation of detonations will yield important fundamental information concerning ignition processes. On the other hand, carefully controlled experiments may contribute to our understanding of the transition from deflagration to detonation, which is one of the important unsolved problems in combustion.

PART II

EXPERIMENTAL STUDIES OF REACTIONS BEHIND SHOCKS

V. ON THE PRODUCTION OF CHEMICALS IN SHOCK TUBES

During the early stages of shock tube investigations, some unsuccessful attempts were made to develop an engine cycle for the production of a suitably selected chemical compound. We proceed to summarize relevant ideas and the preliminary results which led us to abandon the initial program on the production of hydrazine from ammonia. The failure to obtain any indication that hydrazine can be produced through a non-equilibrium reaction from ammonia simply indicates the difficulties which one should expect to find in a process depending on unknown timing requirements and on the hypothetical "freezing" of chemical intermediates which are presumed to form in measurable concentrations. On the other hand, the production of chemicals by "freezing" equilibrium components offers a hopeful method of approach for shock tube applications. This last technique, which is familiar from the technical production of NO from air by using pebble-bed chilling, is presumably being developed by A. Hertzberg and his collaborators who have studied the production of NO in the "chemical shock tube" (see Section IV A(1)).

High temperatures and pressures can be achieved by isentropic compression and by non-isentropic shock waves. Rapid cooling can be accomplished by isentropic steady expansion through a short de Laval nozzle or through an isentropic non-steady rarefaction wave. The use of these methods permits two possible manufacturing processes: (1) a gas turbine process using the steady compression and expansion in a turbocompressor and gas turbine combination; (2) a wave engine process using the compression and expansion generated

by shock waves and expansion waves.

A. A Gas Turbine Cycle*

The gas turbine process has been considered previously for the manufacture of nitric oxide from air.(76)

A schematic diagram of the suggested experimental arrangement is presented in figure 25. Air is first compressed by turbocompressors to about 20 atmospheres. The temperature of the compressed hot air is further increased by passing it through a heat exchanger connected to the turbine exhaust. The heated compressed air, which is at a temperature of about 1300°K, is used to burn added hydrocarbon fuel in the combustion chamber. With an optimum amount of fuel the temperature reaches 2500°K and the concentration of nitric oxide is somewhat greater than 2 °/o (see fig. 23).

The hot gas mixture can be cooled rapidly by expanding the gas through a short de Laval nozzle. If we use a constant specific heat for nitric oxide, namely, $\gamma = 1.3$, and assume a temperature ratio equal to 4, then the exit Mach number is 4.5. The flow speed at the entrance to the de Laval nozzle is very small and we may take an average flow speed through the nozzle of about 1500 ft/sec. Thus the time of passage of the gas through the four inch nozzle is 1/(3x1500) sec and the rate of cooling is 8.1×10^6 °K/sec. At the nozzle exit the gas is cool but it still has a high kinetic energy corresponding to high stagnation temperature.

---

* A more complete discussion of the gas turbine process applied to the production of nitric oxide will be found in reference 76.

By expanding the combustion products through the gas turbine, energy is extracted and transformed into mechanical energy, which may be utilized to drive the compressor (fig. 25) and, if there is a surplus of energy, to drive also an electric generator. Since it is of primary importance for NO production to have very rapid cooling, the first stage of the gas turbine should be of the impulse type so that the temperature of the gas can be immediately reduced to a low value, say 1600°K, in order to "freeze" the nitric oxide concentration after some losses at about 1 °/o. Thus the pressure ratio of the first impulse stage of the turbine should be approximately 8. The pressure of the gas behind the first stage is thus 2.5 atmospheres. The remainder of the stages of the turbine can be of the more efficient reaction type. The turbine exhaust gases are further cooled by passing through the heat exchanger. The result is a relatively cool gas containing about 1 °/o NO.

Present day aircraft turbojet engines have an air flow rate as high as 300 lbs per sec at ground level. A gas turbine of comparable size could thus process 13,000 tons of air a day. At 1 °/o nitric oxide production, this machine can produce 130 tons of NO per day, or 60 tons of fixed nitrogen per day. An important by-product of the gas turbine process is the surplus power generated. For a machine of the size indicated, the surplus power may be as high as 15,000 kw.

The conventional gas turbine fails to produce nitric oxide in appreciable concentrations simply because its combustion products do not reach sufficiently high temperatures and because the first stage of its turbine is of the reaction type, which cools the combustion products too slowly. Both of these design features introduce difficult engineering

problems such as cooling of the turbine nozzle and turbine blades. However, these problems do not seem insurmountable in the light of present knowledge of high temperature designs and high speed flows. In conclusion it is, however, important to note that the principal cost of NO production by this method will involve the cost of recovery of NO which is present at very low concentrations. Until far more efficient recovery processes are developed than are now available, commercial production of NO from a turbine cycle, even at concentrations as high as 2 $^{o}/o$, will not be competitive with other currently used methods.

B. A Wave Engine Cycle*

The shock tube can be used to study the production of chemicals utilizing shock waves and rarefaction waves. To demonstrate the application of a shock tube to a continuously operating cycle, we visualize a cylindrical tube with quick opening valves at both ends. Again we consider the production of nitric oxide.**

The sequence of events is sketched in figure 26. In figure 26(a) both ends of the tube are open with the left side of the tube connected to the low-pressure exhaust vessel and the right side of the tube connected to the fresh air supply. The fresh air is already heated to about 600^{o}K by passage through a heat exchanger. Fresh air at a low pressure (atmospheric) is flowing from right to left. The tube has now

---

* This term was given to a similar class of machines by A. Kantrowitz.[77] The Brown Boveri Co. of Switzerland is currently developing a power plant on this principle which they call the "Comprex".[78]

** It is important to note that, even though higher temperatures are available in a shock tube than in the gas turbine cycle, the maximum cooling rate eventually limits the yield.

been charged. When the fresh air reaches the left end of the tube, the valve at that end closes. The momentum of air will then produce a compression wave which travels towards the right. When this compression wave reaches the right end, the end valve closes. This compression process is shown in figure 26(b). When the right end valve closes, or even somewhat earlier, the left end valve is opened again, but this time connection is made with a high-pressure chamber. Then a strong shock is sent towards the right and compresses the fresh air charge in the tube to a very high pressure and temperature. This is shown in figure 26(c). When the shock wave reaches the closed right end valve, it is reflected, and the pressure and temperature of the gas behind the reflected shock are still higher [see figure 26(d)]. When the reflected shock is close to the left end of the tube, the left end of the tube is disconnected from the high-pressure source, connected again to the low-pressure exhaust vessel, and a strong expansion travels towards the right [see figure 26(e)]. When the expansion wave reaches the right end of the tube, the right end valve is opened and connected with the fresh air supply. The cycle is then completed.

Application of the shock tube to the continuous production of chemicals requires complicated valving and precise timing. However, the shock tube process has the advantage over the turbine process in that the tube is only subjected to the high temperatures intermittently. Thus, cooling of materials is greatly simplified. In addition, the shock tube process offers greater flexibility in temperature and pressure (versus time) cycles (see Section II) than the gas turbine process.

The valve cycling can be accomplished by mounting a number of

pipes (or shock tubes) radially around and parallel to a shaft which can be driven at a high velocity. The valving is done by appropriate port openings between the moving pipes and the stationary end compartments.

C. Remarks on the Production of Chemicals

The first step in a research program on the gas-dynamical production of chemicals requires the selection of promising reactions for shock-tube experiments. For preliminary experiments, a simple shock-tube arrangement (see Section II) is adequate. A. Hertzberg[43] has demonstrated that nitric oxide, a chemical which exists in appreciable concentrations in air at equilibrium, is produced in a shock tube. However, the wave engine process can be used also to produce chemicals which are not present at equilibrium. Non-equilibrium products, which might conceivably be "frozen" out of reacting gas mixtures, are hydrazine (N_2H_4) formed from ammonia (NH_3) and ethylene (C_2H_4) or acetylene (C_2H_2) formed from methane (CH_4).

Instrumentation of a shock tube for the study of reactions must, of course, permit the analysis of the progress of the chemical reaction. A monochromator, set at an appropriate wavelength region, can be used to follow the reaction with time. The experimental conditions should be varied systematically to yield a wide range of temperature (pressure) versus time histories. The approximate temperature versus time histories can be calculated theoretically by making use of the theory of characteristics. The results of a representative calculation for a "chemical shock tube" with a one foot driver section are given in figure 27. A comparison of the temperature cycle and the chemical production data obtained from the monochromator permits,

in principle, a theoretical analysis which should uncover the optimum conditions for the production of the desired chemical. The theoretical considerations may then be verified experimentally. The final step in the chemical production program is the design of a pilot plant, utilizing a properly selected cycle.

D. Preliminary Shock-Tube Experiments for the Production of Hydrazine*

Hydrazine offers attractive possibilities both as a fuel in bi-propellant rocket engines and as a monopropellant or a gas generant. The current production cost of hydrazine is about $2 per pound. For this reason, methods for producing hydrazine more cheaply are of obvious interest.

In the following paragraphs we describe unsuccessful attempts to produce hydrazine from ammonia in a shock tube. The initial work was handicapped by the lack of funds and equipment. The program was discontinued when we became convinced that only a remarkable stroke of luck could lead to a successful selection of useful operating conditions.

(1) Formation of Hydrazine from Ammonia

Hydrazine is produced commercially by combining chlorine and caustic in an excess of ammonia. A one percent yield of hydrazine results.

Devins and Burton[79] have recently conducted some basic research on the production of hydrazine in a glow discharge. The

---

* Anhydrous hydrazine freezes at 2°C, boils at 113.5°C at 760 mm, and has a heat of formation of 12 Kcal/mole.

fraction of NH_3 converted to N_2H_4 was found to be 0.02 °/o under optimum conditions and corresponds to the production of 30 g of N_2H_4 per kw. hr. at the cathode end of the discharge tube at a pressure of 5 mm of Hg, and a volume flow rate of 4.56 cc/sec at STP. The work by Devine and Burton[79] suggests that, under suitable non-equilibrium conditions, NH_3 can possibly be converted to N_2H_4. The particular experimental conditions required to produce N_2H_4 in a shock tube have to be determined experimentally.

The overall reaction is

$$4\,NH_3 + O_2 \longrightarrow 2\,N_2H_4 + 2\,H_2O\,. \qquad (13)$$

An excess of oxiding agent is necessary to reduce the ammonia and produce hydrazine. At high temperatures the ammonia reacts with the oxidizing agent and the reaction goes to completion forming water and nitrogen-oxygen compounds, but no hydrazine. At low temperatures, the ammonia does not react with oxygen. If the production of hydrazine in a shock tube is to be successful, one must hope that the NH_3 and O_2, which undergo complicated kinetic reactions, will produce N_2H_4 in sufficient amounts to make quenching effective for the production of N_2H_4.

(2) Apparatus for the Production of Hydrazine in a Shock Tube

A one inch diameter "chemical shock tube", utilizing two diaphragms and a vacuum chamber (see fig. 28), was designed and constructed to give maximum flexibility of flow conditions and time-temperature histories (see figs. 8 and 9). The metal sections were stainless steel with O-ring seals. The low-pressure section was primarily pyrex tubing (fig. 28). The pyrex tubing withstood 100 psia

static pressure safely, and, on occasion, could be taken to 300 psia static pressure without failure; most failures seemed to be due to fatigue rather than to the impulsive loading of the shock wave. The lengths of the driver section and of the low-pressure pyrex section could be varied in one foot increments. The upstream vacuum chamber had a volume of 10 ft^3.

The low-pressure gas handling system is represented schematically in figure 29. It consisted of a manifold, a two-stage cold trap, and locations for tapping samples of the gas from the shock tube into vacuum-tight flasks. In order to insure adequate mixing of the NH_3 and O_2 under pressure, it was necessary to stir the mixture by shaking a large number of glass beads in the mixing vessel. This mixture was then allowed to stand for at least 12 hours before performing the experiment.

(3) The Double-Diaphragm Breaking Mechanism

Accurate control of the time-delay between diaphragm breakings is essential if the full flexibility of a "chemical shock tube" is to be utilized.

Hertzberg[43] used powerful, precisely controlled, plungers to pierce 0.020 inch thick, hardened, aluminum sheet in a 3 inch shock tube. To drive the plungers with the proper time-delay, an auxiliary shock tube was used. The shock generated by the auxiliary shock tube was divided and was made to travel through two variable-length branches to drive the two plungers at the end of each branch. The time-delay was determined by the difference in length of the two branches. The apparatus gave delays accurate to within 0.1 millisecond.*

* The quoted time-delay accuracy refers to the difference in time of contact of the two plungers with their respective diaphragms.

An electronic method of puncturing two diaphragms at a known time interval was developed to improve upon the inherent inertial uncertainty of a mechanical system. The system utilized an electronic delay line and a concentrated, high energy, discharge which burned a hole in the metal diaphragm.

The electronic delay circuit was both accurate and flexible. The closure of a switch applied a 270 volt signal to one thyratron grid directly and to a second thyratron grid through an L-C delay-line and pulse transformer (fig. 30). The delay-time could be varied in 20 μ sec increments from 240 μ sec to 680 μ sec. The experimental uncertainty in the thyratron discharge time was less than one microsecond.

The high energies were handled with maximum safety. Two 1.5μ fd capacitors charged to 10,000 volts supplied the energy required to burn the holes in the diaphragms. The high-voltage terminal of each capacitor was connected to the plate of its respective thyratron (see fig. 30). A 10 volt positive signal applied to the grid of the PL-5C22 thyratron caused it to discharge and to ground instantaneously the high voltage side of the capacitor. At this time the stored charge on the ground side of the capacitor saw a high inductive load to ground and, as a result, jumped the small gap to the diaphragm. The high energy discharge burned a hole in the copper diaphragm. This electronic arrangement made it possible for the shock tube to be at ground potential at all times.

The spark gap was located in the high-pressure section of the shock tube to avoid collision with the highly destructive breaking copper diaphragm and also to avoid an electrical discharge in the low-

pressure, reactive, gas sample.

The spark gap section of the shock tube is shown in figure 31. The high-voltage lead entered the high-pressure section of the shock tube through a lucite rod, which shielded the conducting center rod from the shock tube. A threaded 1 $\frac{1}{2}$ mm spark probe was suspended on the axis of the shock tube by a thin cantilever spring which protruded from the conducting center rod (fig. 31). The end of the spark probe was filed down to a sharp point to facilitate the spark discharge. A nozzle was used to confine the electrical energy to a small portion of the diaphragm (fig. 31). An unconfined electric discharge from the spark probe tended to spread out over an area on the diaphragm described by a circle 8 mm in diameter. Without confinement, the copper diaphragm was only heated, and no reliable diaphragm rupture resulted. A nozzle (see detail in fig. 31) was used to concentrate the energy released from the spark probe. The minimum constriction was 0.16 mm. The nozzle was made from micolite which stood up very well under the experimental conditions.

The reliability of the nozzle-spark probe arrangement depended upon both the energy release and upon the separation between the spark probe point and the diaphragm surface. Larger holes were burned with larger energies. Thus, using a 2 mil half-hard copper diaphragm and a 1.5 μ fd capacitor, the following results were observed: no hole at 17 kv without nozzle, 5 mm hole at 10 kv with nozzle, 2 mm hole at 7.5 kv with nozzle, no hole at 5 kv with nozzle. In addition, it was found that the maximum size hole was obtained when the spark probe point was backed away from the diaphragm surface by seven

turns of a 0-80 thread (see detail, fig. 31). The thin, protruding, cantilever spring forced the nozzle lightly against the diaphragm as it expanded under pressure and the nozzle spaced the probe correctly from the diaphragm surface.

This electronic delay circuit and high-energy discharge produced holes in the diaphragms at time intervals predictable to within less than two microseconds. Thus an improvement of several orders of magnitude was obtained over the mechanical system developed by Hertzberg.[43]

The greatest uncertainty in establishing known flow conditions arose from non-uniform diaphragm rupture. The magnitude of this effect was determined qualitatively by using zero delay time between the discharge of the two capacitors (see fig. 30) so that the two holes were burned in the diaphragms within at least one microsecond. The high-pressure section for this experiment was two feet long. Barium titanate crystals were located in the tube twenty diameter lengths (i.e., 20 inches) downstream from each diaphragm to determine the time of arrival of each shock. The trigger to the thyratron tube was delayed a millisecond and then triggered a Du Mont dual-beam scope. The two mil copper diaphragms were stressed to 100 psi (their breaking pressure was 110 psi). During twenty trials, the two shocks arrived only twice at the same distance as much as a one hundred μsec apart. In all other cases the time difference was less than 50 μsec. The 50 μ sec time difference was attributed to the non-uniform opening of the two diaphragms.

The method described above for breaking two diaphragms at a predetermined time interval can be extended to shock tubes of larger

I. D. than one inch. However, as the thickness of the diaphragm increases, the necessary energy requirements increase rapidly.

(4) Experimental Results

To determine if hydrazine could be formed in a shock tube, the experimental conditions were varied systematically over a wide range. On the completion of each run, a sample of the low-pressure gas was drawn from the end-plate of the downstream section of the shock tube (fig. 28, "detail B"). Both a qualitative chemical test and a quantitative mass spectrographic analysis were made on each gas sample.

(i) Selenium Oxychloride Chemical Test

The presence of N_2H_4 causes a bright red precipitate to form in a warm solution of selenium oxychlorde and 10 °/o HCl. This test is positive for concentrations of N_2H_4 corresponding to 1 ppm of solvent (or roughly to 50 ppm for the entire mixture).

This chemical test gave non-positive results for all fifteen gas samples.

(ii) Mass-Spectrographic Analysis

The mass spectrographic analyses were generously made by the Union Oil Company. Unfortunately, the gas samples were generally not analyzed until at least one week after the experiment had been performed.

Fifteen gas samples drawn from the shock tube were analyzed and compared with a control sample. The gas samples yielded concentrations of N_2H_4 running from 47 ppm to 81 ppm $\pm$ 20 ppm. The blank was reported to contain 36 ppm $\pm$ 20 ppm of hydrazine. These results show that no positive evidence was obtained for the production of N_2H_4 in significant amounts from NH_3.

VI. CARBON FORMATION BEHIND REFLECTED SHOCK FRONTS

Optical techniques are the primary tools which are available for the study of fast chemical reactions in shock tubes. In spite of strong emphasis on shock-tube research in recent years, refinement of optical measurements behind shock fronts is necessary before many useful studies on the production of chemicals in shock tubes can be carried out.

The development of optical techniques reported in this thesis represents the beginning of a long-range program on the study of carbon formation from acetylene. The pyrolysis of hydrocarbons to form carbon is of fundamental interest. Also carbon formation is of practical importance in a variety of propulsion applications. The thermal decomposition of hydrocarbons involves intense emitted light, the formation and growth of carbon particles, and perhaps measurable ionization. The mechanism of pyrolysis is as yet incompletely understood.

The pyrolysis of acetylene is an interesting problem suitable for study by shock-tube techniques. The production of acetylene from methane has commercial possibilities. Mass spectrometric analyses of the gaseous products formed during pyrolysis of hydrocarbons always indicate the presence of large amounts of acetylene.

One of the theories of carbon formation from hydrocarbons, advanced particularly by G. Porter,[80] involves the assumption that carbon formation is always preceded by the production of acetylene, viz., "The thermal decomposition of hydrocarbons results

in dehydrogenation and cracking to smaller molecules and the last stable hydrocarbon to be observed before carbon formation is acetylene". The shock tube offers a unique tool for preparing acetylene, under uniform conditions, at high temperatures where the decomposition rates may be studied conveniently.

The following topics will be considered in subsequent sections: calculation of gas properties behind shocks, prior to chemical reaction (Section VI A); minimum time at peak temperature behind a reflected shock (Section VI B); apparatus and experimental procedure (Section VI C); determination of the minimum pressure ratio required for carbon formation (Section VI D); simultaneous light absorption and emission measurements behind carbon-forming shocks (Section VI E); induction period experiments (Section VI F); the two-color method of temperature measurement behind carbon-forming shocks (Section VI G).

A. Calculation of Gas Properties Behind Shocks, Prior to Chemical Reaction

In order to plan and interpret shock-tube experiments, the state of the gas must be determined prior to the occurrence of chemical reaction. The equations for incident and reflected shocks, for the case of complete thermal equilibrium, will be presented. The results of equilibrium calculations for four hydrocarbons (methane, acteylene, benzene, and n-heptane) are given. The results of similar calculations, assuming constant specific heats for the gases, can be found in the literature.[4, 5] Finally, the effects of the interaction of the reflected shock with the contact surface will be discussed briefly.

The following assumptions are made to develop the normal shock equations for the case of complete thermal equilibrium:

(1) The shock tube has a uniform cross-section (figure 1).

(2) The gases obey the ideal gas law.

(3) The viscous and heat conduction effects of a real fluid are confined to the narrow region of the shock wave (i.e., there is no boundary layer and the flow may be considered to be one-dimensional).

(4) There is no radiative or conductive heat loss from the gas.

(5) There are no body forces.

(6) The internal relaxation times are short compared with the times necessary for chemical reactions, i.e., the gas is assumed to be in thermal equilibrium before chemical reactions occur.

The conditions behind a shock front are determined by applying these assumptions to the conservation equations in a coordinate system fixed with respect to the shock wave. The equation for conservation of mass becomes

$$\rho_1 v_1 = \rho_2 v_2 \quad . \tag{14}$$

The condition for conservation of momentum is

$$p_1 + \rho_1 v_1^2 = p_2 + \rho_2 v_2^2 \quad . \tag{15}$$

The relation for conservation of energy can be written as

$$h_1 + \frac{v_1^2}{2} = h_2 + \frac{v_2^2}{2} \quad . \tag{16}$$

For ideal gases, the equation of state is

$$p = \rho R_g T \quad . \tag{17}$$

The preceding equations can be solved for the temperature ratio $\frac{T_2}{T_1}$ and for the velocity of the gas behind the incident shock relative to the shock wave, v_2. The results are*

$$\frac{T_2}{T_1} = -\sqrt{v_1^2 + 2\,(h_1 - h_2)}\,\left(\frac{1}{v_1} + \frac{v_1}{R_g T_1}\right) - \frac{v_1^2 + 2(h_1 - h_2)}{R_g T_1} \quad , \tag{18}$$

and

$$v_2 = -\sqrt{v^2 - 2\,(h_1 - h_2)} \quad , \tag{19}$$

where

$$u_2 = -\,(v_1 - v_2) > 0$$

The values of the specific enthalpy for a wide range of hydrocarbons, as a function of temperature, are given in the literature.[82, 83] The shock velocity $u_s = -\,v_1$ can be computed from equation 18 for various values of T_1 and T_2 by using tabulated data for h_1 and h_2.

---

* For details see reference 81.

The conditions behind the reflected shock can be determined by applying equations 14 through 17 in a coordinate system fixed with respect to the reflected shock. The value of the temperature T_5 behind the reflected shock may be determined from relation*

$$T_5 = \left\{(h_5 - h_2) - \frac{(v_1 - v_2)^2}{2}\right\} \left\{\frac{T_2}{(h_5 - h_2) + \frac{(v_1 - v_2)^2}{2}} + \frac{1}{R_g}\right\} . \quad (20)$$

Equation 20 must be solved for T_5 by an iteration procedure using the data for h_5 given in the literature.[82, 83] The velocity of the reflected shock may be computed from the relation

$$u_{sr} = \frac{h_5 - h_2}{v_1 - v_2} + \frac{v_1 - v_2}{2} . \quad (21)$$

The pressure ratio across the incident shock can be calculated by making use of equations 14 and 17. The pressure ratio is found to be

$$\frac{p_2}{p_1} = \frac{v_1 T_2}{v_2 T_1} \quad (22)$$

when R_g is assumed to be constant. A similar relation may be obtained for the pressure ratio p_5/p_2 across the reflected shock. The product of the pressure ratios across the incident and the reflected shocks, p_5/p_1, is given by

---

* For details see reference 81.

$$\frac{p_5}{p_1} = \frac{p_5}{p_2}\,\frac{p_2}{p_1} = \frac{(h_5 - h_2) + \dfrac{(v_1 - v_2)^2}{2}}{(h_5 - h_2) - \dfrac{(v_1 - v_2)^2}{2}} \cdot \frac{v_1}{v_2} \cdot \frac{T_5}{T_1} \quad . \quad (23)$$

The initial pressure ratio across the diaphragm may be determined from the computed velocity of the gas behind the incident shock u_2. For a backward-facing rarefaction wave (in a gas of constant specific heat such as helium) the relation

$$u_3 + \frac{2}{\gamma_4 - 1}\, a_3 = \frac{2}{\gamma_4 - 1}\, a_4 = \text{constant} \qquad (24)$$

holds, where $\underline{a}$ is the local velocity of sound and γ_4 refers to the specific heat ratio for the gas initially in region 4.

The pressures are related to the local sound velocity for isentropic processes by the relation

$$\frac{p_4}{p_3} = \left(\frac{a_4}{a_3}\right)^{\frac{2\gamma_4}{\gamma_4 - 1}} \quad . \qquad (25)$$

Solving equation 24 for a_4/a_3 in terms of u_3/a_4 and substituting the results into equation 25, we obtain

$$\frac{p_4}{p_3} = \left(1 - \frac{\gamma_4 - 1}{2} \cdot \frac{u_3}{a_4}\right)^{-\frac{2\gamma_4}{\gamma_4 - 1}} \quad .$$

The boundary conditions between region 2 and region 3 (see Section II) are that $p_3 = p_2$ and $u_3 = u_2$. Thus the initial pressure ratio across the diaphragm can be related to the resulting shock pressure ratio p_2/p_1 through the relation

$$\frac{p_4}{p_1} = \frac{p_2}{p_1}\left(1 - \frac{\gamma_4 - 1}{2} \cdot \frac{u_2}{a_4}\right)^{-\frac{2\gamma_4}{\gamma_4 - 1}} . \quad (26)$$

Computations using the foregoing equations have been made for shocks traveling through methane, acetylene, benzene, and n-heptane. The values of p_4/p_1, T_2/T_1, u_2/a_1, u_{sr}/a_1, p_2/p_1, and p_5/p_1 have been plotted against the initial shock Mach number (u_s/a_1) for each of the four gases in figures 32 to 47.

The experimental results reported in this Section VI deal exclusively with studies using helium as the driver gas and acetylene as the driven gas. Preliminary experiments with other driven gases required much greater initial pressure ratios for carbon formation. Thus, in order to pyrolyze pure methane, initial pressure ratios p_4/p_1 of the order of several thousand were found to be necessary.

B. The Minimum Time at Peak Temperature Behind a Reflected Shock

The time at peak temperature (for a fixed geometry) is limited either by the arrival of the rarefaction wave or of a reflected wave associated with the interaction of the reflected shock and the contact surface (see Section II B (4)).

In the following paragraphs the calculations which are necessary to determine the minimum time at peak temperature behind the reflected shock, the position of closest approach of the contact surface, and the time of arrival of the rarefaction wave will be discussed.

In figure 48 is shown a schematic drawing of the complex interactions which we wish to consider in detail. For the moment, it is assumed that the reflected rarefaction wave does not arrive until

long after the experiment has been completed. The time at which the reflected shock interacts with the contact discontinuity t_c is easily determined to be

$$t_c = \frac{x_c}{u_2} = \frac{x_e}{u_s} + \frac{x_e - x_c}{u_{sr}} \quad .$$

The preceding equation can be solved for t_c and x_c in terms of the calculated shock parameters. The results are easily expressed in non-dimensional form, viz.,

$$\frac{x_c}{x_e} = \frac{u_s + u_{sr}}{u_2 + u_{sr}} \cdot \frac{u_2}{u_s} \tag{27}$$

and

$$\frac{t_c a_1}{x_e} = \frac{a_1}{u_s} \cdot \frac{u_s + u_{sr}}{u_2 + u_{sr}} \quad . \tag{28}$$

Observations behind the reflected shock wave have to be made in the region between the contact surface and the end of the tube (x_e). In figure 49 is plotted the ratio $(x_e - x_c)/x_e$ versus the initial shock Mach number for the case of acetylene using an equilibrium value for γ . A conservative estimate can be made for the length of time the gas (region 5) is at T_5 by estimating the time interval between the passage of the reflected shock at the observation window (t_o) and the intersection of the reflected shock with the contact surface. If the observation window is placed at the end of the tube (x_e), then the maximum conservative estimate for the time available for observation at the uniform temperature T_5 is given by $(t_c - t_e)$. The relation

$(t_c - t_e)/x_e$ is plotted in figure 50 as a function of the initial shock Mach number for acetylene, again using an equilibrium value for γ. The dimensional ratio is plotted against Mach number in figure 50 in order to emphasize the fact that the calculation applies only for acetylene and for the case of equilibrium heat capacity ratio.

Times and distances computed from equations 27 and 28 are significant only if the time t_r required before the first reflected rarefaction wave intersects the contact surface is longer than t_c. The time t_r can be expressed analytically as a function of the design variables by using ideal shock-tube theory. The result is given, for example, in reference 84 and is, in our notation,

$$\frac{t_r\, a_4}{x_\ell} = 2\left(\frac{p_4/p_1}{p_2/p_1}\right)^{\frac{\gamma_4 + 1}{4\gamma_4}} \tag{29}$$

where x_ℓ is the length of the high-pressure section of the shock tube. A non-dimensional plot of equation 29, for different but constant values of γ will be found in figure 51.

For experiments on the determination of the threshold temperatures and pressures necessary for carbon formation (Section VI D), as well as in experiments for the determination of the induction time before the onset of carbon formation (Section VI F), it is important to note that the temperatures T_5 and pressures p_5 represent the maximum temperatures and pressures to which the acetylene is subjected. An upper limit can be computed for the temperature rise associated with the shock reflected from the contact surface, for the incident shock strengths employed in our experiments,

by using an equilibrium value of γ (see reference 81) and the theory of characteristics.[3-5] The results of such a calculation for the three experimental conditions most often employed in the carbon formation experiments are listed in table II. The temperature rise from region 5 to region 6, associated with an incident shock Mach number of 4.3, is 30°K (see table II).

It is interesting to note that the gas in region 6 is moving toward the end of the tube with a sizable velocity (see table II). Thus the contact surface, even in ideal shock-tube theory, does get closer to the end of the tube than one would predict from equation 27.

Actually the flow in region 6 is very turbulent, as is verified by schlieren studies of this region;[84] therefore, the results given in table II cannot be taken literally. The turbulence is created by interaction of the shock with the contact surface which is no longer a discontinuity but a broad region with steep gradients of temperature and composition (see the schlieren pictures showing the growth of the contact surface given in reference 84). Interpretation of chemical reactions which take place in region 6 is complicated by the presence of this turbulence (see Section VI H(5)). For instance, experiments of other investigators show that the theoretical values of $(x_e - x_c)$ and $(t_c - t_e)$ may be reduced by a factor of two for very strong shocks.

C. Apparatus and Experimental Procedure

The apparatus and the experimental procedure used will now be discussed. Specialized instrumentation will be described in conjunction with appropriate experiments.

(1) The Shock Tube

Two shock tubes were used in the course of the carbon formation experiments.

A one inch I.D. stainless steel shock tube, which had been used for experiments on the production of chemicals, was modified for preliminary spectral studies of carbon formation. The two diaphragm-breaking sections (see figure 31) were redesigned to hold pressure pickups (utilizing barium titanate crystals) for shock velocity measurements. Optical measurements were made through a fused quartz tube section two inches long and with a 1/4 inch wall thickness. A screw plunger was used to break the half-hard copper diaphragms at known pressures.

The small shock tube was not used in the final experiments. The one inch internal dimension limited the optical path and, in addition, measurable shock velocity attenuation was observed for incident shock Mach numbers of three or greater.

A three inch diameter shock tube was designed and constructed out of cold-drawn steel tubing. Pressure and vacuum seals between flanged tube sections were made with neoprene O-rings. A carbon steel structure, thirty-two inches high, twenty-four inches wide, and bolted to the laboratory floor, served as a rigid support for the tube.

The length of the downstream section could be varied from five feet to over forty feet in one foot steps. The low-pressure section had a wall thickness of 1/8 inch. Observation windows or transducers could be mounted in any of three pairs of one inch circular openings in the side of the tube. An over-sized nut held either the window or the

transducer against an O-ring seal. The window material was either glass or lucite. The distance between two stations could be made as small as one foot. An additional shock tube section was fitted to hold and seal a pair of 1/4 inch thick optically-clear sapphire windows which could be used for observations out to six microns in the infrared. The end of the low-pressure section was sealed with a quickly opening, coarsely threaded, plug. The length of a tightly fitting plunger inserted in the end of the shock tube before each run determined the distance between the last observation window and the end of the tube. In most of the carbon-forming experiments reported here, the distance between the center of the last observation station and the end of the tube was 9/16 inch.

The high-pressure sections had wall thicknesses of 1/4 inch and were hydraulically tested to 1800 psi. The length of the high-pressure section could be varied from one to seven feet in one foot increments. A screw-plunger, whose axis coincided with the shock-tube axis, was used to break the stressed half-hard copper diaphragms at the correct pressure (see figure 52). The high-pressure section rested on roller bearings so that the tube could be easily separated for cleaning and changing of the diaphragms.

(2) Gas-Handling System

The gas supply to the low-pressure section of the shock tube was handled with a six-valve manifold. Commercial acetylene was used as the driven gas. The absolute pressure of the low-pressure gas was measured with a Wallace and Tiernan mercury manometer which could be read to 0.2 mm Hg.

The gas supply to the high-pressure section of the shock tube was handled with a three-valve manifold. Commercial grade helium was used as the driver gas. The pressure in the high-pressure section was measured with a calibrated Bourdon gauge which could be read to one psi.

A Kinney high-capacity vacuum pump, capable of reducing the pressure to 0.01 mm of mercury (absolute), was used to evacuate both high- and low-pressure sections of the shock tube before admitting the gas.

The diaphragm material was 0.003 or 0.005 inch half-hard copper shim stock and was used in one or more thicknesses.

(3) Shock-Velocity Measurements

Barium titanate pressure pick-ups (see Section III A) were used as triggers to determine the shock velocity. The pressure pick-ups were designed so that there was some degree of isolation between the pick-up and the shock tube wall. In spite of this precaution, tube ringing associated with the rupture of the diaphragm caused a measurable output signal preceding the arrival of the shock. When p_4 was increased significantly above 300 psi (with $p_1 \sim$ 1 psia), the tube ringing which preceded the arrival of the shock resulted in a signal level which was comparable to the signal caused by the incident shock. In order to avoid these troubles and to improve the accuracy of the shock velocity measurements, a schlieren system trigger is now under construction (see Section III B(3)). In the meantime, no experiments were conducted with $p_4 >$ 300 psi.

The barium titanate crystals, used in the velocity-triggering

system, were circular wafers 1/2 inch in diameter, 1/8 inch thick, with the sensitive surface perpendicular to the 1/2 inch dimension. A shock wave traveling at 4000 ft/sec requires 10 μ sec to go a distance of 1/2 inch. The experimentally determined rise-time for these pressure pick-ups varied between 5 and 10 μ sec for shock strengths of this magnitude. The rise-time of these pressure pick-up pulses leads to a maximum uncertainty of $\pm$ 2 % in the shock-velocity measurement. The maximum variation in the measured shock velocity for uniform initial conditions was $\pm$ 1.3 %.

It is interesting to make a rough estimate of the variation in shock velocity that would be predicted from the uncertainty in the measurement of the initial pressure ratio across the diaphragm. The initial pressure ratio p_4/p_1 was measured to about one percent. In figure 32 is shown the pressure ratio p_4/p_1 as a function of the incident shock Mach number for an equilibrium value of γ. A one percent variation in p_4/p_1 leads to approximately a $\pm$ 1/3 % variation in the shock velocity.

In practice, the shock velocity pick-ups were mounted two feet apart. The center of the second pressure pick-up was located directly opposite the observation window and was, as stated previously, located 9/16 inch from the end of the shock tube.

The incident shock velocity was measured by sending the output of the pressure pick-ups directly to a Berkeley Universal Electronic Counter and Timer, Model 5510. A sudden pressure rise of five or ten psi yielded about a one volt output, which was sufficient to start or stop the counter. The velocity was determined by dividing

the distance between the two pick-ups (2 feet) by the displayed counter time.

The velocity-measuring system was tested for accuracy before each set of new runs by displaying simultaneously the output from the two pressure pick-ups on one scope trace and by displaying the counter gate signal output on a second scope trace. The velocity-measuring system was working correctly if the counter gate signal coincided with the pressure pick-up signals associated with the passage of the shock at the two stations.

The average measured shock velocity was 3.3 $^{o}/o$ below the value which would be predicted from the initial pressure ratio across the diaphragm using ideal shock-tube theory and an equilibrium value of γ .

The signal from the last pressure pick-up, which was produced by the reflected shock, was at least three times as large as the signal associated with the incident shock. This signal was used to trigger the oscilloscope sweeps when observations were being made behind the reflected shock.

(4) Auxiliary Equipment

Two oscilloscopes were used: a Tektronix, Type 535, with a 53C plug-in preamplifier and a Tektronix, Type 513D. The oscilloscope traces were photographed by using Polaroid Land Cameras, Type 2620.

A Jarrel - Ash Model 8200 scanning monochromator was used for spectroscopic studies. This instrument has an Ebert mounting, a suitable photomultiplier tube behind the exit slit, and a Leeds and

Northrup recorder and high-voltage power supply for the phototube. The scanning range is 2000 to 8000 Å. A 52 x 52 mm grating ruled at 1200 lines per mm gives a dispersion of 16 Å in the first order at the plane of the exit slit.

In all experiments the monochromator was operated with a 20 micron entrance slit and an exit slit which was about three millimeters in width.

The interference filters used in two-color temperature measurements were purchased from the Baird Company and had a one-half pass band width of 70 Å. Thus, the spectral region observed both by the monochromator (50 Å) and by the interference filters (70 Å) were of comparable size.

D. Determination of the Minimum Pressure Ratio Required for Carbon Formation

Preliminary experiments of carbon formation from acetylene using the one-inch shock tube revealed three interesting results: (1) there exists a well-defined threshold condition which just causes carbon formation; the density of the carbon deposits changes from "very light" to "very heavy" with only a small increase in the initial pressure ratio; (2) the formation of detectable amounts of carbon is accompanied by the intense emission of light in the visible spectrum; (3) the narrowly defined threshold limits can be modified by changing the length of the shock tube. This last result suggests that there is an induction period (a definite time at the temperature T_5) associated with the onset of carbon formation.

Bennett[81] used the three-inch shock tube to study quantitatively

the minimum pressure ratio required for carbon formation in both acetylene and acetylene-argon mixtures. A simple optical technique, utilizing light absorption by solid carbon particles, was used to detect carbon formation. A beam of light was directed through two windows at the end of the shock tube onto the sensitive portion of a 931-A photomultiplier tube. The photomultiplier output was observed before the experiment and immediately after the cessation of any strong emission. A decrease in photomultiplier output always correlated (visually) with the formation of carbon.

The use of a photomultiplier made it possible to determine qualitatively the degree of carbon formation. Bennett found that, at the threshold level for carbon formation, a change of 2 $^{o}/_{o}$ to 5 $^{o}/_{o}$ in the initial pressure ratio caused a carbon deposit density change from "very light" to "very heavy".

Our experiments showed that intense emitted light invariably accompanies carbon formation. In Section VI E we discuss experiments which verify the fact that the onset of light emission and the onset of carbon formation coincide (to within the several μ sec limit of experimental error).

Bennett[81] made rough calculations of the temperature rise which would be associated with the exothermic reaction

$$C_2H_2\,(g) \longrightarrow 2\,C(s) + H_2(g) \qquad (30)$$

for various assumed models of excitation of the internal degrees of freedom. By comparing the results of these calculations with the temperature measurements (see Section VI G) for equivalent shock

strengths he was able to show that the effective specific heat ratio probably approaches the equilibrium value.

E. Simultaneous Light Absorption and Emission Measurements Behind Carbon-Forming Shocks

Absorption measurements behind carbon-forming shocks are complicated because of the intense emitted radiation associated with the chemical reaction. A method for distinguishing between the transmitted and absorbed light has been developed which is suitable for studies of the rate of carbon-formation.

The emitted light may be separated from the transmitted light by the use of two carefully matched photomultiplier tubes.* One photocell is used to observe both the transmitted and the emitted light through a suitable slit system. The second photocell is used to observe only the emitted light in a narrowly defined region adjacent to that observed by the first photocell. The transmitted light component is calculated by subtracting the output of the second photocell from that of the first photocell.

Another method of measuring the transmitted light involves the use of chopped transmitted light and one photomultiplier tube (see fig. 53). The envelope of the chopped photocell signal can be distinguished easily from the emitted (unchopped) photocell signal. However, the chopping rate places an upper limit on the rates of reaction

---

* Experiments of this type were carried out by Mr. W. J. Hooker at the General Electric Company in Schenectady, New York.

that can be studied. A Kerr cell* using nitrobenzene can be used to modulate the light at frequencies greater than 10 megacycles without appreciable attenuation. Thus, a Kerr cell operating as a shutter can be used to modulate the transmitted light to make simultaneous absorption and emission measurements behind shocks.

A series of experiments was conducted to determine the usefulness of a Kerr cell as a light chopper and also to determine what relation existed between the intense emitted light behind carbon-forming shocks in acetylene and absorption of radiation by carbon. A schematic drawing of the experimental arrangement is shown in figure 53.

The minimum time-delay between the trigger signal from the shock tube and the operation of the Kerr cell - light source combination** was of the order of one millisecond. The amplified signal from a barium titanate crystal, which was taped to the outside of the shock-tube wall close to the diaphragm, served as a reliable trigger for these experiments.

The light source was a General Electric Type 524 xenon lamp. A 240 μfd capacitor charged to 4000 volts was discharged through a thyratron tube and through the xenon lamp so that its peak radiation corresponded in time to the onset of carbon-formation. Operated in this fashion, the lamp had a peak radiation lasting 400 microseconds and a peak intensity of more than 50 million lumens.

---

* This use of the Kerr cell was suggested by Dr. N. Davidson.

** The author is indebted to Dr. A. T. Ellis for the use of his Kerr cell and power supplies.

The modulating circuit was originally designed by A. Ellis to operate a Kerr cell as a shutter for a very high-speed camera. The modulating circuit applied a 14.5 kilovolt signal to the plates of the Kerr cell for one-tenth of a microsecond. The repetition rate of these pulses could be varied continuously over a wide range. For the Kerr-cell experiments discussed here, the repetition rate was set at either 250 or 1000 kilocycles per second.

The light from the xenon lamp was directed through the Kerr cell, the windows W in the end of the shock tube, and then onto the sensitive surface of a photocell (see fig. 53). A 95 ohm load resistor was used with the photomultiplier tube to give a fast response-time to the circuit. The photocell output was displayed on the scope and photographed.

Drawings of the actual scope trace records for two experiments may be found in figures 54 and 55. The experiment represented by figure 54 was carried out with an initial pressure ratio of 1100 and an initial downstream pressure p_1 equal to 10 mm Hg (absolute). The Kerr-cell repetition rate was 250 kilocycles per second. The initial pressure ratio p_4/p_1 for the experiment represented by figure 55 was 720, the initial low pressure p_1 was 15 mm Hg (absolute), and the repetition rate was one megacycle.

The portion of the trace to the left of the vertical dashed line aa represents the photocell output preceding the onset of either carbon formation or of light emission.

The lower heavy solid line to the left of the vertical dashed line aa represents a zero DC photocell output. The difference

between the upper envelope and the lower heavy solid line represents the chopped light which is transmitted through the shock tube at any instant of time.

The region of interest lies between the dashed vertical line aa and the solid vertical line bb in the trace reproduction. Light emission begins at the vertical line aa, as can be seen from the increase in the DC level of the photocell output (lower heavy solid line). The transmitted component of the light (the difference between the upper envelope and the lower solid line) begins to decrease at the onset of emission. Thus it seems plausible to conclude that carbon formation occurs simultaneously with light emission within the error of several microseconds of reading the photographic record.

A decrease in the total light flux, following the onset of carbon formation, is shown in figure 55. The explanation is obvious: the formation of carbon during the early stage of the experiment leads to absorption of light and a greater reduction in intensity than corresponds to the emitted radiation during the initial phases of the chemical reaction.

The use of extremely bright light sources and low initial densities of acetylene makes it possible to observe a small component of the transmitted (AC) signal throughout the duration of the experiment. If the experiment is conducted in this manner, a measure of the percentage of light absorption can be obtained.

Another experiment using the Kerr cell as a light chopper illustrates the necessity for using intense light sources. In connection with the two-color temperature measurements (see Section VI H(4)),

it was necessary to observe emitted light simultaneously at two wavelengths. An attempt was made to chop one beam of filtered light and then to focus both the modulated and the unmodulated signals on one photocell. The filter reduced the light incident on the photomultiplier tube by several orders of magnitude. As a result, the electronic noise associated with the Kerr cell electronics obscured the modulated light signal.

Our experiments demonstrate that a Kerr cell can be used to make simultaneous light absorption and emission measurements. A simultaneous spectral study of the emitted and absorbed light can also be obtained if the source light and emitted radiation are sufficiently intense.

F. Induction Period Experiments

As has been stated previously, carbon formation occurs under well-defined conditions of temperature and pressure. When the high-pressure section of the shock tube was lengthened, under otherwise constant conditions, a different set of threshold values for carbon formation was found. The new threshold values were, in all cases, below the threshold values determined by experiments using shorter driver sections. The effect of lengthening of the driver section is to increase the distance which the head of the rarefaction wave (F) has to travel before it reaches the end of the tube. Increasing the length of the high-pressure section, therefore, increases the length of time spent by the gas behind the reflected shock at the high temperature T_5. These crude experiments establish the obvious fact that there is an induction period associated with the formation of carbon from

acetylene in a shock tube.

The induction period is defined here as the length of time during which the gas is subjected to the high temperature behind the reflected shock before carbon just begins to form. A barium titanate pressure pick-up mounted directly opposite to the observation window in the three-inch shock tube was used to trigger the scope sweep when the reflected shock passed. The Kerr cell light absorption experiments (Section VI E) showed that the onset of carbon formation is accompanied (within several microseconds) by light emission. The induction time was determined by measuring the distance between the start of the scope sweep and the onset of intense emission as shown by a photocell output. The output rise-time of the titanate pressure pick-up (for the reflected shock) was found to vary between 20 and 30 μ sec. Thus the scope sweep trigger coincides with the passage of the shock to no better than $\pm$ 10 μ sec. The photomultiplier tube detected light which originated from a several mm wide region of the observation window, as defined by a narrow slit system. A possible source of confusion arose from an uncertain interpretation of the two types of emission which were observed. Strong shocks, which gave temperatures well above the threshold values, caused the radiation to increase more or less rapidly until a peak value was reached. Shocks, which created temperatures only slightly above the threshold value, were followed by radiant energy emission which increased very slowly with time (and then, in some cases, decreased) before rapidly increasing to some peak value in the manner described for stronger shocks. The time between the first detectable signs of light

emission and the rapid increase of light emission for the weaker shocks was often longer than one hundred microseconds.

The computed pressures p_5 and the computed temperatures T_5 are plotted as functions of the induction time in figures 56 and 57, respectively. The pressures and temperatures behind the reflected shocks were computed from the measured incident shock velocities using equations 20 and 23, which were derived for an equilibrium value of γ. There are two sets of experimental points shown in figures 56 and 57. The empty circles represent induction times based upon the first detectable signs of radiation. The solid circles represent induction times based upon the time at which the radiation reached an arbitrary, but fixed, level equal to about 1/6 of the peak intensity. This fixed level of intensity was chosen to be the minimum intensity for which all of the experimental data displayed the rapidly increasing emission which is characteristic for the stronger shocks.

No Kerr-cell absorption experiments were conducted near the threshold conditions (see Section VI E). It seems possible that the gradually increasing and decreasing light emission near the threshold values does not correspond to the onset of carbon formation. Experiments which will be discussed presently in detail, indicate that the temperature associated with the first detectable signs of light emission behind carbon-forming shocks not under threshold conditions, is always at least 1800°K. The highest computed gas temperature T_5 behind the reflected shock was 1275°K (see fig. 56). Reflected shock interaction with the contact surface will raise this gas temperature by no more than 100°K (see table II). Thus the first detectable signs

of emission must accompany an exothermic chemical reaction. Whether or not the first sign of emission is always characteristic of the same amount of carbon formation is a question which cannot be answered without following the reaction as a function of time spectroscopically.

Most of the experimental scatter (see figs. 56 and 57) is probably due to inaccurate shock-velocity measurements. For example, the computed temperatures T_5 are uncertain by about 50°K. A shock-velocity measurement which was inaccurate by 4 °/o would cause an error in the computed temperature of about 50°K. The maximum error in the shock-velocity measurement was $\pm$ 3 °/o. The schlieren trigger system which is being developed should reduce the scatter of the experimental results.

A rough kinetic interpretation of the experimental data shown in figures 56 and 57 can be given in the following manner. The incipient rate of change of carbon concentration is presumably described by a relation of the type[85]

$$\frac{d\,C(s)}{dt} = B \exp(-E'/RT)\,(p_5)^n , \qquad (31)$$

where n is a small number, E' is the effective molar activation energy, B equals the frequency factor which is independent of temperature, and R is the molar gas constant. The thermal decomposition of hydrocarbons often follows first-order kinetics;[86] therefore, a choice of n near unity appears to be reasonable.

We now assume that the induction time Δt measured experimentally is the time required for minimum detectable carbon formation, and that the minimum detectable amounts of carbon are

roughly the same for each experiment. Therefore

$$\Delta C(s) \simeq \text{constant}$$

for all values of p_5, T_5 and Δt determined experimentally. For these conditions, equation 31 becomes

$$E' = 2.303\ R\ \frac{d \log_{10} (p_5 \Delta t)}{d\ (1/T_5)} \quad . \tag{32}$$

Since the activation energy is independent of temperature and pressure, a plot of log $(p_5 \Delta t)$ versus $1/T_5$ should be linear with a slope equal to $E'/2.303\ R$. Such a plot is given in figure 58 for the values of T_5, p_5 and Δt calculated from the experimental data. A straight line has been drawn through the experimental points. The effective value of the activation energy obtained from the crude induction time measurement is 34 Kcal/mol for an induction time based on the first detectable signs of light emission, and 30 Kcal/mol for an induction time based upon the fixed level of radiant energy.

Bennett made an accurate determination of the initial conditions which just cause carbon formation.[81] He was able to reduce the scatter of the computed values of p_5 and T_5 (based upon an equilibrium value of γ) to one or two percent of the absolute value. Bennett made use of equation 31 in the form

$$E' = \frac{2.303\ n\ R\ d \log_{10} p_5}{d\ (1/T_5)} \tag{33}$$

where he assumed that the rates of carbon formation are roughly similar for the conditions of minimum detectable carbon formation

with fixed times at peak temperature. Plotting $\log_{10} p_5$ versus $1/T_5$ he found that a linear relation did not exist for pure acetylene. This is explained by the fact that the maximum time at p_5 and T_5 varied between 100 and 2000 μ sec for his initial conditions. However, he did find that a linear relation exists when $\log_{10} p_5$ is plotted versus $1/T_5$ for a mixture of 5 °/o acetylene and 95 °/o argon. In this case, the time at p_5 and T_5 did not vary much with his initial conditions. The value obtained for the effective activation energy, corresponding to carbon formation in the argon-acetylene mixture, was about 54 n Kcal/mol, assuming that the equilibrium value of γ applies.

The value of 34 n Kcal/mol obtained from our induction time experiments was very strongly dependent upon one experimental point (see fig. 58). This experimental point corresponds to a short induction time and a low pressure. The computed pressure could be incorrect because of an error in the velocity measurement. As explained previously, the measured induction time (for short times) is inaccurate to about $\pm$ 10 μ sec. If one experimental point is ignored, an acceptable correlation for the remaining data is found to correspond to an effective activation energy of 56 Kcal/mol (see fig. 58). It may therefore be concluded that the value of the effective activation energy computed for acetylene-argon mixtures[81] and based on threshold experiments, and for pure acetylene (based on induction time experiments) are in semi-quantitative agreement. Before a more precise value of the effective activation energy can be obtained from the induction time experiments, the errors in shock-velocity measurements and the uncertainty in the start of the oscillo-

scope sweep will have to be reduced.

G. The Two-Color Method of Temperature Measurement

Spectral studies of the emitted light behind carbon-forming shocks show considerable scatter but suggest, nevertheless, that the emitted radiation, after some time, follows a greybody distribution law. A two-color method has therefore been employed successfully to yield continuous temperature versus time data.

(1) Definitions

A blackbody is defined as a source which emits light with a spectral distribution given by Planck's equation for isothermal radiation. A greybody has an emissivity ($E < 1$) which is independent of wavelength.

The brightness temperature T_{br} at the wavelength λ is defined as the temperature at which the radiator under study emits the same spectral intensity of radiation as a blackbody. The brightness temperature is related to the true temperature by the relation

$$\frac{1}{T} = \frac{1}{T_{br}} + \frac{\lambda}{c_2} \ln \varepsilon_\lambda \qquad (34)$$

where λ is the wavelength at which the brightness temperature is measured ($\mathring{A}$), c_2 is the second radiation constant (cm-^{o}K), and ε_λ is the spectral emissivity of the emitter at the wavelength λ. An optical pyrometer may be used to measure the brightness temperature T_{br} by comparing the brightness of the emitted light at a given wavelength with the brightness of a calibrated strip filament source.

The color temperature T_c of an emitter for specified wave-

lengths λ_1 and λ_2 is defined as the temperature at which a blackbody emits radiation having the same ratio of radiant intensities at the wavelengths λ_1 and λ_2 as the emitter under study. The color temperature T_c is related to the true temperature through the expression

$$\frac{1}{T} = \frac{1}{T_c} + \frac{1}{c_2 \left(\frac{1}{\lambda_1} - \frac{1}{\lambda_2}\right)} \ln \frac{\varepsilon_{\lambda_1}}{\varepsilon_{\lambda_2}} \quad . \qquad (35)$$

The color temperature is evidently the true temperature for a greybody emitter since $\varepsilon_{\lambda_1} = \varepsilon_{\lambda_2}$ in this case.

If the radiation associated with carbon formation follows a greybody distribution law, then a two-color method can be used to make a continuous temperature versus time study (see Section III D(2)).

(2) Calibration of the Optics

A Jarrel-Ash monochromator was used to determine the spectral intensity of the emitted radiation. Two 931-A photomuliplier tubes, each preceded optically by an appropriate interference filter, were used to measure simultaneously the color temperature as a function of time. For direct quantitative measurement, the system must, of course, be calibrated.

The two-color temperature measurements were made for intensities at which the photomultiplier tubes had linear response curves. When the sensitivity of the phototube was varied by changing the load resistor, the range of the linear operation was modified. For instance, when the photocell was operated at high sensitivity, the peak emitted radiation (for an initial downstream pressure

p_1 = 1/2 psia) was beyond the range of linearity. When the photocell was operated with a small load resistor, the peak intensities were in the range of linear response; however, the reduced photocell sensitivity made it impossible to determine an accurate two-color temperature measurement at the onset of luminosity when the radiant energy flux was low. Thus, for each experiment, the light intensity range determined by the sensitivity of the photocells, on the one hand, and the region of linear response, on the other hand, defined the time during which the signal from the photocells could be used for temperature measurements.

The spectral response S_λ of the monochromator and its associated optics varies with wavelength. The effective value of S_λ was determined by placing a tungsten strip filament lamp on the axis of the slit system (see fig. 18) and at a distance from the slits corresponding to the inside face of the shock-tube window. A Leeds and Northrup optical pyrometer was used to determine the brightness temperature of the filament. The brightness temperature was converted to the true temperature by using equation 34 and the emissivity data for a tungsten ribbon given by De Vos.[87] The intensity of the tungsten source was measured with the spectrometer over the range of wavelengths from 3500 Å to 7000 Å. In order to obtain the spectral response, S_λ, the measured intensities at each wavelength were divided by the value of the greybody spectral distribution at that wavelength for the corresponding true temperature. Actually, a correction should be applied to the greybody spectral distribution in order to take into account the fact that a tungsten

source is not strictly grey. However, this correction is small (e.g., at 1600°K, $\varepsilon_{4400\ \mathring{A}} = .476$ and $\varepsilon_{6575\ \mathring{A}} = .499$) and was neglected because the scatter in the experimental results was greater than the value of the correction.

For the calibration, a stable DC source was used to apply different voltages to the tungsten lamp filament in order to vary its temperature. The brightness temperature was measured, the apparatus was exposed to the light source, and the two photocell outputs were photographed on an oscilloscope face. The ratios of the intensities transmitted through the red filter (6575 Å) and through the blue filter (4400 Å), R(T), are shown as a function of brightness temperature (for several repeated calibration runs but identical optical system) in figure 59. The smooth curve drawn through the experimental points in figure 59 was used to deduce an equivalent brightness temperature from experimental shock-tube emission data. The scatter of experimental points corresponds to an uncertainty in temperature of about $\pm$ 100°F.

The equivalent brightness temperature can be converted directly to the true temperature in the two-color calibration experiments (using equation 34) if the source is grey. Since the emissivity of tungsten varies slightly between 4400 Å and 6575 Å (see reference 87), an additional correction of about 25°K is required in order to calculate the true temperature from the brightness temperature. This correction was neglected in the present applications.

(3) The Spectral Distribution of the Light Emitted Behind a Reflected Shock in Acetylene

The one-inch shock tube was used to make 119 consecutive

runs, under similar initial conditions, to determine the nature of the radiation emitted behind carbon-forming shocks in acetylene. The initial pressure ratio was 465 and the initial pressure of the acetylene, p_1, was 24 mm of Hg. Because of shock-wave attenuation in the one-inch tube, the average Mach number of the incident shock, just before reflection, was 3.9.

The light intensity was measured as a function of time in 100 Å intervals for the spectral range between 3000 Å and 7500 Å. In general, the peak intensity of the radiation at a given wavelength was not consistent from one run to the next. As many as seven runs were made for a specified wavelength to try and establish a trend. The scatter in the data was considerable. For example, in figure 60 is shown the rise-time (measured as the time between the onset of measurable radiation and the time of peak radiation) as a function of wavelength for about seventy separate runs. The rise-time is seen to vary from 130 to 450 μ sec. The data shown in figure 60 show no positive correlation between rise-time and wavelength of the emitted light. Other experiments showed that the absolute value of the scatter decreased as the strength of the incident shock wave increased.

The corrected intensities have been plotted as a function of wavelength for three different times: 100 μ sec and 200 μ sec after the onset of measureable emission, and for the time when the emitted intensity was a relative maximum. The relative peak intensities showed the smallest scatter and followed roughly the blackbody distributions curve for isothermal radiation at a temperature of 2000°K (see fig. 61). Of the original 119 experimental runs, peak intensities

from 105 are plotted in figure 61; for four runs the intensity trace went off the oscilloscope screen; the corrected peak intensities of 10 runs would not fit within the scale of the figure. A method for reducing experimental scatter will be presented later on.

Additional experiments have been conducted with the one-inch shock tube to determine if there was any intense radiation which occurred at wavelengths corresponding to the C_2 and CH emission bands commonly observed in hydrocarbon flames. No discrete radiation was observed at any of these wavelength regions. Thus it seems likely that the radiation behind carbon-forming shocks, after some elapsed time, has a greybody spectral distribution.

The two-color method can only be applied to determine the temperature as a function of time during the times for which the emitted light has a greybody spectral distribution. Before the two-color method can be relied upon to yield meaningful temperatures at the onset of emission and long after the time of peak emission, the spectral character of the light at these times must be measured. Unfortunately, a monochromator capable of scanning hundreds of Angstrons in several microseconds is not yet available (see, however, Section III F (4)). Two photocell-filter combinations and a Jarrel-Ash monochromator were used to perform experiments in a three-inch shock tube. Using this equipment, it should have been possible to follow the emitted radiation as a function of time at three widely separated wavelength regions and to determine if the spectral distribution of the emitted light deviated from that of a greybody at the onset of light emission. Unfortunately, the sensitivity of the photo-

cells was found to be so low at 6575 Å that it was not possible to make an accurate relative calibration between the 6575 Å filter-photocell combination and the monochromator set at 6575 Å.

The scatter in the monochromator results can be reduced by making use of a filter-photomultiplier output averaged over several runs. In figure 62 are plotted the relative outputs from the 6575 Å filter-photocell combination for several consecutive runs. The experimental points (circles) for a particular run are connected by a thin line. It appears that the photocell output versus time fluctuates from one run to another around an average value. The heavy line (figure 62) is a rough average curve through the experimental points.

The fluctuations in the filter-photocell outputs are related to the fluctuations in the monochromator output. In figures 63 through 66 are shown the simultaneous relative outputs of the photocell-filter combinations and of the monochromator as a function of time for representative runs. These data indicate that the filter and the monochromator outputs fluctuate with time in a similar manner. This result can be used, for example, to reduce all of the 6575 Å filter-photocell data to a common curve (see figure 62) and to correct the corresponding monochromator output data by the same factor. The monochromator data, reduced in this fashion and plotted as a function of wavelength at the time of peak emission, show somewhat less scatter than the data plotted in figure 61.

(4) Two-Color Temperature Measurements

The three-inch shock tube was used for the two-color temperature measurements. The calibration of the two photomultiplier tubes

has been described in Section VI F (2) .

Accurate measurements of the ratio of the red filter-photocell output to the blue filter-photocell output have been made as a function of time. The oscilloscope sweep was operated in such a fashion that the output from the two photomultiplier tubes was alternately displayed, for five microsecond intervals, on the oscilloscope face. The ratio of the two photocell outputs could be measured accurately every five microseconds at the time of the discontinuity in the oscilloscope trace.

The temperature obtained from two-color measurements behind reflected shocks (see Section VI G (2) for a discussion of the corrections which should be applied to these values) are plotted as a function of time in figures 67 and 68 for several experiments of nearly identical initial shock velocities. The initial pressure p_1 of acetylene was 25 mm Hg and the incident shock Mach number varied from 4.18 to 4.28. The peak radiation occurred about 80 μ sec after passage of the reflected shock. The average true temperature at the time of peak radiation (see fig. 67) was 2150°K. Since the theoretical equilibrium gas-dynamic temperature (see fig. 32) behind the reflected shock was roughly 1300°K, our results again show that the greybody radiation from carbon-forming shocks follows exothermic chemical reactions.

The spectral distribution of the peak values of the radiated light plotted in figure 61 strongly suggests that the temperature is about 2000°K. The data shown in figure 61 were obtained with the one-inch shock tube and an incident Mach number of about 3.9, which

corresponds to a gas-dynamic temperature $T_5 = 1100^{\circ}K$.

The measured temperature obtained from the two-color experiments in the three-inch shock tube and the equivalent greybody temperature obtained from the experiments with the one-inch shock tube show satisfactory agreement.

The two-color temperature of the emitted light also was measured for stronger incident shocks with a Mach number equal to 5.2. The equivalent gas temperature, based on an equilibrium γ, before any chemical reaction, was about $1600^{\circ}K$. The maximum temperature measured by the two-color method (see figure 69) was only about $150^{\circ}K$ greater than the two-color temperature obtained for initial Mach numbers of 4.2.

(5) High-Speed Photographs of the Emitted Visible Radiation

The erratic fluctuations in the photocell output during emission (see fig. 65) may be understood after an examination of high-speed pictures of the emission behind the reflected shock. Some results of these studies are given in figures 70 and 71.

The high speed camera was similar to the one shown in figure 19. The pictures were taken at the end of the shock tube through the observation window and perpendicular to the tube axis (see fig. 53). The camera had a field of view of 3/16". The time resolution of the photographs shown in figures 70 and 71 is 13.7 μ sec per inch. Time runs from right to left. The vertical dimension in the photograph is the image of the vertical field of view just inside the observation window, magnified four times.

Examination of the high-speed photographs indicates that the emission behind carbon-forming shocks is non-uniform across the field of view of the camera. The slit system used in the two-color measurements defines about twice the vertical field of view that is represented in these photographs. Thus the erratic fluctuations in the photocell output are correlated with this non-steady and non-uniform emission.

(6) Some Additional Comments Concerning the Two-Color Experiments

The results of the two-color experiments (fig. 67) suggest also that the radiation behind carbon-forming shocks is indeed grey over a considerable length of time. If the emitted radiation were the result of chemiluminescence, then one would expect the ratio of the intensities at two wavelengths to change radically with time. However, the experimental ratios fluctuate within small and rather well-defined limits.

It does not seem likely that the two-color method can be used to measure temperatures during the initial stages of chemical reactions. After the chemical reactions begin, but before any solid carbon has formed, one might expect the radiation to be characteristic of strong emitters such as C_2 and CH. The spectral distribution of such radiation is far from that of a greybody.

The initial stages of the chemical reaction were studied using the monochromator and filter-photocell combinations. However, no emission was observed during the initial stages of the chemical

reactions which could be attributed to selective emitters. In addition, the first measureable ratios always coincided with true temperatures well above the gas temperatures (T_5) calculated for an equilibrium value of γ behind the reflected shock. Thus, in practice, we were only able to observe radiation which seemed to be associated with the onset of carbon formation and which occurred some time after the onset of chemical reactions.

It is not possible to interpret the observed dependence of light intensity on time quantitatively. The intensity of the emitted radiation depends on the number of carbon particles, the size distribution, the temperature of the emitters, and so forth. The lack of reproducibility of emitted intensity is probably largely the result of the fact that the emitting region is physically non-uniform across the field of view (see figs. 70 and 71).

VII. CONCLUSIONS AND RECOMMENDATIONS

Theoretical and experimental studies on the production of hydrazine and on carbon formation behind reflected shocks have been described in the preceding sections.

The unsuccessful attempt to produce hydrazine in a shock tube typifies the difficulties which one should expect to find in a process depending on unknown timing requirements and on the hypothetical "freezing" of chemical intermediates which are presumed to form in measureable concentrations. On the other hand, the production of chemicals by "freezing" equilibrium components offers a hopeful method of approach for shock-tube applications.

The studies on carbon formation behind reflected shocks in acetylene constitute the beginnings of a larger study on the mechanism of carbon formation at elevated temperatures and pressures.

The principal conclusions are the following:

(1) The effective values of the specific heat ratio γ, for the incident and reflected shocks, probably are close to the equilibrium values.

(2) Simultaneous light-absorption and emission experiments can be made behind shock waves using the Kerr cell as a light chopper. Light emission and absorption experiments behind carbon forming shocks indicate that the onset of radiation coincides with the onset of carbon formation (within a few microseconds).

The rates of reaction studied by use of the Kerr cell technique are only limited by the chopping rate, which can be greater than 10 megacycles per second. The Kerr cell, operated as a light

chopper, may be a valuable research tool also in light scattering experiments behind carbon-forming shocks. Theoretically it is possible to determine the average size and number density of the carbon particles as a function of time by observing the scattered light simultaneously at two different wavelengths.

(3) Well-defined conditions of temperature and pressure, in the times available for a fixed shock-tube geometry, determine whether or not carbon will be formed behind the reflected shock.

(4) The induction time (the time between the passage of the shock and the onset of emission) varies with temperature and pressure; this variation can be used to make crude estimates for the overall activation energy.

(5) The maximum radiant energy in carbon-forming experiments follows the grey- (or black-) body distribution curve in the wavelength region between 3500 and 7000 $\mathring{A}$. The intense CH and C_2 emission bands, which occur in this spectral region, could not be distinguished from the continuous background radiation.

(6) Assuming that the emitted radiation follows a blackbody distribution curve as a function of time (during periods of appreciable emission), a simple two-color technique has been developed for the measurement of the temperature as a function of time. The peak temperatures measured by the two-color technique correspond, within $\pm$ 200^{o}K, with those calculated from the measured blackbody spectral distribution of the radiation.

REFERENCES

1. P. Vieille, Compt. Rend. 129, (1899), p. 1228.

2. W. Payman, and F. Shepherd, Proc. Roy. Soc. (London) 186A, (1946), p. 293.

3. R. Courant, and K. O. Friedrichs, Supersonic Flows and Shock Waves, Interscience Publications, New York (1948).

4. J. Lukasiewicz, "Shock-Tube Theory and Applications", National Research Council (Canada) Report No. MT-10, Ottawa (1950).

5. G. Rudinger, Nonsteady Flow in Ducts, D. Van Nostrand Co., Inc., New York (1955).

6. K. Lobb, "The Study of Supersonic Flows in a Shock Tube", Ph. D. Thesis, University of Toronto, Toronto (1950).

7. F. W. Geiger, and C. W. Mantz, "The Shock Tube as an Instrument for the Investigation of Transonic and Supersonic Flow Patterns", Engineering Research Institute, University of Michigan, Ann Arbor (1949).

8. E. L. Resler, S. C. Lin, and A. Kantrowitz, J. Appl. Phys. 23, (1952), p. 1390.

9. K. Lobb, "On the Length of a Shock Tube", UTIA, Canada, Report No. 4, Toronto (1950).

10. W. Doering and G. Burkhardt, Translation Technical Report No. F-TS-1227-IA (GDAM A9-T 46), Air Material Command, (1949).

11. Y. A. Yoler, "The Hypersonic Shock Tube", Ph.D. Thesis, California Institute of Technology, Pasadena (1954).

12. J. Lukasiewicz, "Flow in a Shock Tube of Non-Uniform Cross-Section", NRC Report MT-11, (Jan. 1950).

13. E. L. Resler, "High-Temperature Gases Produced by Shock Waves", Ph. D. Thesis, Cornell University, Ithaca, N.Y. (1951).

14. J. V. Foa, and G. Rudinger, "Methods of Analysis for Nonsteady Flow", Project SQUID, Semi-Annual Progress Report 14, (Oct. 1952).

15. R. G. Fowler, Phys. Rev. 88, (1952), p. 137.

16. F. A. Jenkins, and H. E. White, Fundamentals of Physical Opitcs, McGraw-Hill Book Co., New York (1937), pp. 68-81.

17. A. Ladenburg, and D. Bershader, Physical Measurements in Gas Dynamics and Combustion, Princeton University Press, Princeton, N. J. (1954), pp. 47-75.

18. W. Bleakney, D. R. White, and W. C. Griffith, J. Appl. Mech. 17, (1950), p. 439.

19. V. H. Blackman, Bull. Am. Phys. Soc., (Jan. 1956), Series II, Vol. I, p. 18.

20. G. B. Kistiakowsky, J. Chem. Phys. 19, (1951), p. 1611.

21. H. Schardin, Ergeb. exakt. Naturw. 20, (1942), p. 303; Verh. deut. Ing. Forschungsheft 367 (5), (1934), p. 1.

22. J. W. Beams, Physical Measurements in Gas Dynamics and Combustion, Princeton University Press, Princeton, N. J. (1954), pp. 26-44.

23. I. I. Glass, and G. N. Patterson, J. Aero. Sci. 22, (1955), p. 73.

24. I. Langmuir, and H. M. Mott-Smith, General Electric Reviews 27, (1924), p. 449; E. J. Johnson, and L. Malter, Phys. Rev. 80, (1950), p. 58.

25. H. F. Calcote, and I. R. King, Fifth Symposium (International) on Combustion, Reinhold Publishing Corp., New York (1955), pp. 423-434.

26. S. C. Lin, E. L. Resler, and A. Kantrowitz, J. Appl. Phys. 26, (1955), p. 95.

27. R. G. Fowler, W. R. Atkinson, and L. W. Marks, Phys. Rev. 87, (1952), p. 966.

28. A. Unsold, Physik der Sternatmospharen, J. W. Edwards, Ann Arbor, Michigan (1948), p. 286 et sez.

29. K. E. Schuler, and J. Weber, J. Appl. Phys. 22, (1954), p. 491.

30. A. J. Chabai, and R. J. Emrich, J. Appl. Phys. 26, (1955), p. 779.

31. J. Rabinowicz, M. E. Jessey, and C. A. Bartsch, J. Appl. Phys. 27, (1956), pp. 97-98.

32. E. Bauer, Le Radium 6, (1909), p. 110.

33. F. P. Bundy, and H. M. Strong, Physical Measurements in Gas Dynamics and Combustion, Princeton University Press, Princeton, N. J., (1954), pp. 343-385.

34. N. Thomas, ibid, pp. 527-567.

35. S. S. Penner, Am. J. Phys. 17, (1949), pp. 422, 491; Selected Combustion Problems - Fundamentals and Aeronautical Applications, Butterworths Scientific Publications, London (1954), pp. 144-166.

36. A. G. Gaydon, and H. G. Wolfhard, Flames, Their Structure, Radiation, and Temperature, Chapman and Hall, Ltd., London (1953), pp. 216-261.

37. J. H. Hett, and J. B. Gilstein, J. Opt. Soc. Am. 39, (1949), p. 909.

38. H. E. Petschek, P. H. Rose, H. S. Glick, A. Kane, and A. Kantrowitz, J. Appl. Phys. 26, (1955), p. 83.

39. E. B. Turner, NSF Conference on Stellar Atmospheres, Indiana University, Bloomington, Indiana (1954).

40. H. Edels, and D. Whittaker, J. Scientific Instruments 32, (1955), p. 103.

41. M. M. Wachtel, and E. J. Sternglass, Bull. Am. Phys. Soc., (1956), Series II, Vol. 1, No. 1.

42. G. R. Cowan, and D. F. Hornig, J. Chem. Phys. 18, (1950), p. 1008.

43. H. S. Glick, W. Squire, and A. Hertzberg, "A New Shock Tube Technique for the Study of High Temperature Gas Phase Reactions", Fifth Symposium (International) on Combustion, Reinhold Publishing Corporation, New York (1955), pp. 393-402.

44. T. Carrington and N. Davidson, J. Phys. Chem. 57, (1953), p. 418.

45. D. Britton, N. Davidson, and G. Schott, Faraday Society Discusions, (1954), No. 17, pp. 58-68.

46. M. Plooster, and D. Garvin, "The High Temperature Hydrogen-Bromine Reaction", The James Forrestall Research Center, Princeton University, Princeton, N. J. (April 1955); D. Britton, and N. Davidson, J. Chem. Phys. 23, (1955), p. 2461.

47. H. E. Petschek, Ph.D. Thesis, Cornell University, Ithaca, N. Y. (Sept. 1955).

48. L. Landau, and E. Teller, Phys. Z. Sowjetunion 10, (1936), p. 34; H. A. Bethe, and E. Teller, Aberdeen Proving Ground Report X-117.

49. R. Schwartz, Z. I. Slawsky, and K. F. Herzfeld, J. Chem. Phys. 20, (1952), p. 1591; R. Schwartz, and K. F. Herzfeld, ibid 22, (1954), p. 8768.

50. K. F. Herzfeld, comments presented at the Second AGARD Combustion Colloquium, Liege, Belgium, (December 1955); Butterworths Scientific Publications, London (in press).

51. H. C. Hottel, Chapter 4 in W. H. McAdams Heat Transmission, McGraw-Hill Book Co., New York (1954).

52. S. S. Penner, et al, J. Appl. Phys. 21, (1951), p. 685; 22, (1951), p. 1164; 23, (1952), pp. 256, 825.

53. S. S. Penner, J. Appl. Phys. 25, (1954), p. 66.

54. R. H. Christian, and F. L. Yarger, J. Chem. Phys. 23, (1955), p. 2042.

55. R. H. Christian, R. E. Duff, and F. L. Yarger, J. Chem. Phys. 23, (1955), p. 2045.

56. W. V. M. Rankine, Phil. Trans. 160, (1870), p. 277.

57. Lord Rayleigh, Proc. Roy. Soc. (London) 84A, (1910), p. 247.

58. G. I. Taylor, Proc. Roy. Soc. (London) 84A, (1910), p. 371.

59. R. Becker, Zeits. f. Physik 8, (1922), p. 321.

60. L. H. Thomas, J. Chem. Phys. 12, (1944), p. 449.

61. C. S. Wang Chang, University of Michigan, Dept. of Engineering Research, Report UMH-3-F (APL/JHU CM-503), (1948).

62. H. M. Mott-Smith, Phys. Rev. 82, (1951), p. 885.

63. K. Zoller, Z. f. Physik 130, (1951), p. 1.

64. D. F. Hornig, Phys. Rev. 72, (1947), p. 179.

65. E. F. Greene, G. R. Cowan, and D. F. Hornig, J. Chem. Phys. 19, (1951), p. 427.

66. E. F. Greene, and D. F. Hornig, J. Chem. Phys. 21, (1953), p. 617.

67. W. M. Flook, Jr., and D. F. Hornig, J. Chem. Phys. 23, (1955), p. 816.

68. W. H. Andersen, and D. F. Hornig, J. Chem. Phys. 24, (1956), p. 767.

69. W. Payman, and H. Titman, Proc. Roy. Soc. (London) 152A, (1935), p. 418.

70. W. C. F. Shepherd, Third Symposium on Combustion, Flame and Explosion Phenomena, The Williams and Wilkins Co., Baltimore (1949), p. 301.

71. J. A. Fay, Fourth Symposium (International) on Combustion, The Williams and Wilkins Co., Baltimore (1953), p. 501.

72. W. R. Gilkerson, and N. Davidson, J. Chem. Phys. 23, (1955), p. 687.

73. D. J. Berets, E. F. Greene, and G. B. Kistiakowsky, J. Amer. Chem. Soc. 72, (1950), p. 1080.

74. A. J. Mooradian, and W. E. Gordon, J. Chem. Phys. 19, (1951), p. 1166.

75. W. J. Hooker, "Ignition of $2H_2$-O_2 Mixtures by Means of Shock Waves", M.S. Thesis, Cornell University, Ithaca, N. Y. (1955).

76. G. J. MacLeod, "Some Considerations in the Application of a Gas Turbine Cycle to the Manufacture of Nitric Oxide", Mechanical Engineer's Thesis, California Institute of Technology (1953).

77. A. Kantrowitz, "The Wave Engine", paper presented before 1946 Annual Meeting of ASME, New York.

78. F. W. Barry, J. Appl. Mechanics (ASME), 17, (1950), p. 47.

79. J. C. Devins and M. Burton, "Formation of Hydrazine in Electric Discharge Decomposition of Ammonia", J. Am. Chem. Soc., 76, (1954), p. 2618.

80. G. Porter, "The Mechanism of Carbon Formation", Combustion Researches and Reviews, AGARDograph No. 9, Butterworths Scientific Publications, London (1955).

81. E. N. Bennett, "Carbon Formation from Acetylene in the Shock Tube", Aeronautical Engineer's Thesis, California Institute of Technology (1956).

82. National Bureau of Standards, Tables and Selected Values of Chemical Thermodynamic Properties, (1949), Series III, Vol. II.

83. F. D. Rossini, et al., Selected Values of Physical and Thermodynamic Properties of Hydrocarbons and Related Compounds, American Petroleum Institute Research Project 44, Carnegie Press, Pittsburgh (1953).

84. I. I. Glass, W. Martin, and G. N. Patterson, "A Theoretical and Experimental Study of the Shock Tube", University of Toronto, Institute of Aerophysics, Report No. 2 (1953).

85. S. S. Penner, Chemical Reactions in Flow Systems, Butterworths Scientific Publications, London (1955).

86. C. N. Hinshelwood, et al., Proceedings of the Royal Society of London, A203, (1950), pp. 486-501; A214, (1952), pp. 20-35.

87. J. C. DeVos, "A New Determination of the Emissivity of Tungsten Ribbon", Physica XX, (1954), p. 107.

TABLE I

Relative rise-time and output characteristics of representative PbS, PbTe, and PbSe photoconducting cells*

Cell	Relative output**	Load resistor in ohms	Temperature in °C	Response time** in μsec	Reported sensitivity range in μ
PbS # 1	1325	150 K	22	40	.3-3
# 2	90	100 K	22	68	.3-3
# 2	670	100 K	- 80	1450	.3-3
PbTe # 1	6.9	1250 K	22	143	Somewhat less than PbSe
# 1	4.0	100 K	- 196	50	
PbSe # 1	16.7	100 K	22	13	0.6-6 or 8
PbSe # 1		25 K	22	6	0.6-6 or 8

* Determined by Windsor at the California Institute of Technology.

** The output and response times of these cells are very sensitive functions of the associated electronic circuitry.

TABLE II

The calculated* state of acetylene gas following interaction of the reflected shock with the contact surface.

M_s	p_6/p_1 **	u_6/a_1 **	T_6/T_5 **	T_5	$M_{re} = \frac{u_{re}}{a_1}$ **
5.18	510	.97	1.06	1625	1.26
4.29	220	.36	1.025	1256	1.106
3.79	138	.10	1.008	1070	1.030

* The calculation to determine the gas state in regions 2 and 5 was based upon an equilibrium value of γ. The calculation of the gas state in region 6 was made on the basis of a constant γ. This last assumption is justified because, even at the lowest temperature, $T_5 = 1070$, the specific heat of acetylene at constant pressure is a slowly varying function of T (e.g., if the temperature is raised from 1070 to 1170°K, the corresponding ratio of specific heats changes only from 1.139 to 1.136).

** See figure 48.

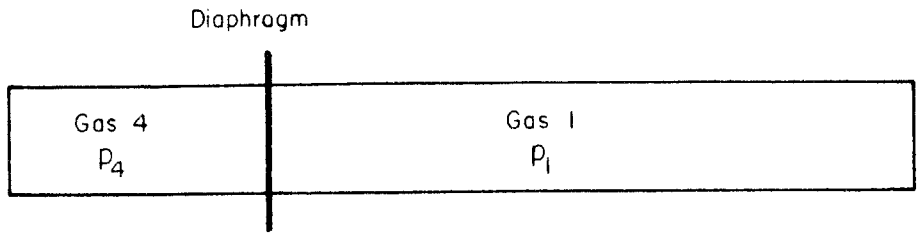

Fig. 1. Schematic diagram of one-dimensional shock tube with uniform cross-section, closed at both ends.

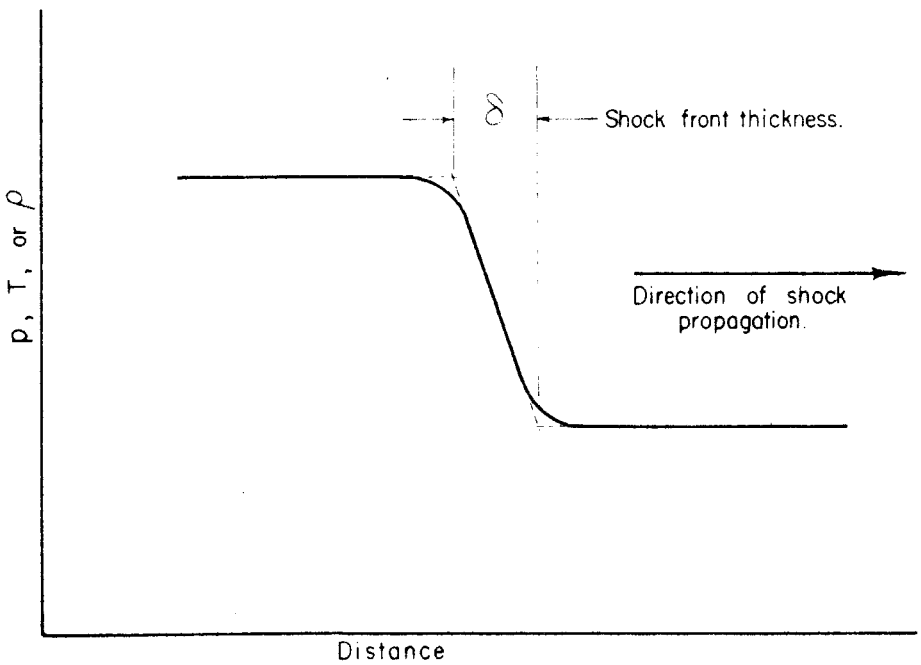

Fig. 2. Pressure (temperature, or density) as a function of distance across an incident shock with no relaxation effects and/or chemical reaction behind the shock front (schematic).

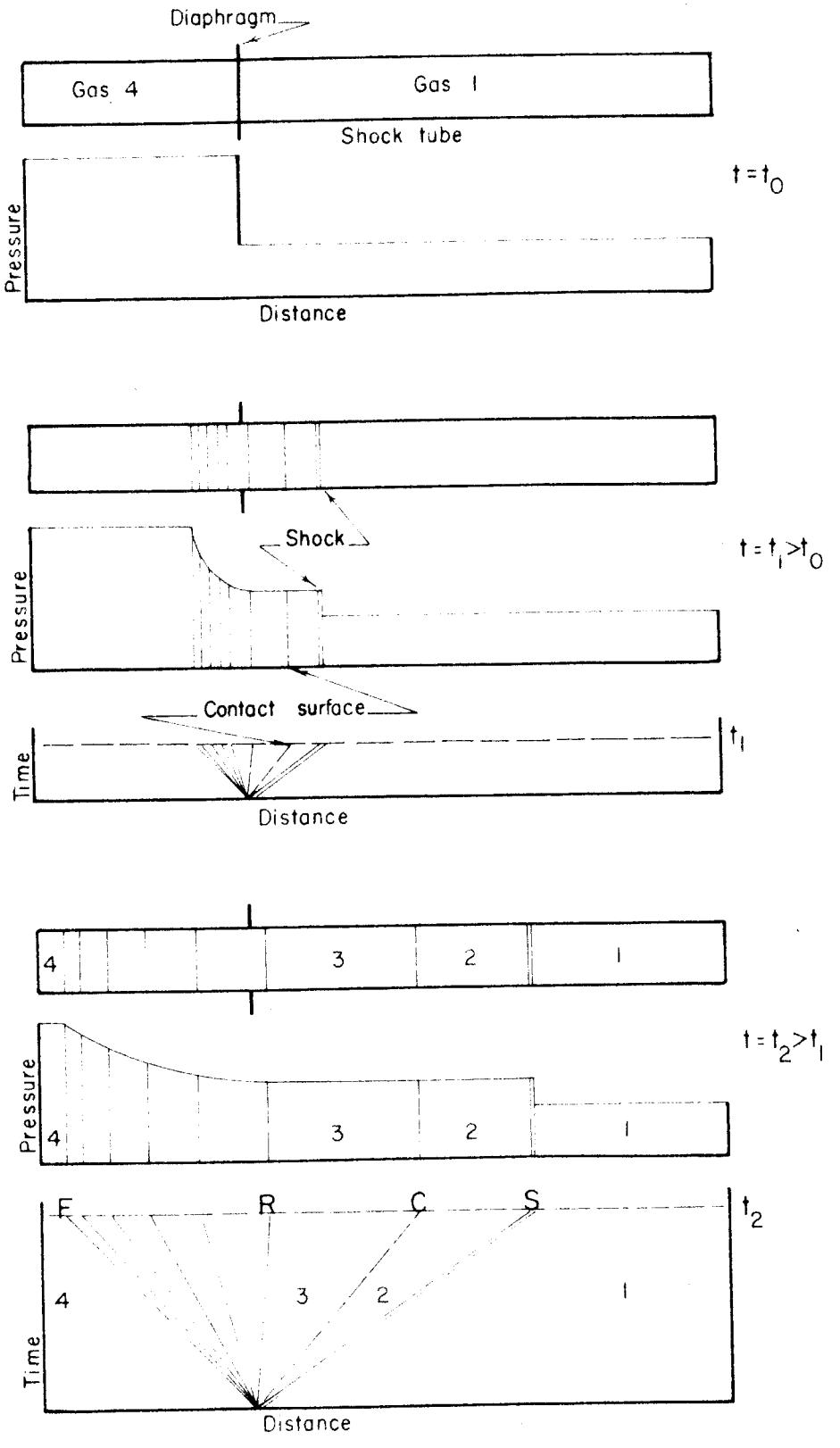

Fig. 3. Gas distribution and pressure profile as a function of time with associated distance-time (x-t) diagram (schematic); S: shock front; C: contact surface; R to F: expansion wave.

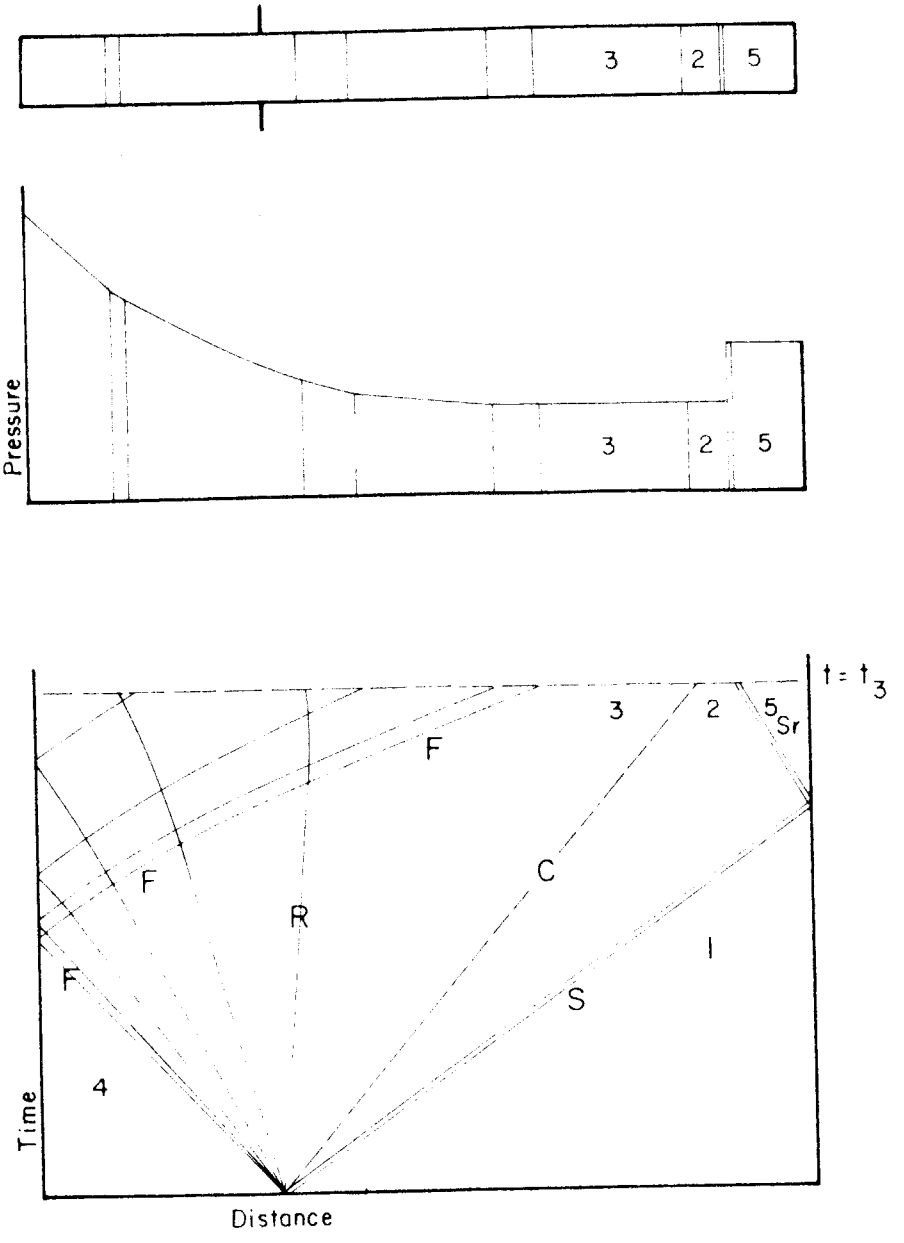

Fig. 4. Gas distribution and pressure profile as a function of time with associated distance-time (x-t) diagram for the case of the reflected shock (schematic); S: shock front; C: contact surface; R to F: expansion wave; S_r: reflected shock.

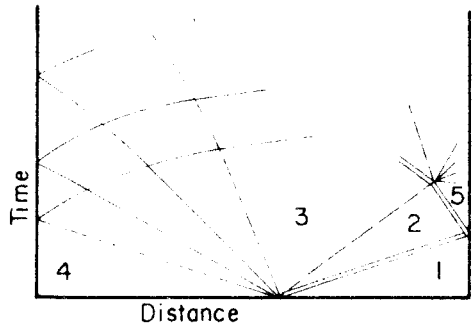

FIG. 5a.

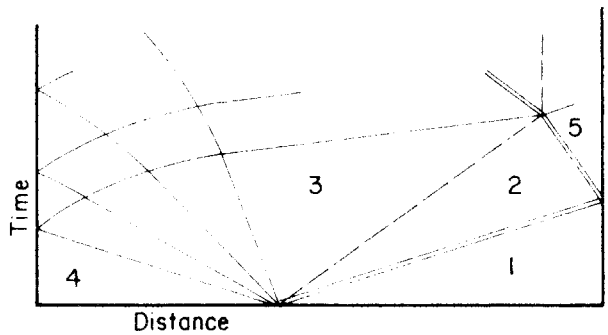

FIG. 5b.

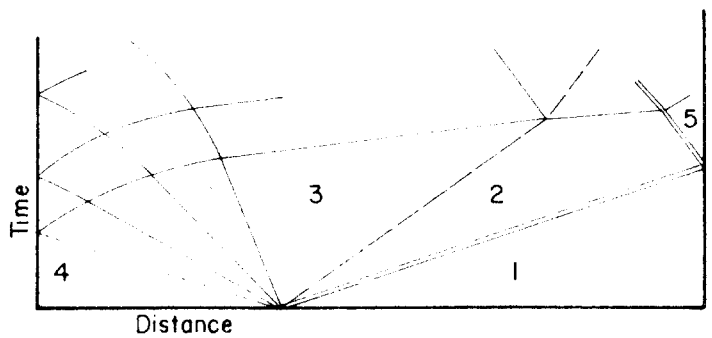

FIG. 5c.

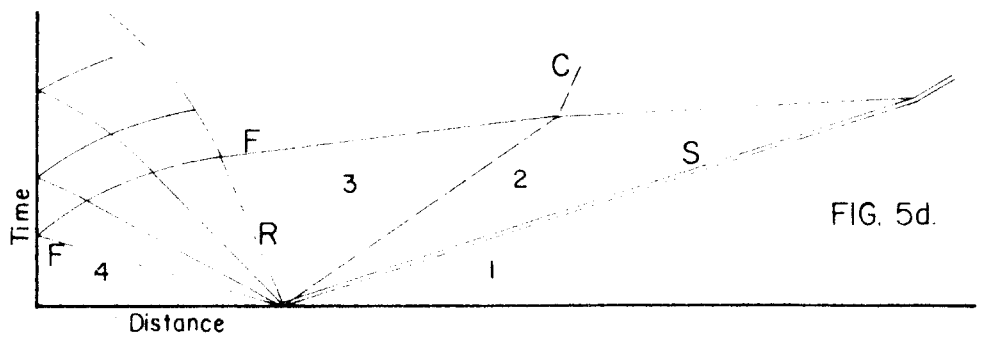

FIG. 5d.

Fig. 5. Influence of length of low-pressure section on gas flow as represented by the x-t diagram; S: shock front; C: contact surface; R to F: expansion wave; S_r: reflected shock.

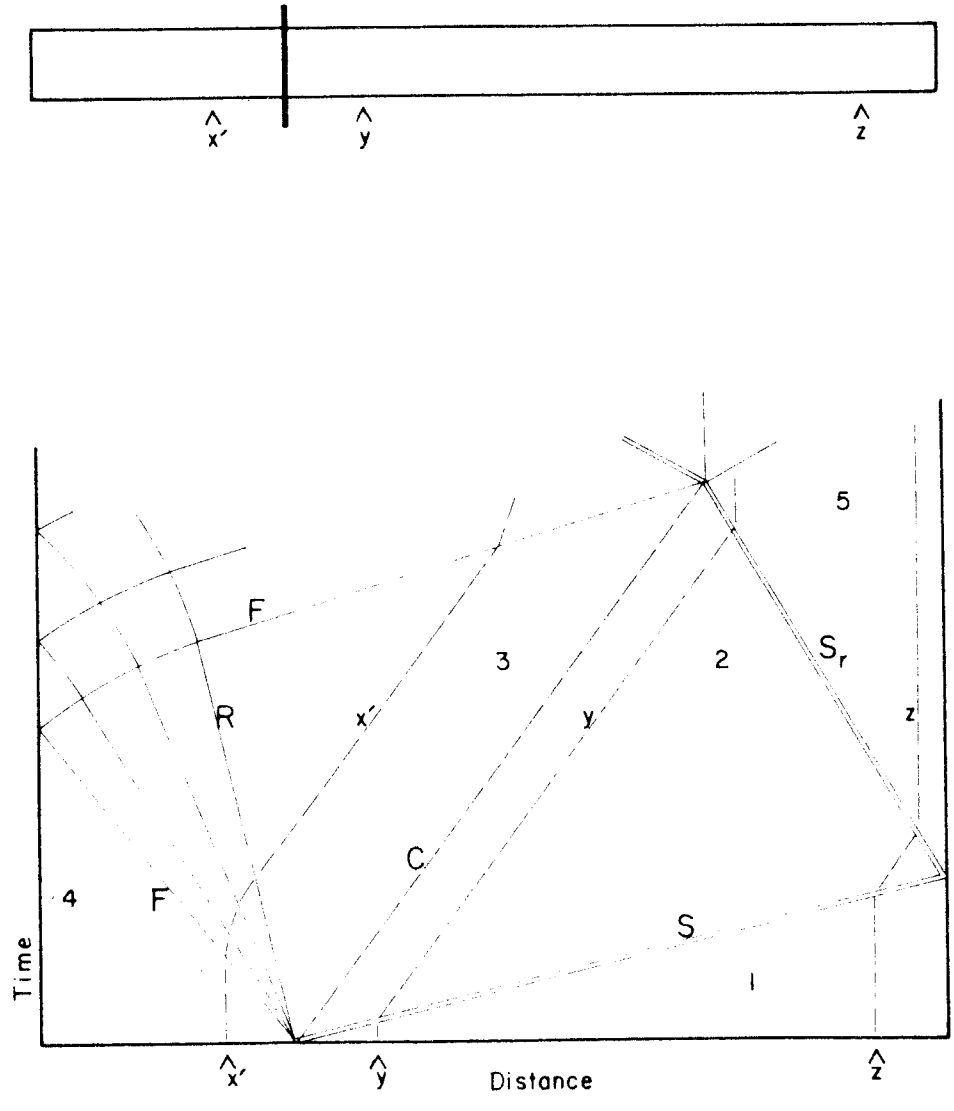

Fig. 6. Particle paths shown in the x-t diagram for selected initial positions; S: shock front; C: contact surface; R to F: expansion wave; x', y, z: particle paths; S_r: reflected shock.

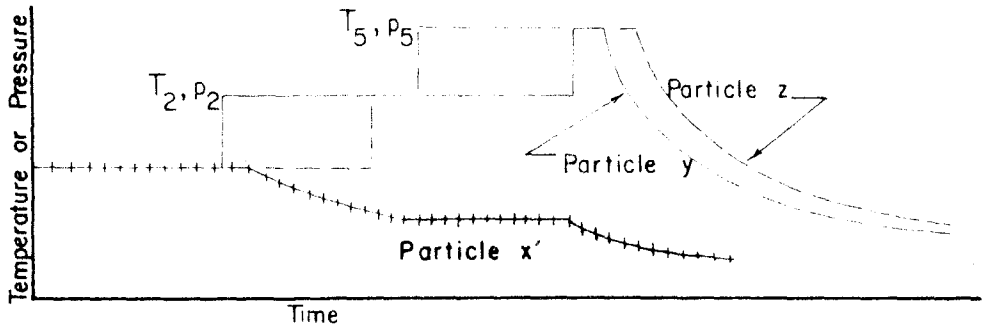

FIG. 7a.

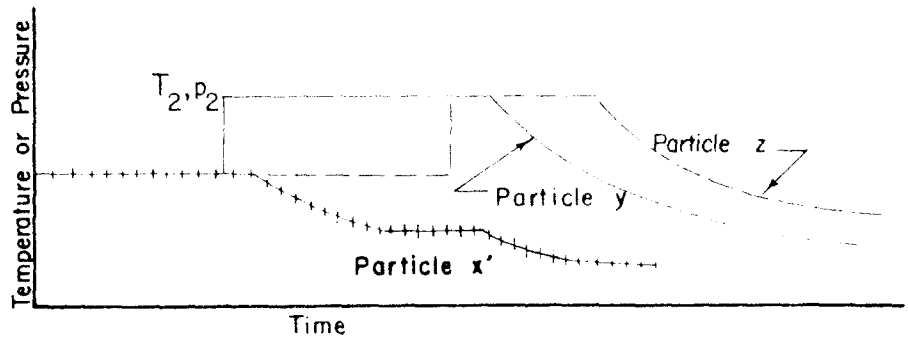

FIG. 7b.

Fig. 7. Temperature (T) versus time (t) diagrams (schematic) for three particles initially located at the positions x', y, and z shown in figure 6. In figure 7a is shown the T vs. t history for the configuration corresponding to figure 5b. In figure 7b is represented the T vs. t history for a design similar to that for which figure 5d applies.

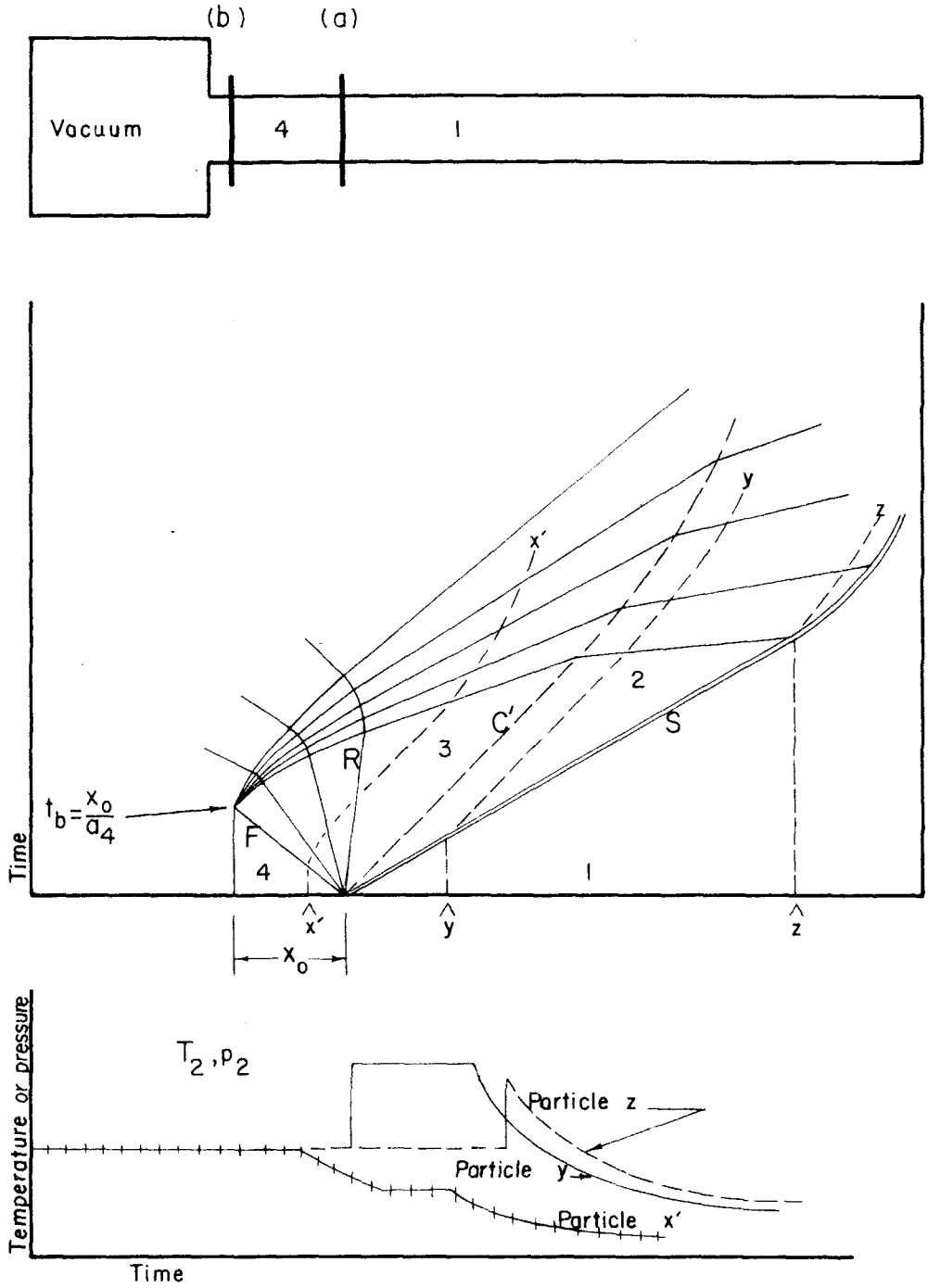

Fig. 8. Description of flow, particle position, and temperature for the incident shock in a modified shock tube using two diaphragms and a large expansion chamber; S: shock front; C: contact surface; R to F: expansion wave.

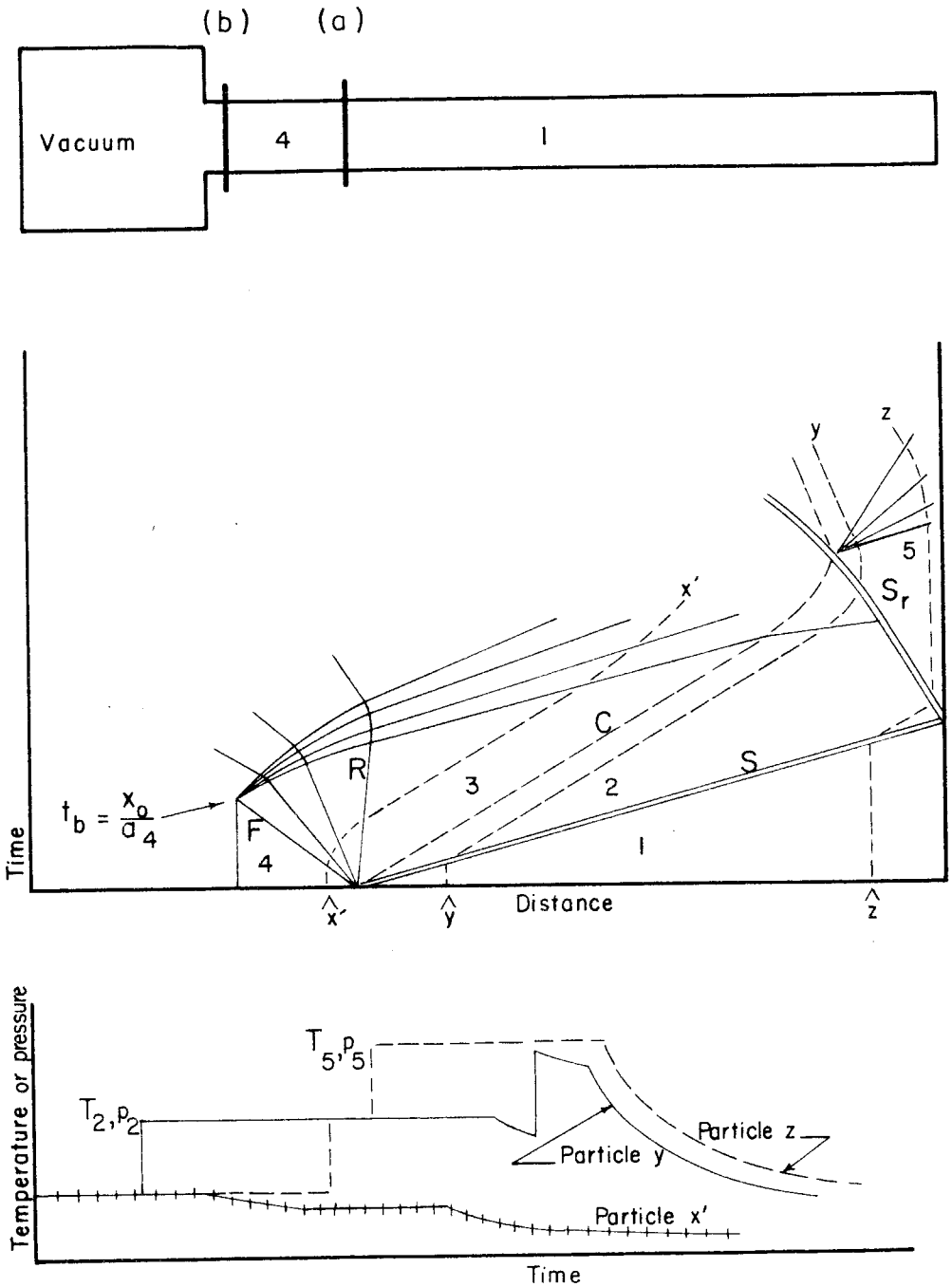

Fig. 9. Description of flow, particle position, and temperature for the reflected shock in a modified shock tube using two diaphragms and a large expansion chamber; S: shock front; C: contact surface; R to F: expansion wave.

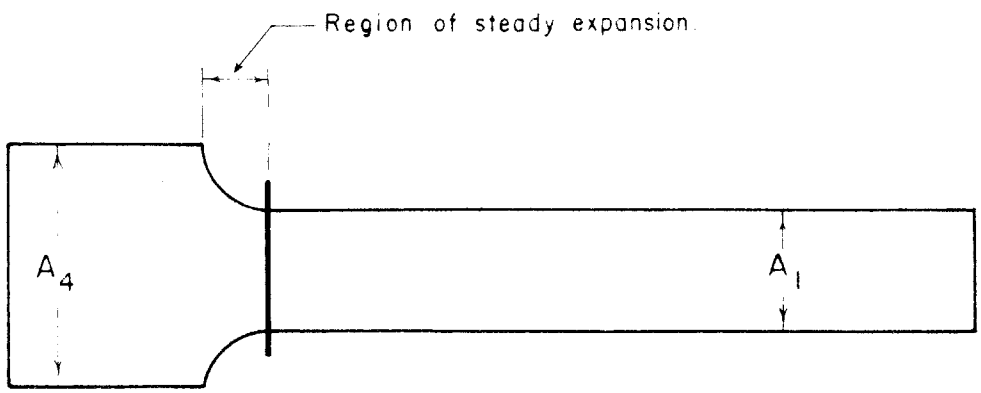

Fig. 10. Schematic diagram of a shock tube utilizing a converging driver section.

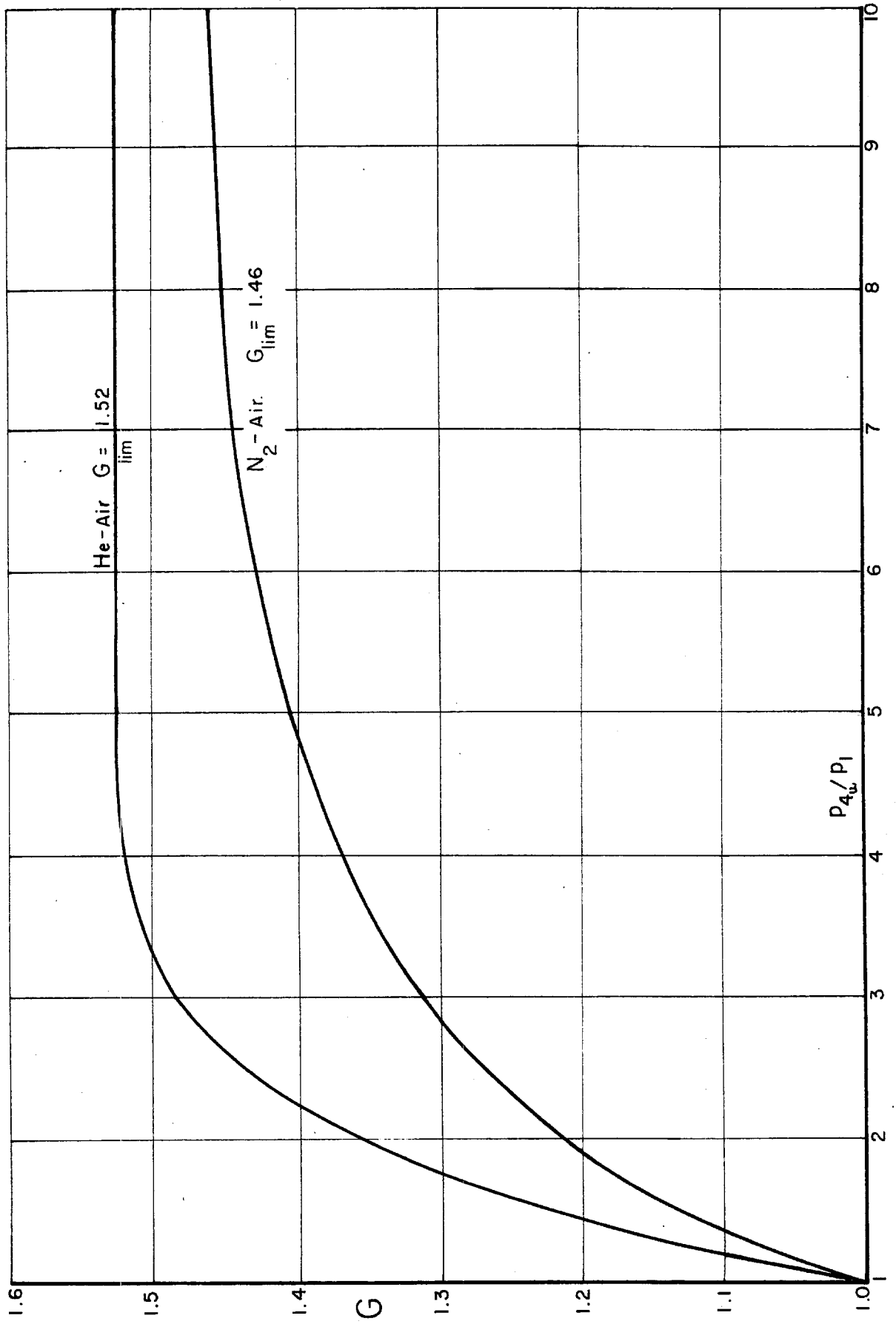

Fig. 11. Gain factor G vs. diaphragm pressure ratio $p_{4_{u1}}/p_1$ for the case of $A_4/A_1 = 2.80$ (from reference 11).

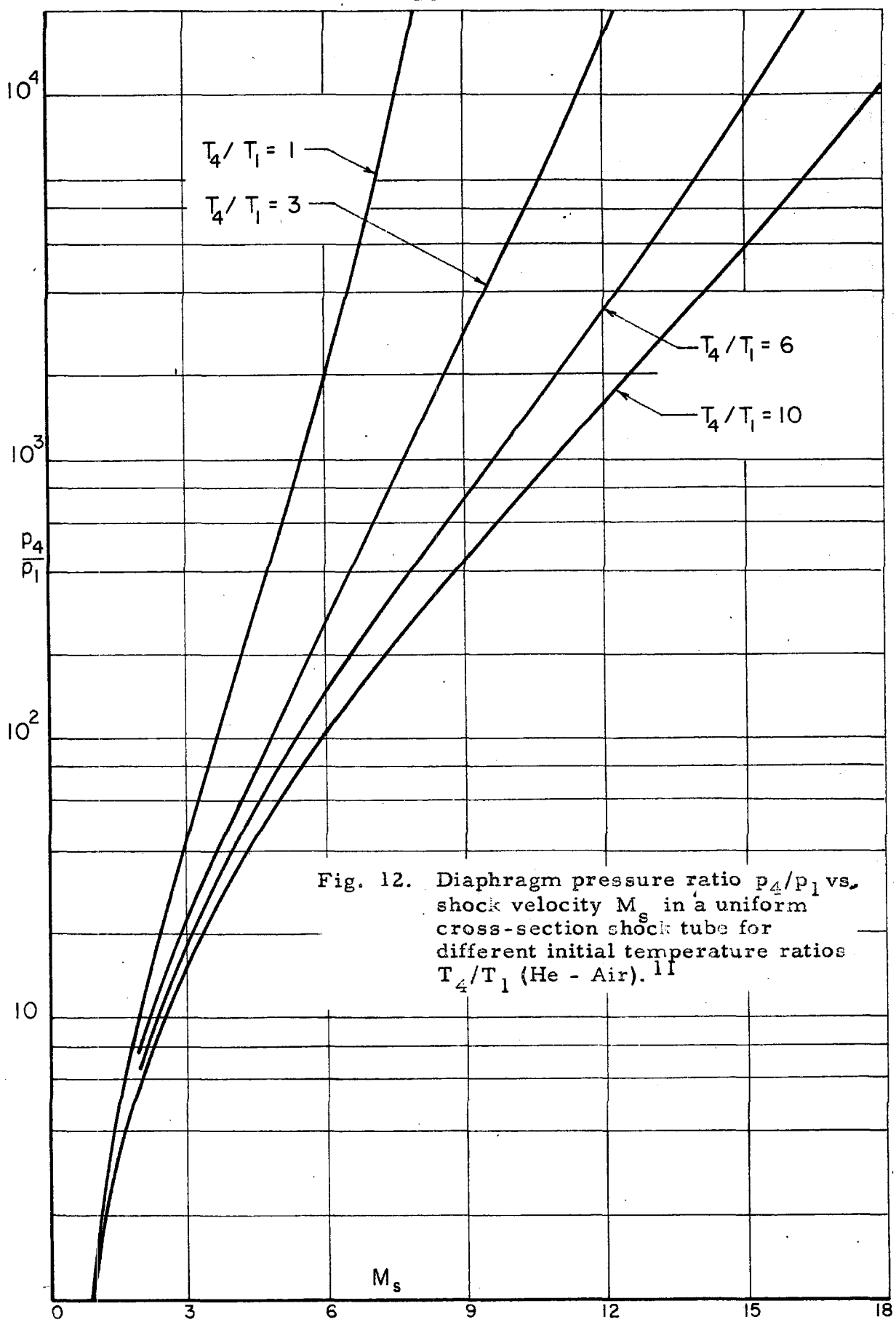

Fig. 12. Diaphragm pressure ratio p_4/p_1 vs. shock velocity M_s in a uniform cross-section shock tube for different initial temperature ratios T_4/T_1 (He - Air).[11]

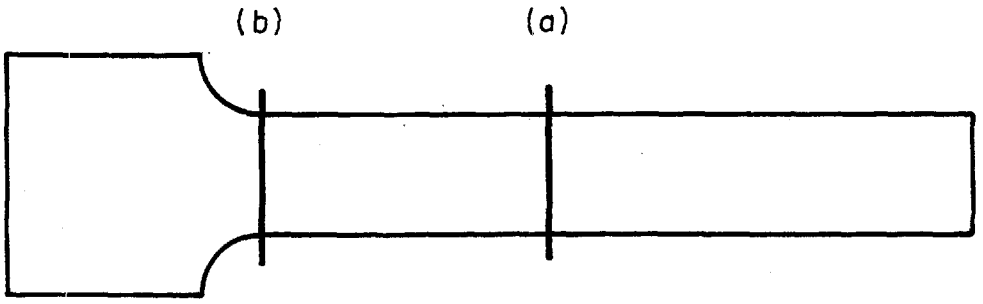

FIG. 13a.

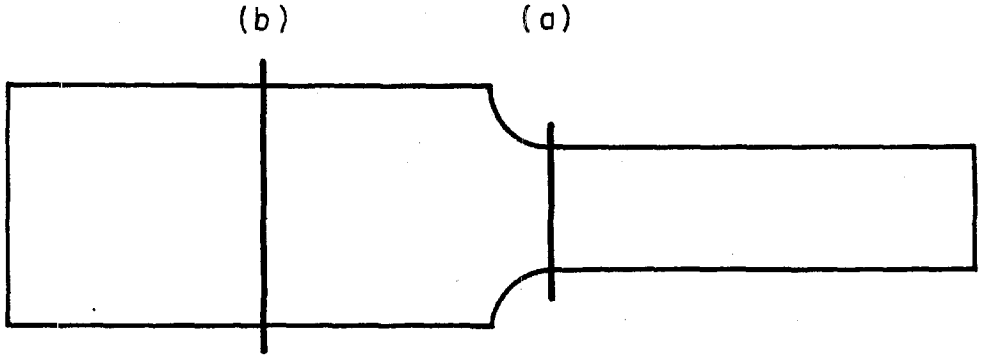

FIG. 13b.

Fig. 13. Two shock tube modifications utilizing both the change-in-area technique and the double-diaphragm method.

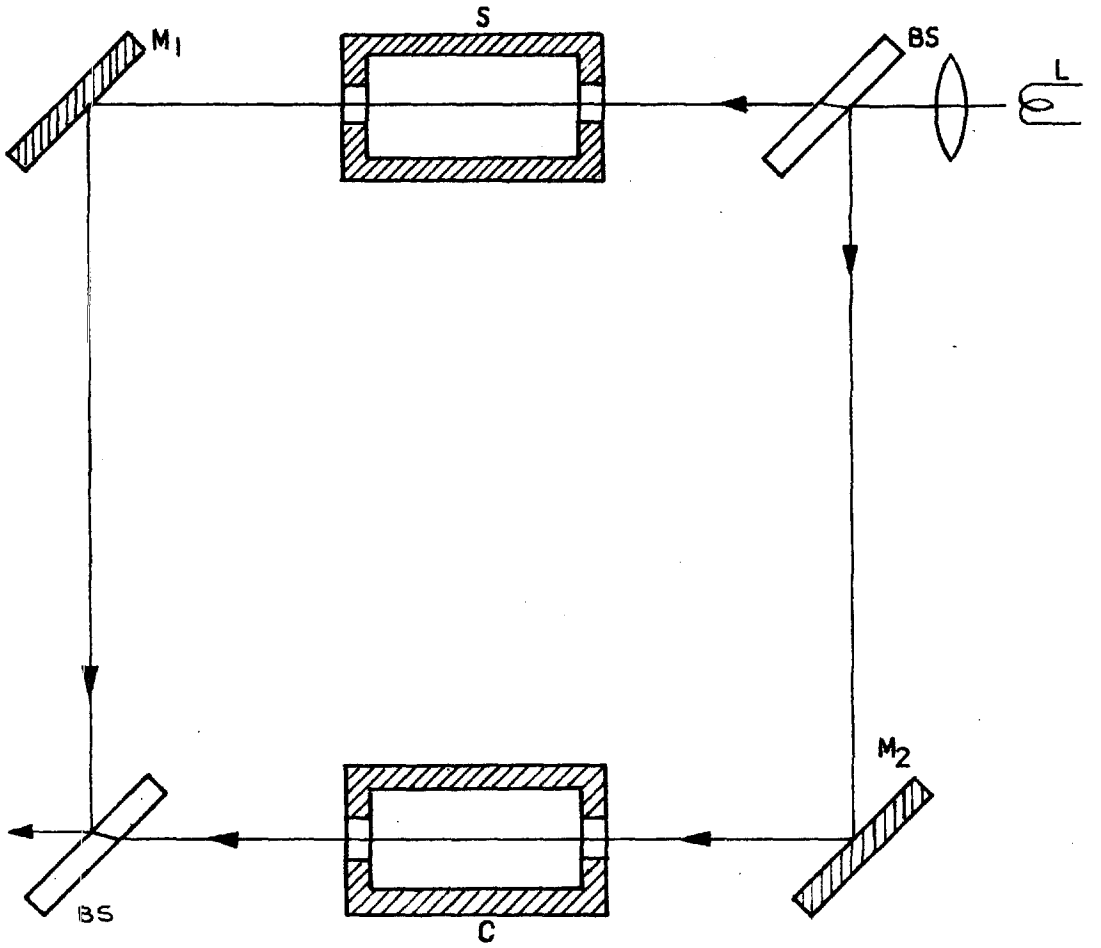

Fig. 14. Interferometer arrangement for the study of density changes behind shock fronts (schematic); L: light source; BS: beam splitter; S: shock tube; M_1 and M_2: plane mirrors; C: compensator.

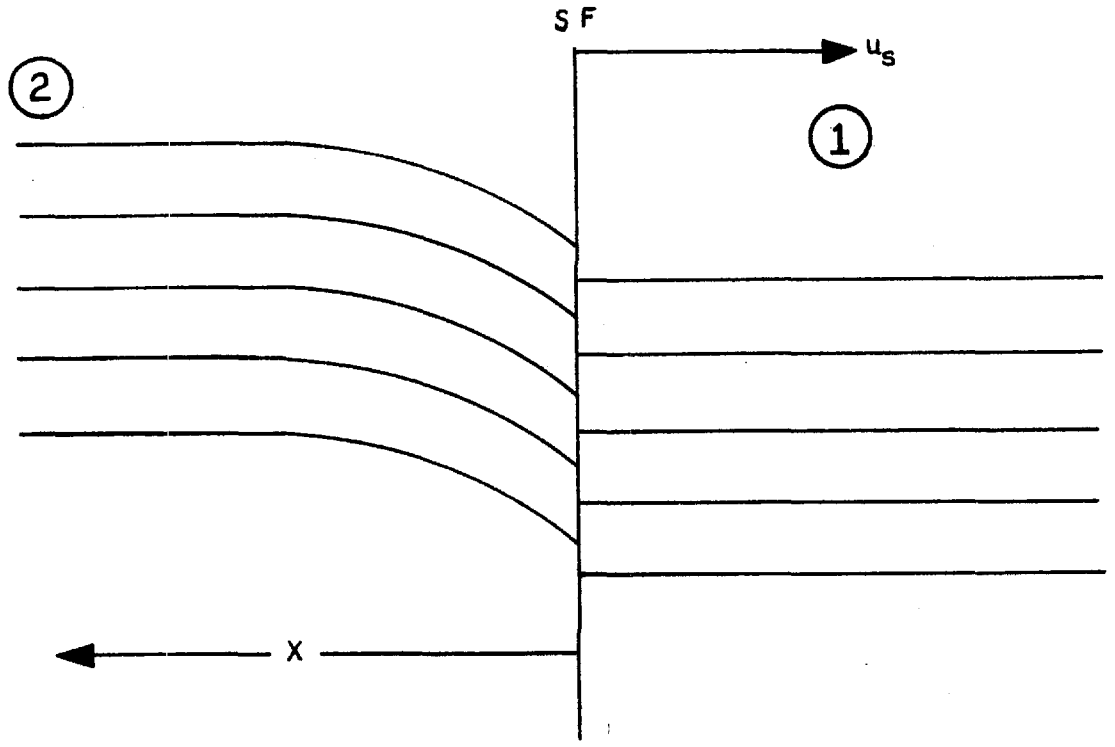

Fig. 15. Interferogram for a shock front (schematic), which is suitable for the determination of vibrational relaxation times; SF: shock front; u_s: shock propagation velocity; x: distance behind the shock front.

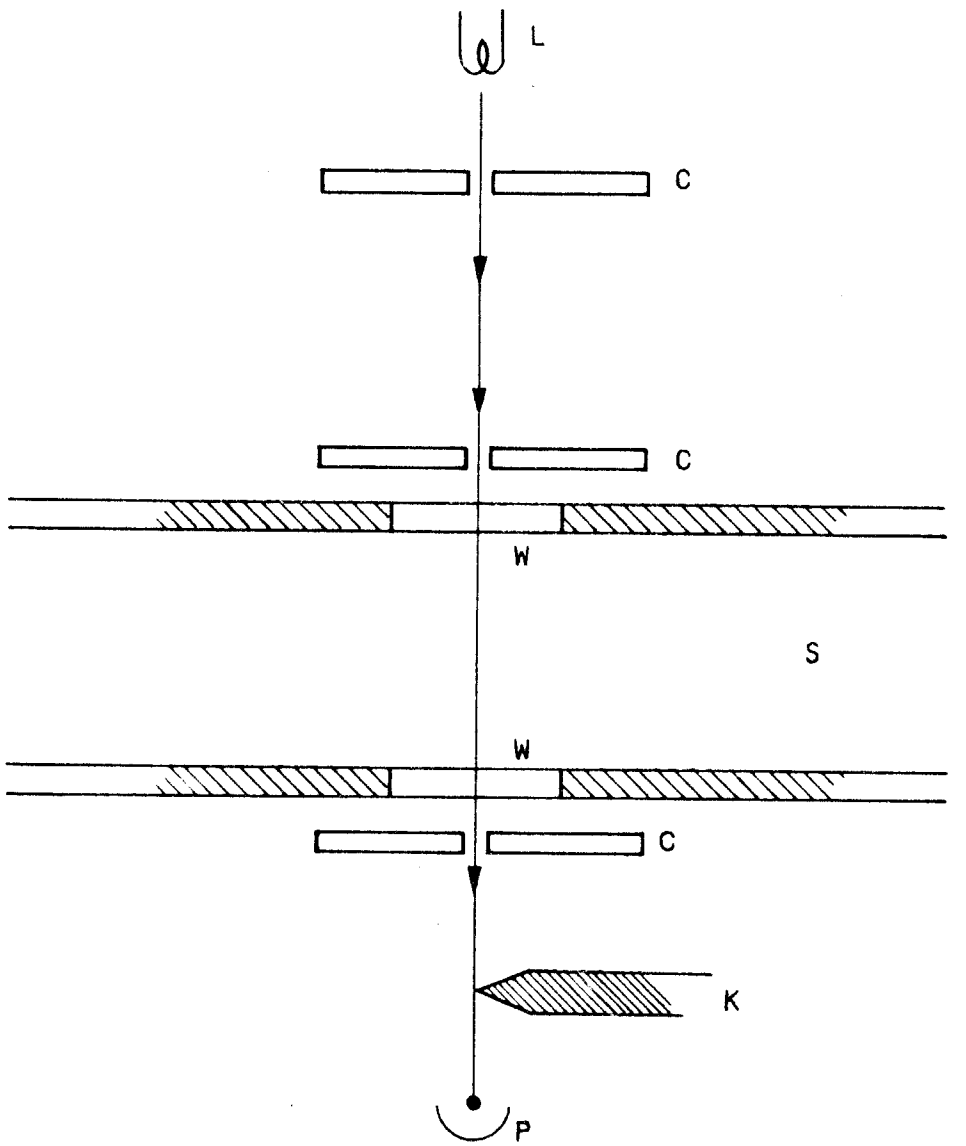

Fig. 16. Schematic diagram illustrating the use of the schlieren method for determining the time at which the maximum density gradient (shock front) passes the observation station; L: light source; C: slits; W: windows; K: knife edge; P: photomultiplier.

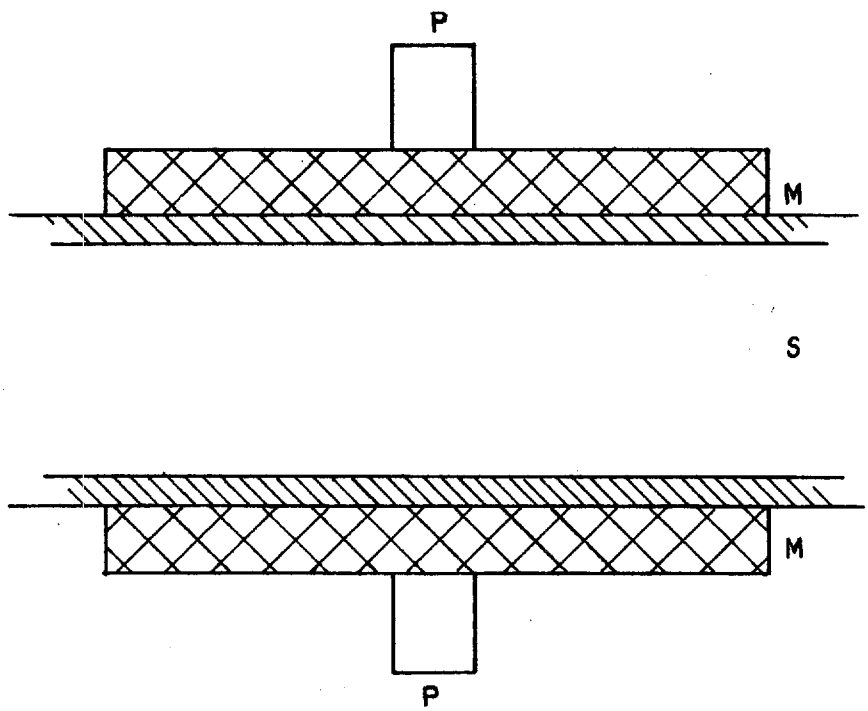

Fig. 17. Schematic diagram of experimental arrangement used for conductivity measurements behind shock fronts; M: field coil; P: pick-up coil; S: shock tube.

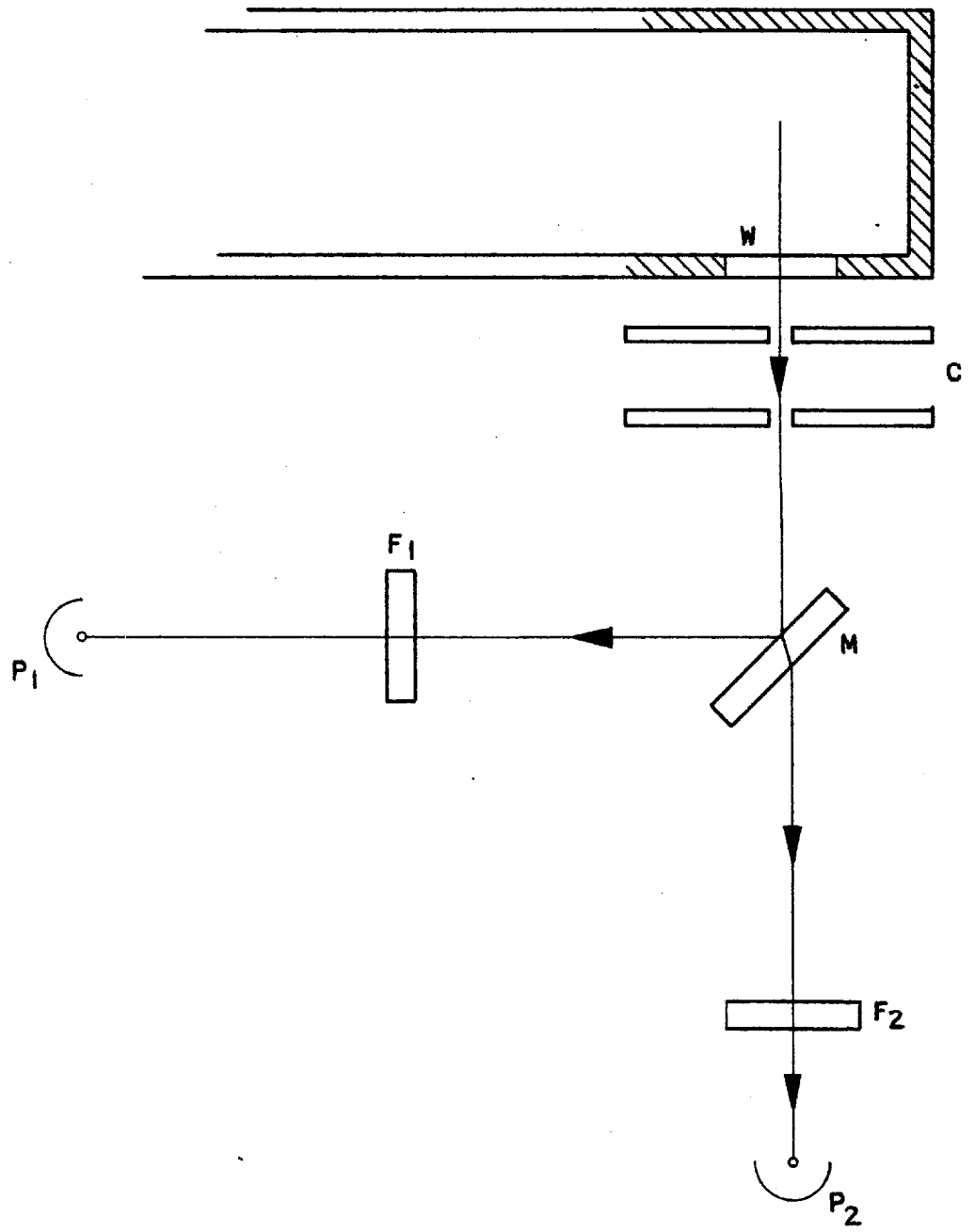

Fig. 18. Schematic diagram showing the experimental arrangement used for determining the temperature behind the reflected shock by use of a two-color technique; W: window near the end of the shock tube; C: collimating slits; M: beam splitter; F_1 and F_2: wavelength (interference) filters; P_1 and P_2: photomultiplier tubes.

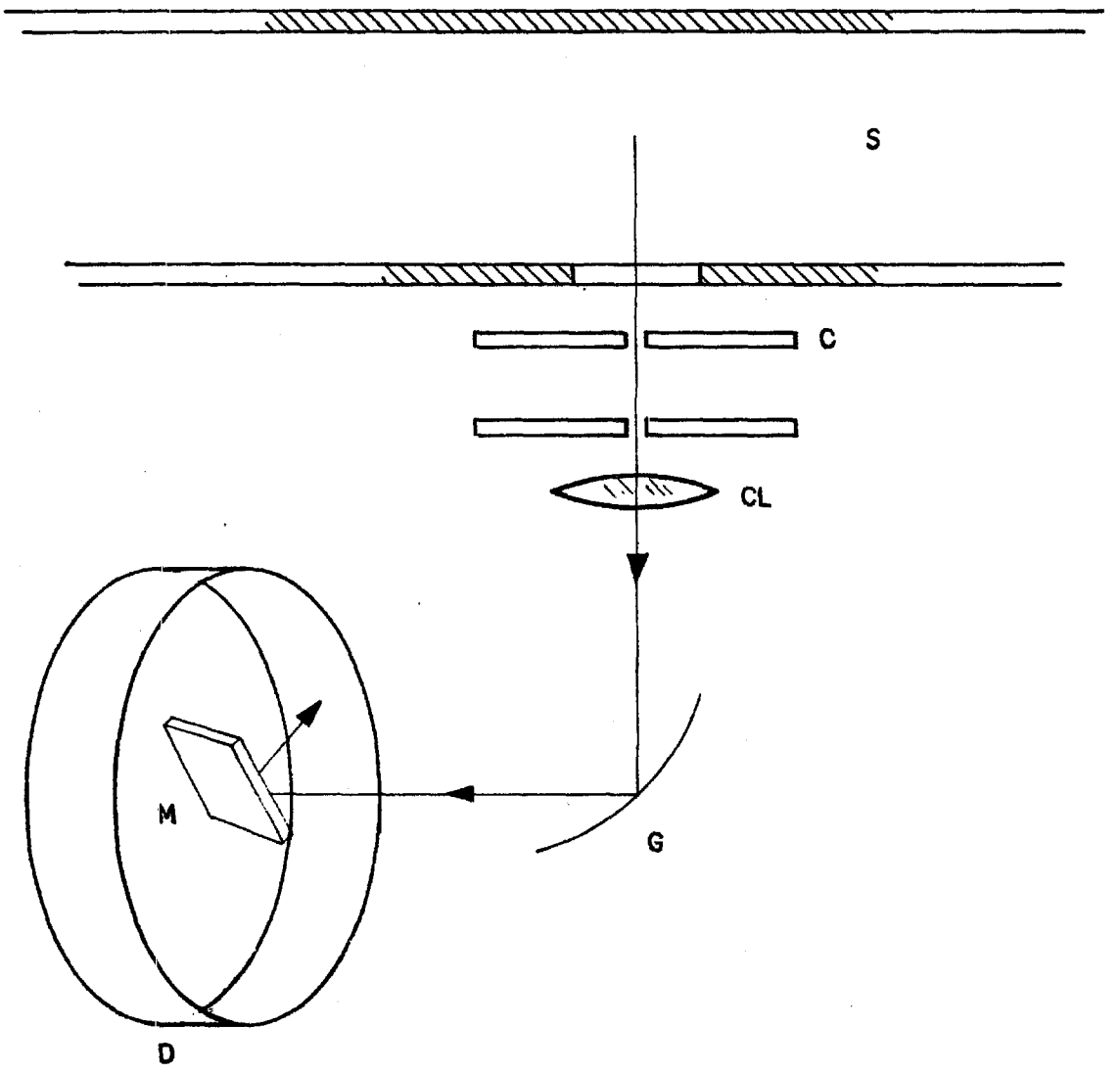

Fig. 19. Schematic diagram showing the optical arrangement used in the rotating-drum-camera-spectrograph combination; S: shock tube; CL: collimating lens; G: concave grating; M: plane mirror; D: drum camera.

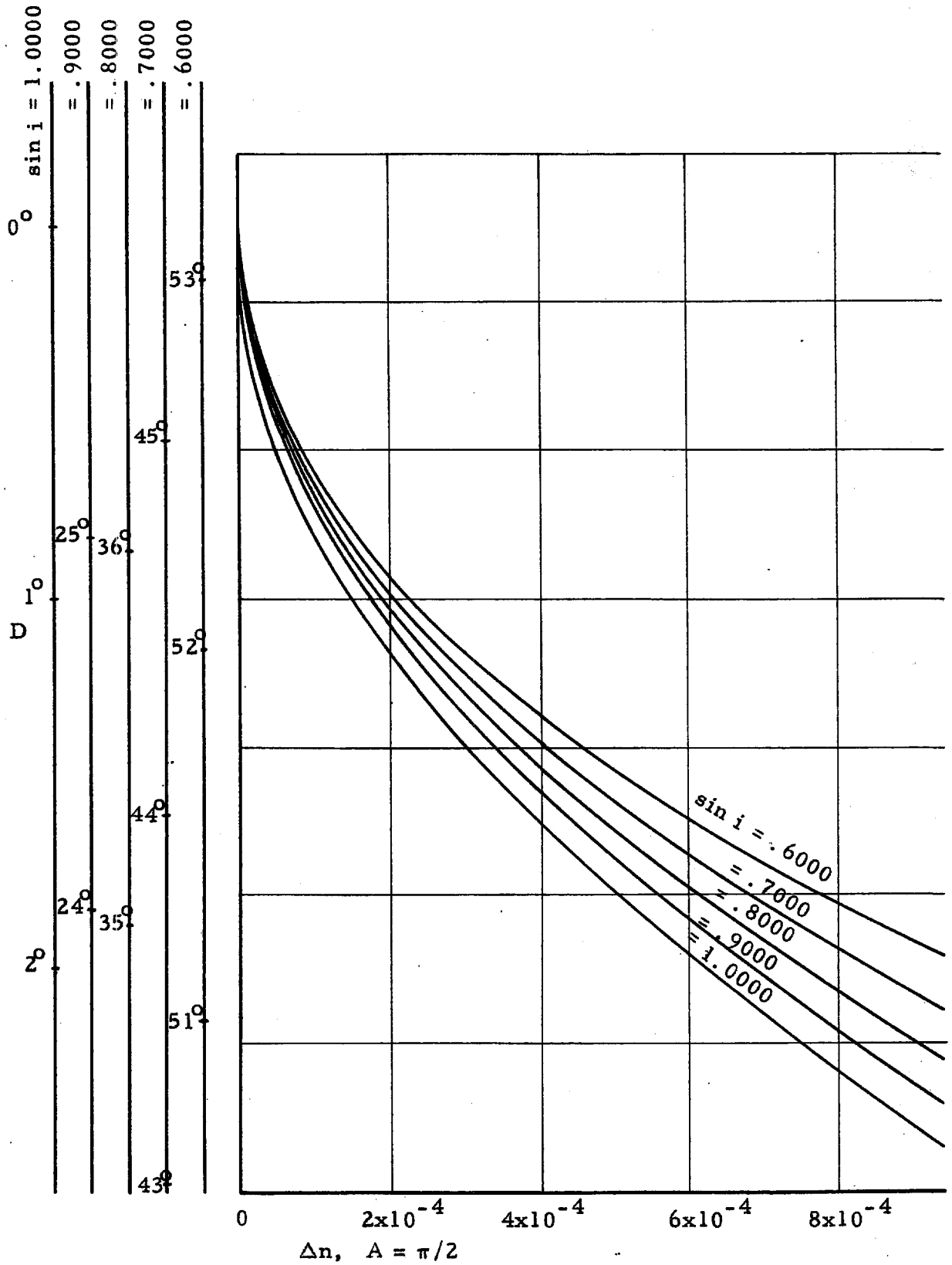

Fig. 20. The deflection angle D as a function of the change in index of refraction (Δn) for various values of the sine of the angle of incidence (sin i) for a prism angle $A = 90^{\circ}$. (Data taken from V. Vali).

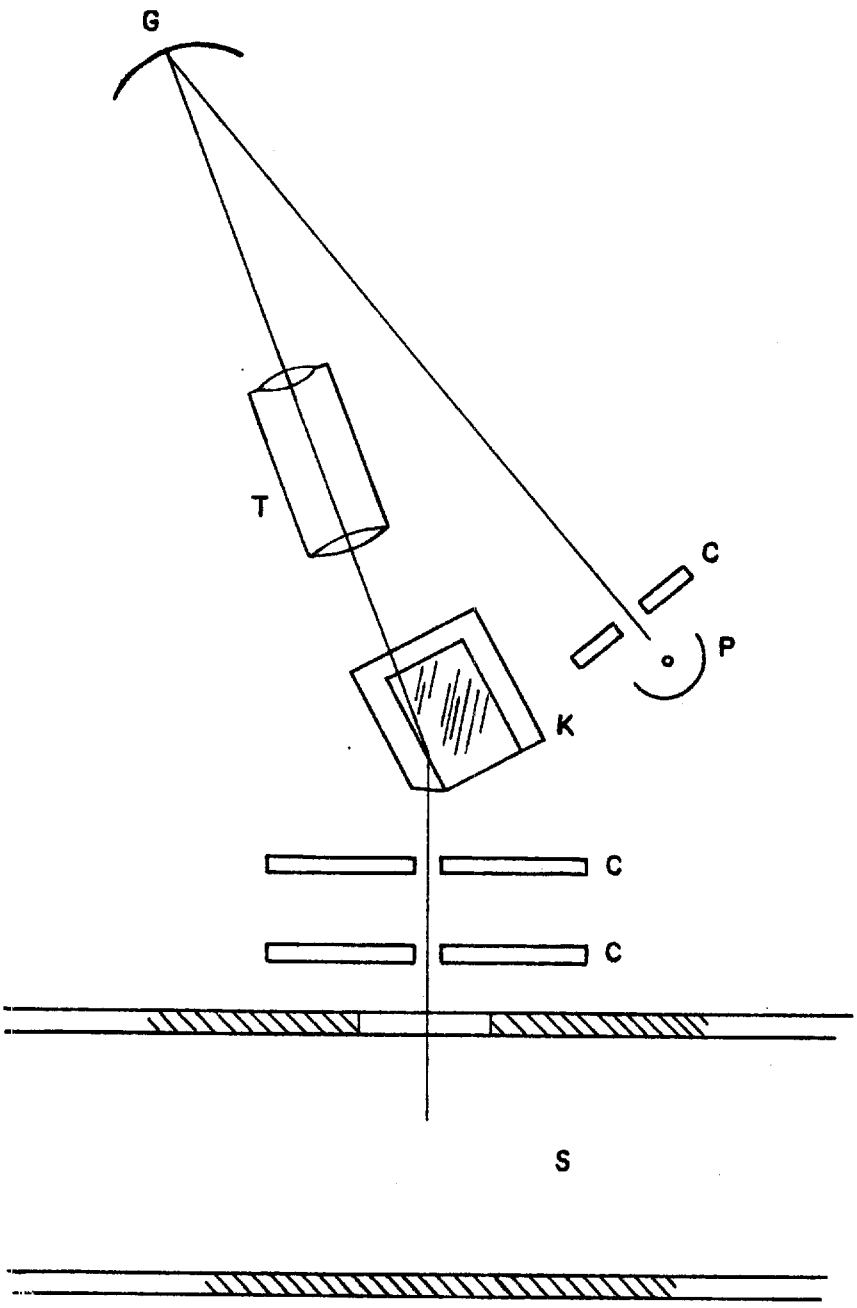

Fig. 21. Scanning spectrograph for shock-tube studies (schematic); S: shock tube; K: Kerr-cell-prism; T: telescope; G: concave grating; C: fixed slit; P: photomultiplier.

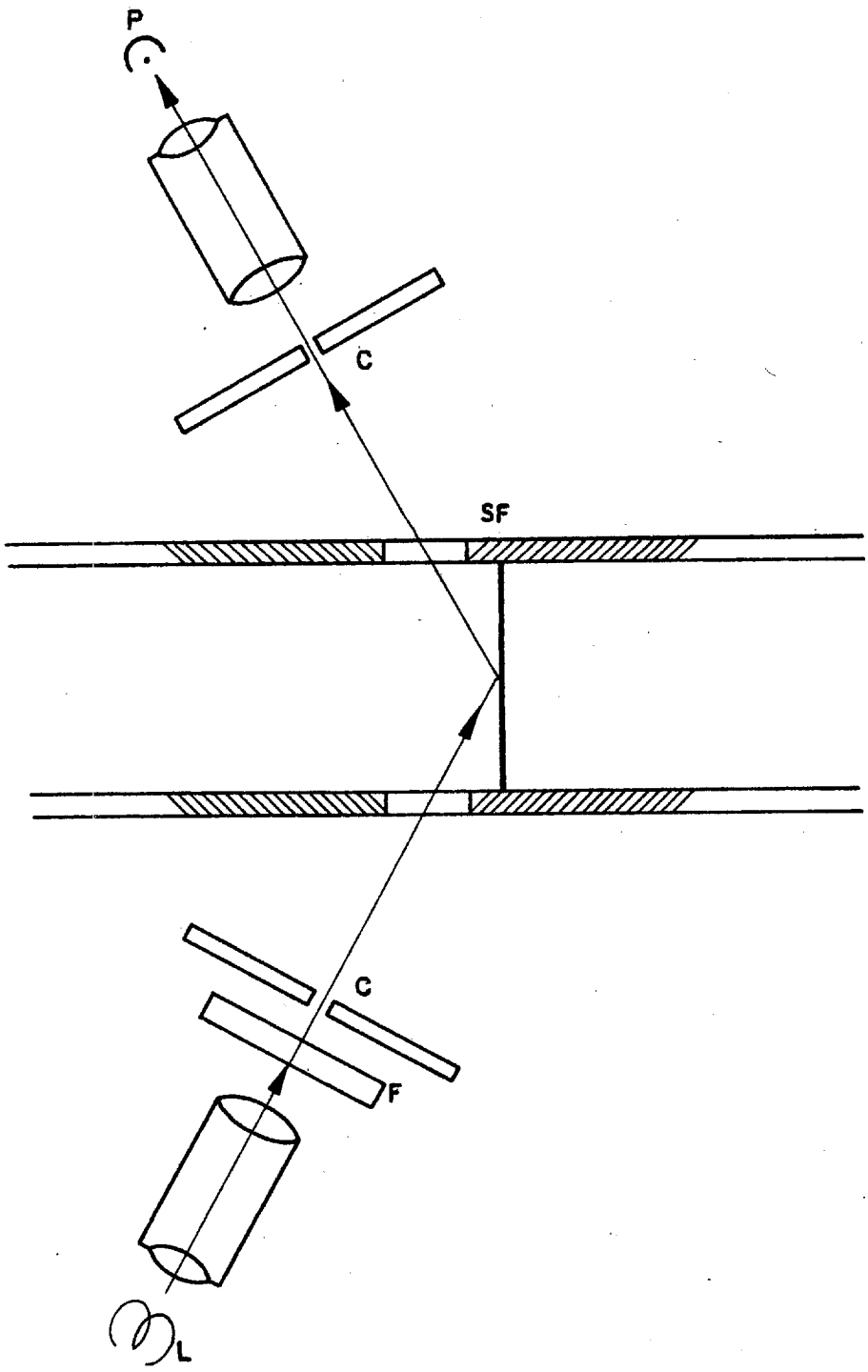

Fig. 22. Schematic diagram showing the optical arrangement used for shock reflection measurements; L: light source; F: filter; C: slits; SF: shock front; P: photomuliplier.

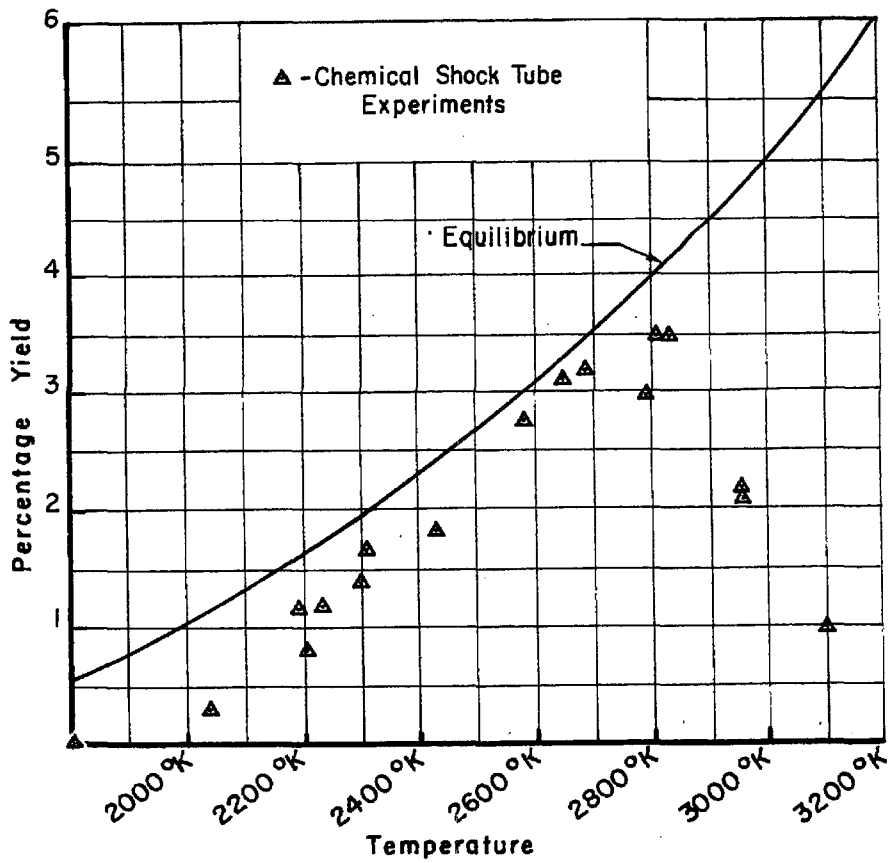

Fig. 23. Nitric oxide concentration formed behind reflected shocks as a function of peak temperature, from reference 43.

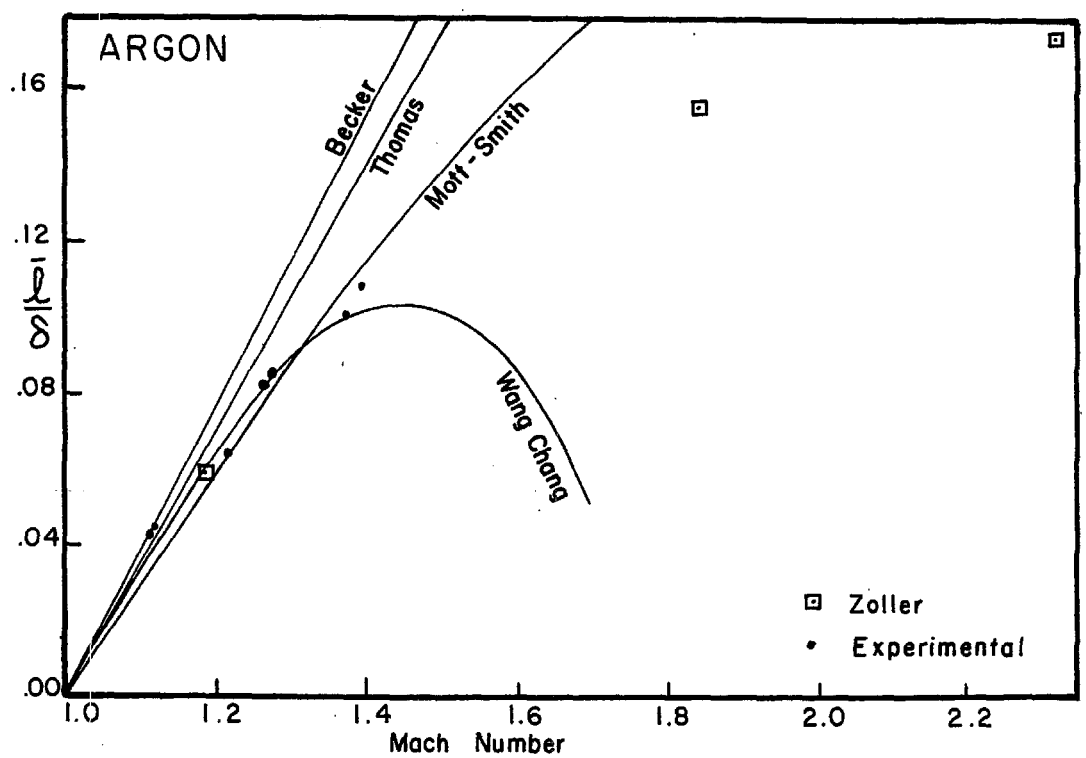

Fig. 24. The ratio of mean free path $\bar{\ell}$ to shock front thickness δ as a function of shock Mach number, from reference 69.

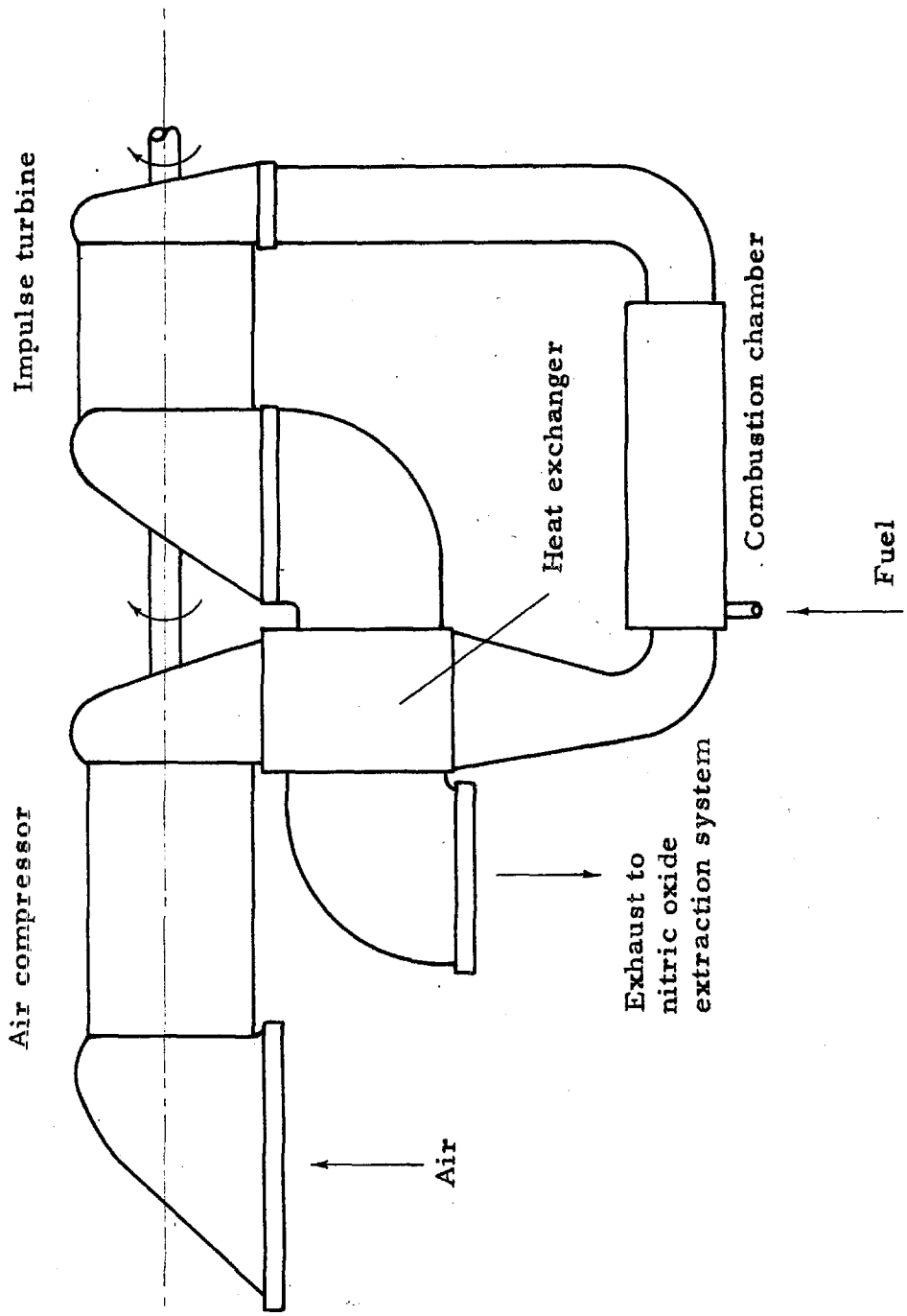

Fig. 25. Gas turbine cycle for the production of nitric oxide from air.

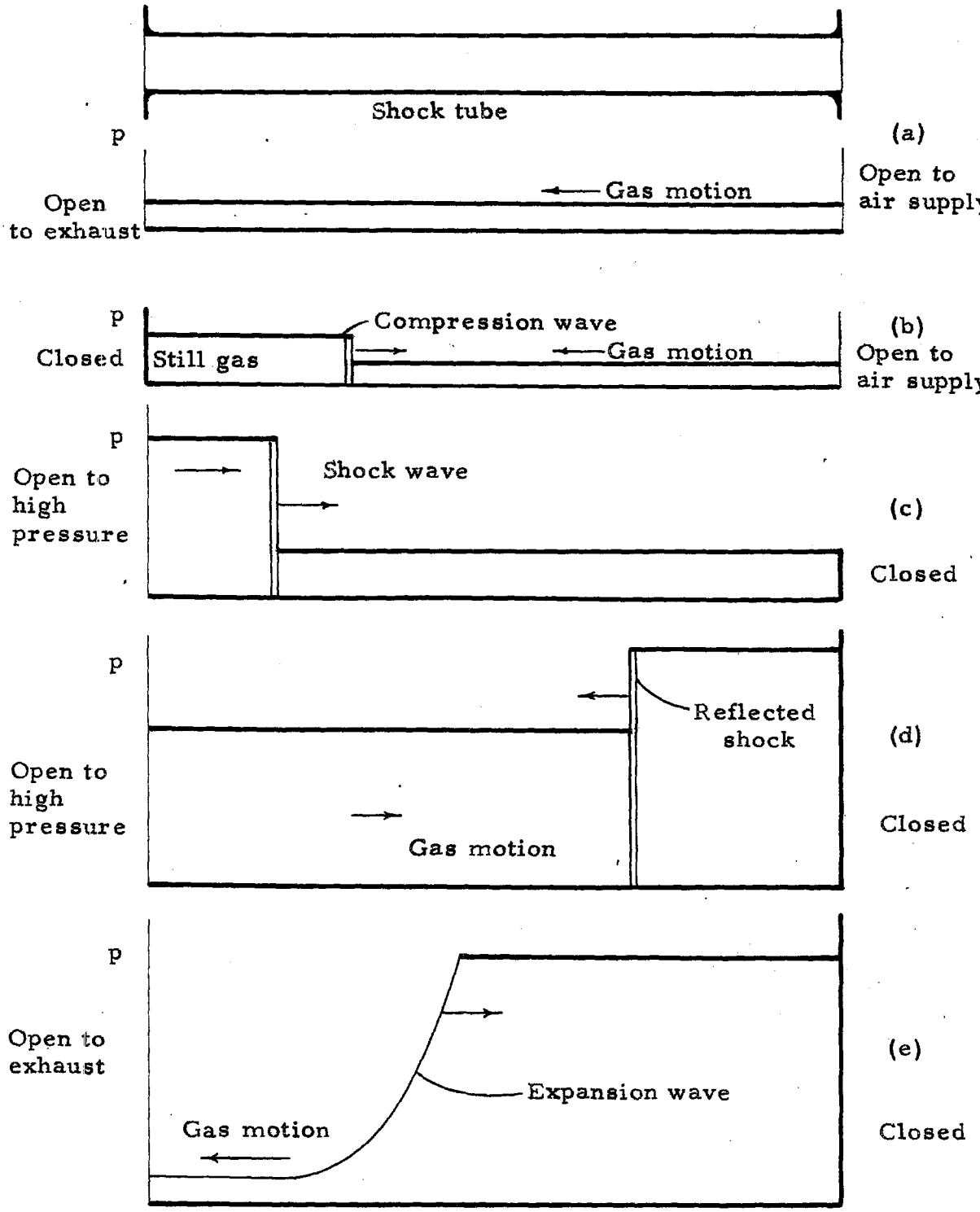

Fig. 26. A cycle for the continuous production of chemicals in a shock tube.

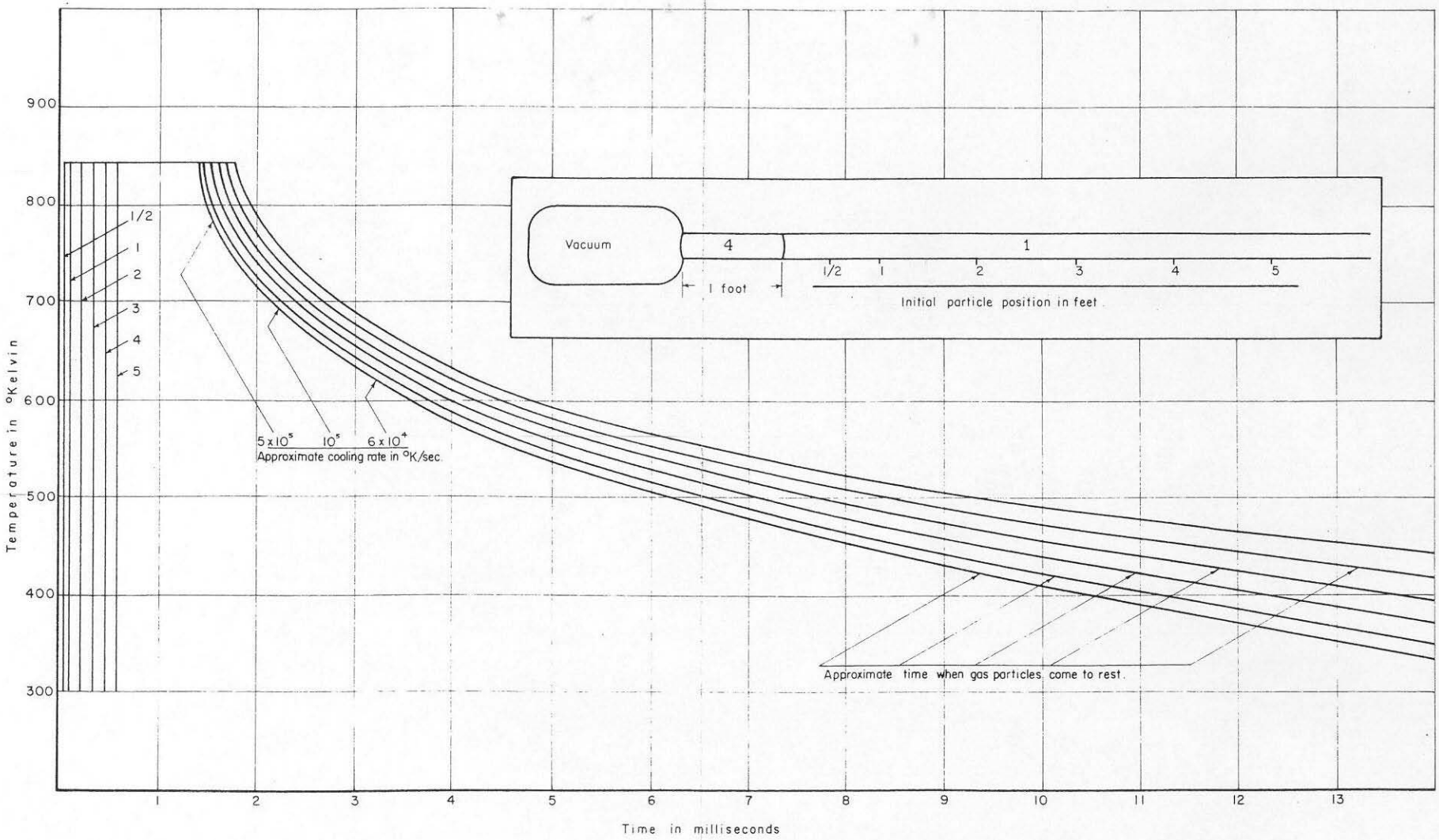

FIG. 27. Calculated temperature versus time history for particles initially located at different positions in the shock tube (see insert); gas 4 = helium; gas 1 = $4NH_3 + O_2$.

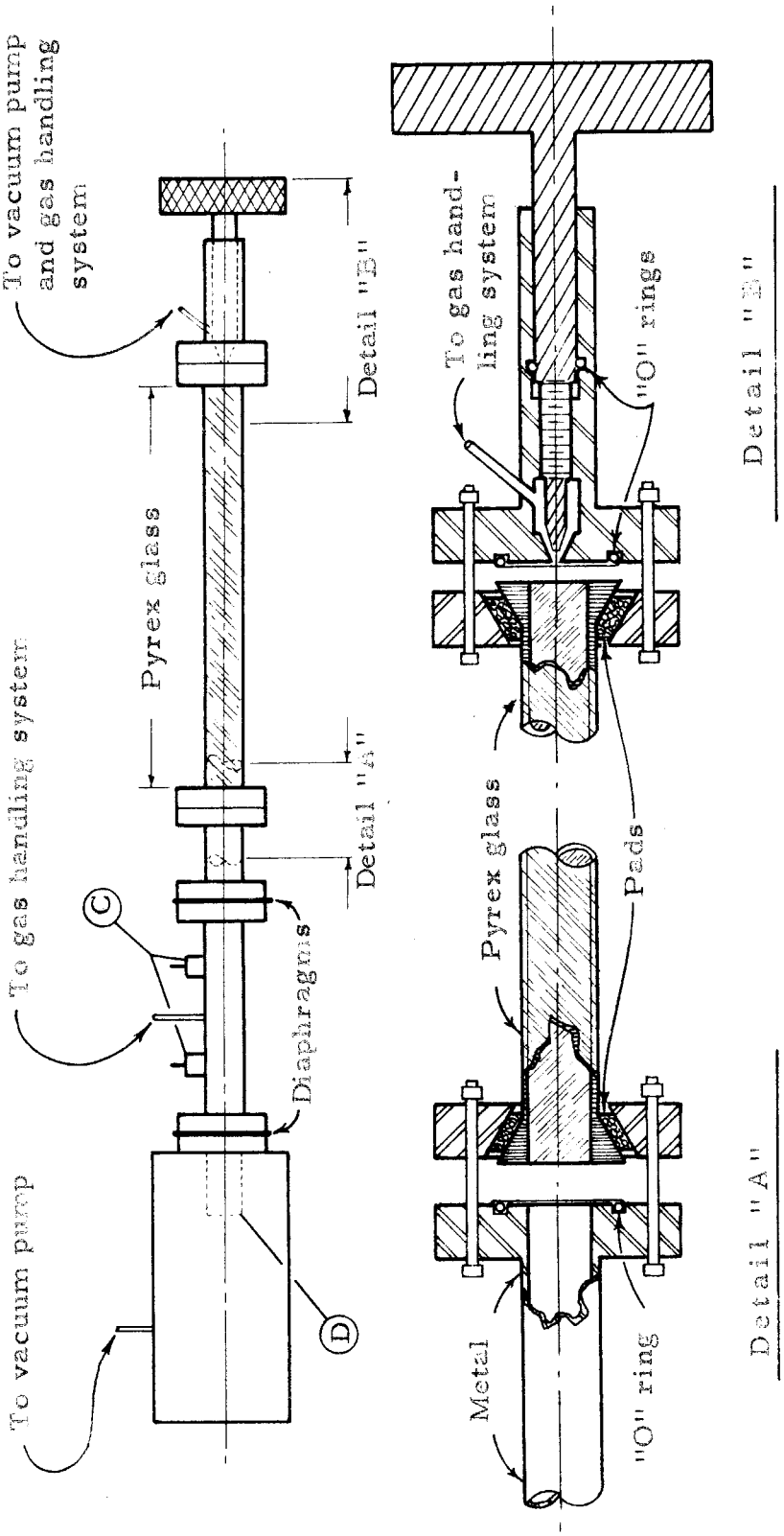

(C) Double-diaphragm breaking mechanism (see fig. 31).

(D) Short shock-tube section to reduce the effect of reflected compression waves.

Fig. 28. The chemical shock tube used for preliminary studies of hydrazine formation.

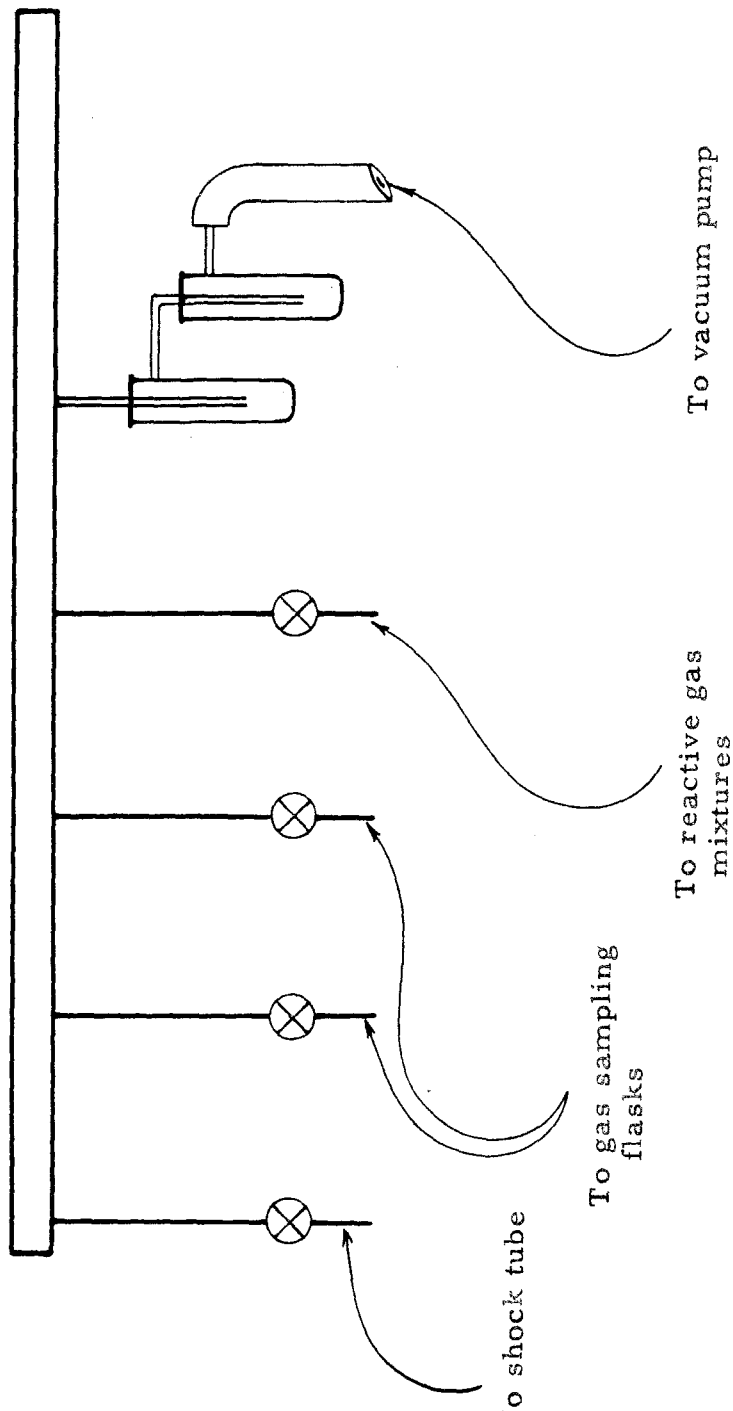

Fig. 29. The low-pressure gas-handling system for the chemical shock tube (schematic).

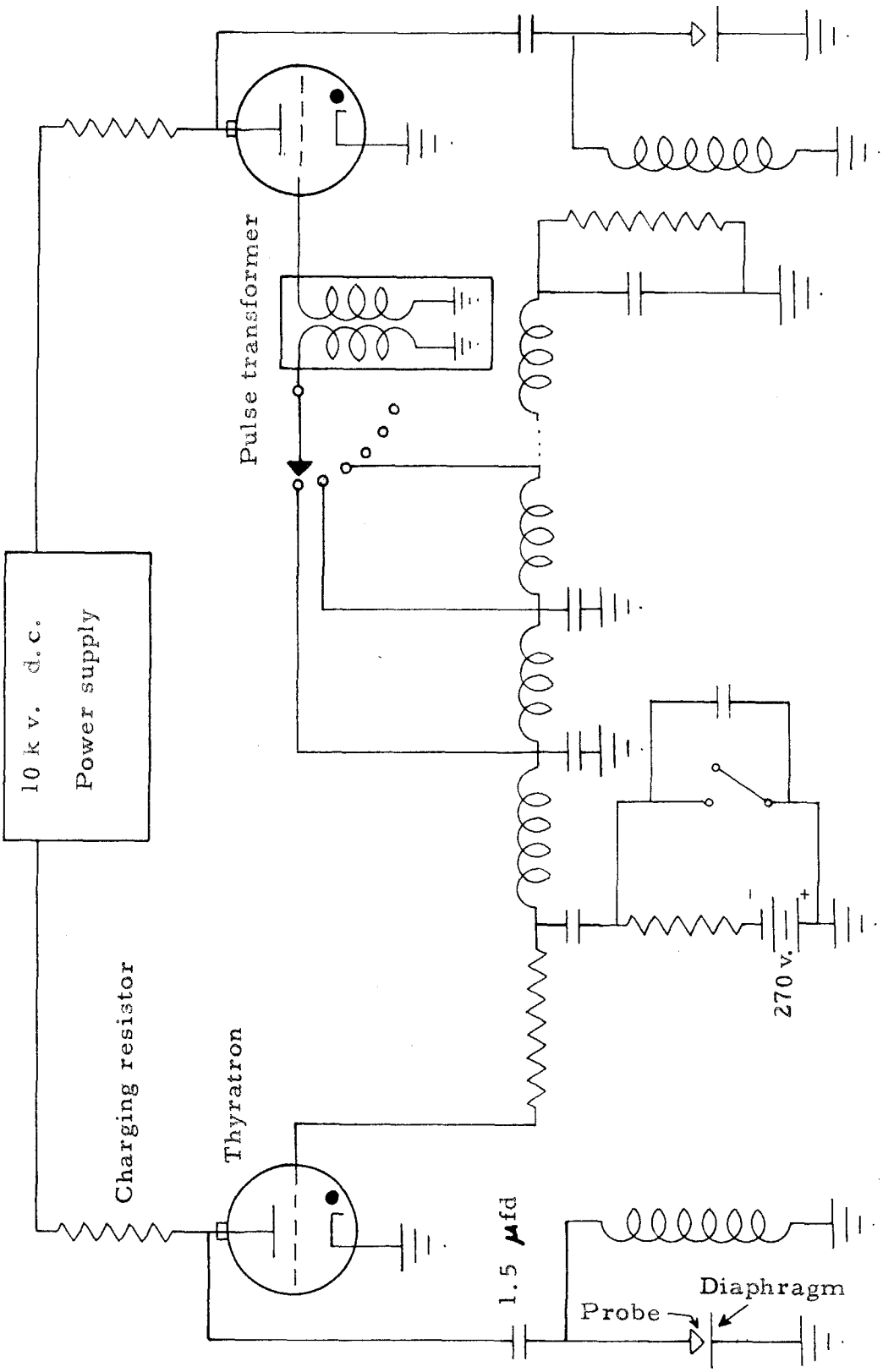

Fig. 30. The electronic circuit used to puncture two diaphragms at a known time interval.

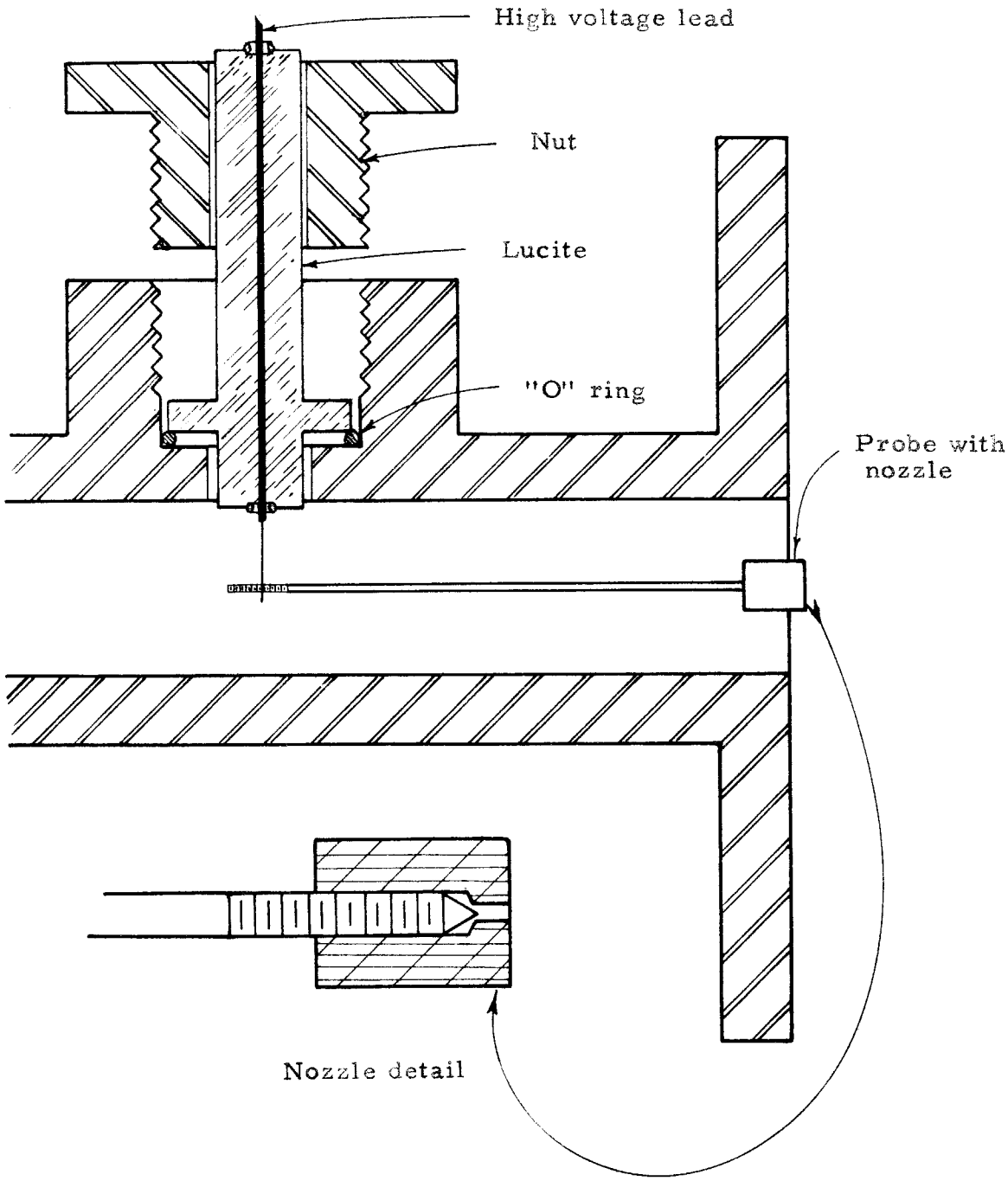

Fig. 31. The high-pressure spark gap section of the chemical shock tube with nozzle detail.

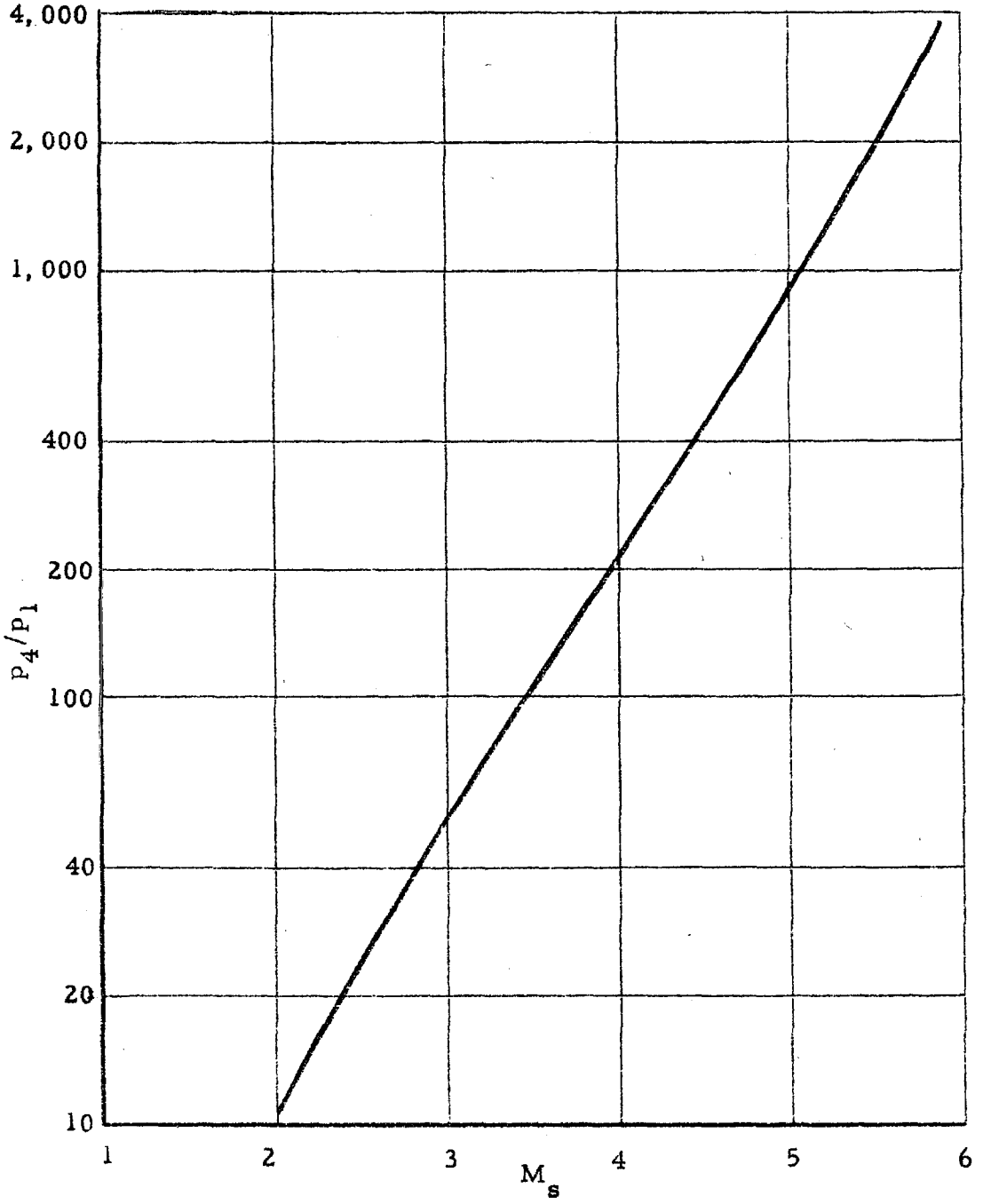

Fig. 32. Pressure ratio p_4/p_1 vs. incident shock Mach number M_s for acetylene; equilibrium value of γ; $T_1 = 300^{\circ}K$ ($a_1 = 1139$ ft/sec).

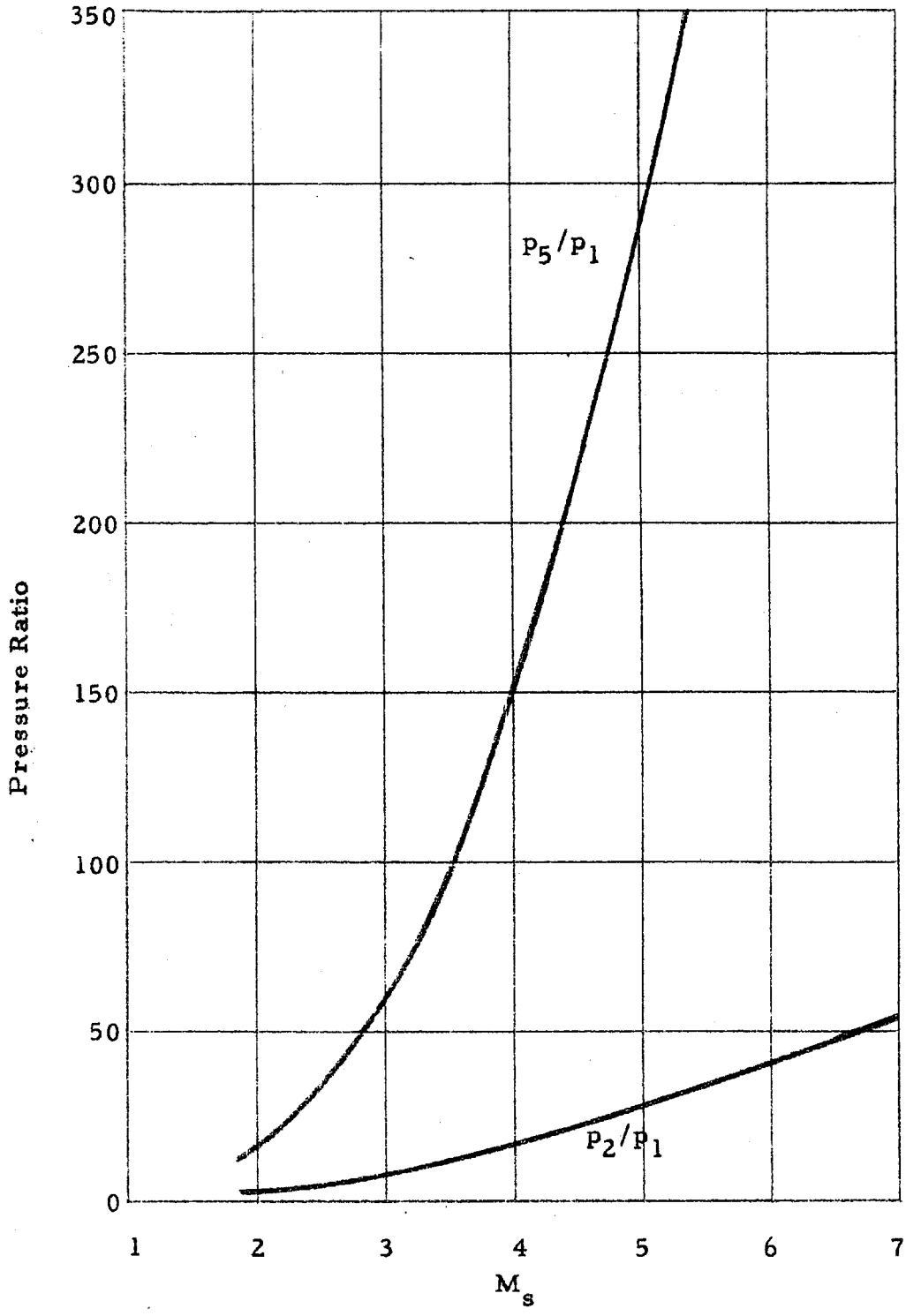

Fig. 33. Pressure ratios p_5/p_1 and p_2/p_1 vs. incident shock Mach number for acetylene; equilibrium value of γ; $T_1 = 300^{\circ}K$ ($a_1 = 1139$ ft/sec).

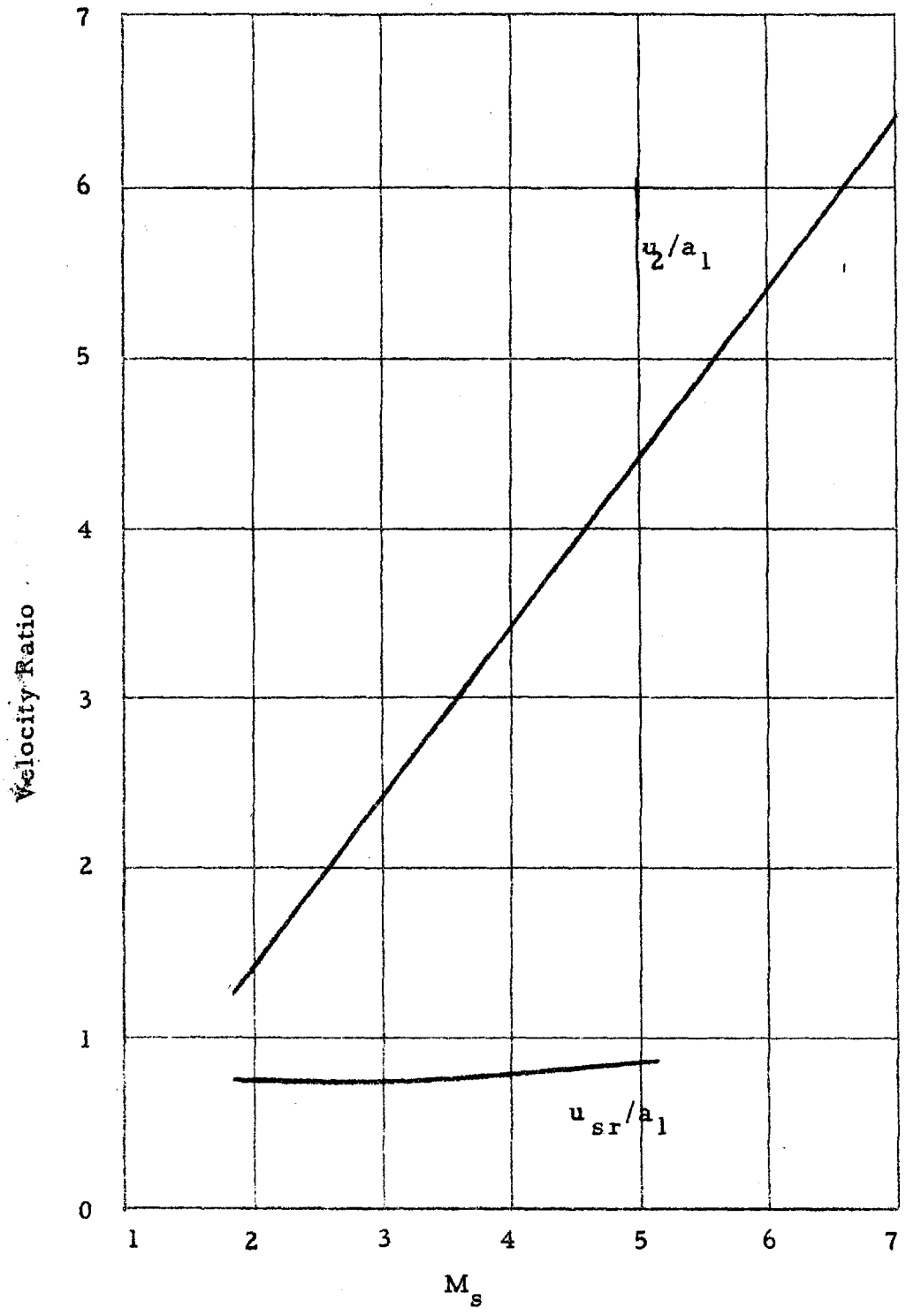

Fig. 34. Velocity ratios u_2/a_1 and u_{sr}/a_1 vs. incident shock Mach number for acetylene; equilibrium value of γ; $T_1 = 300^{\circ}K$ ($a_1 = 1139$ ft/sec).

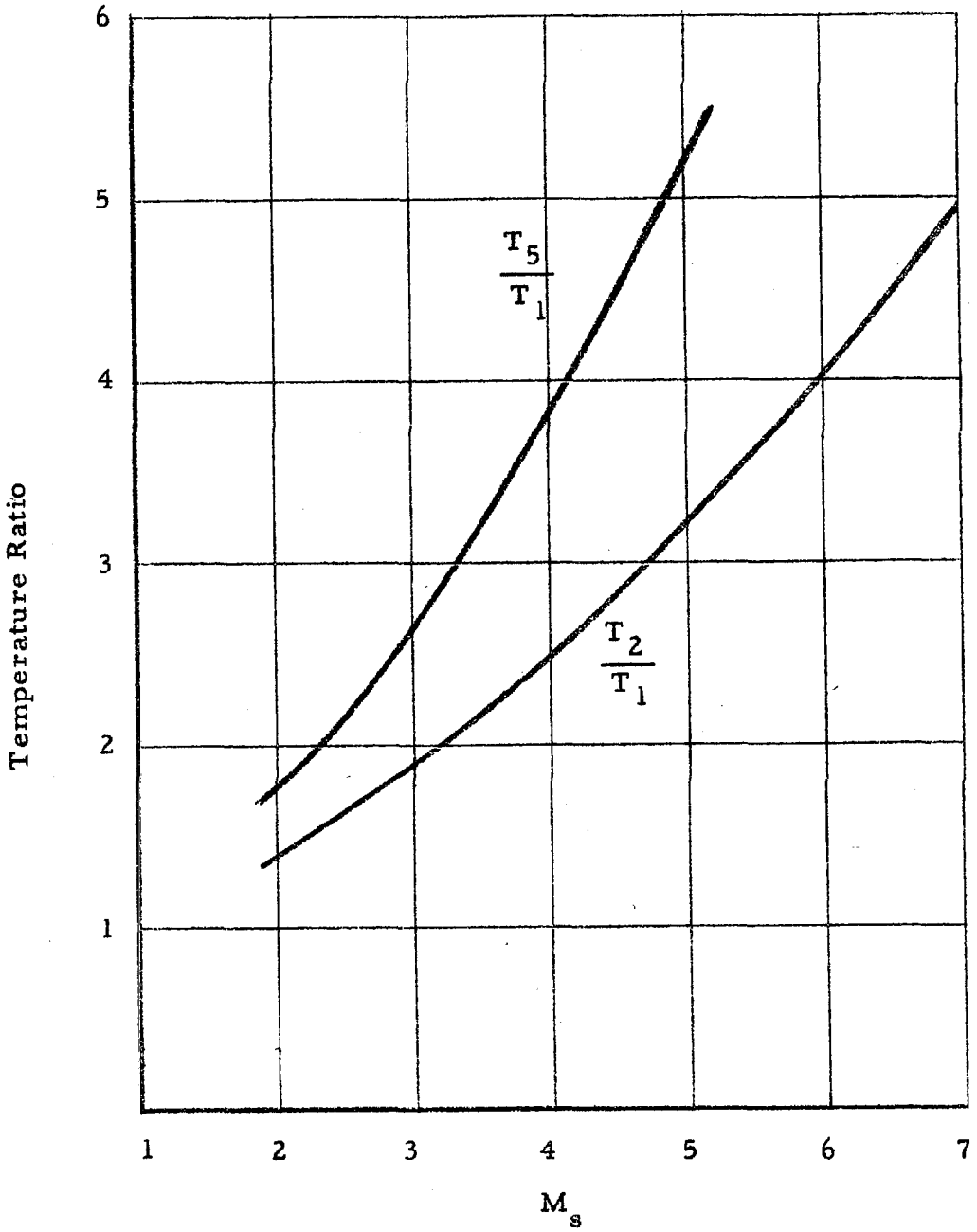

Fig. 35. Temperature ratios T_5/T_1 and T_2/T_1 vs. initial shock Mach number for acetylene; equilibrium value of γ; $T_1 = 300\ ^{o}K$ ($a_1 = 1139$ ft/sec).

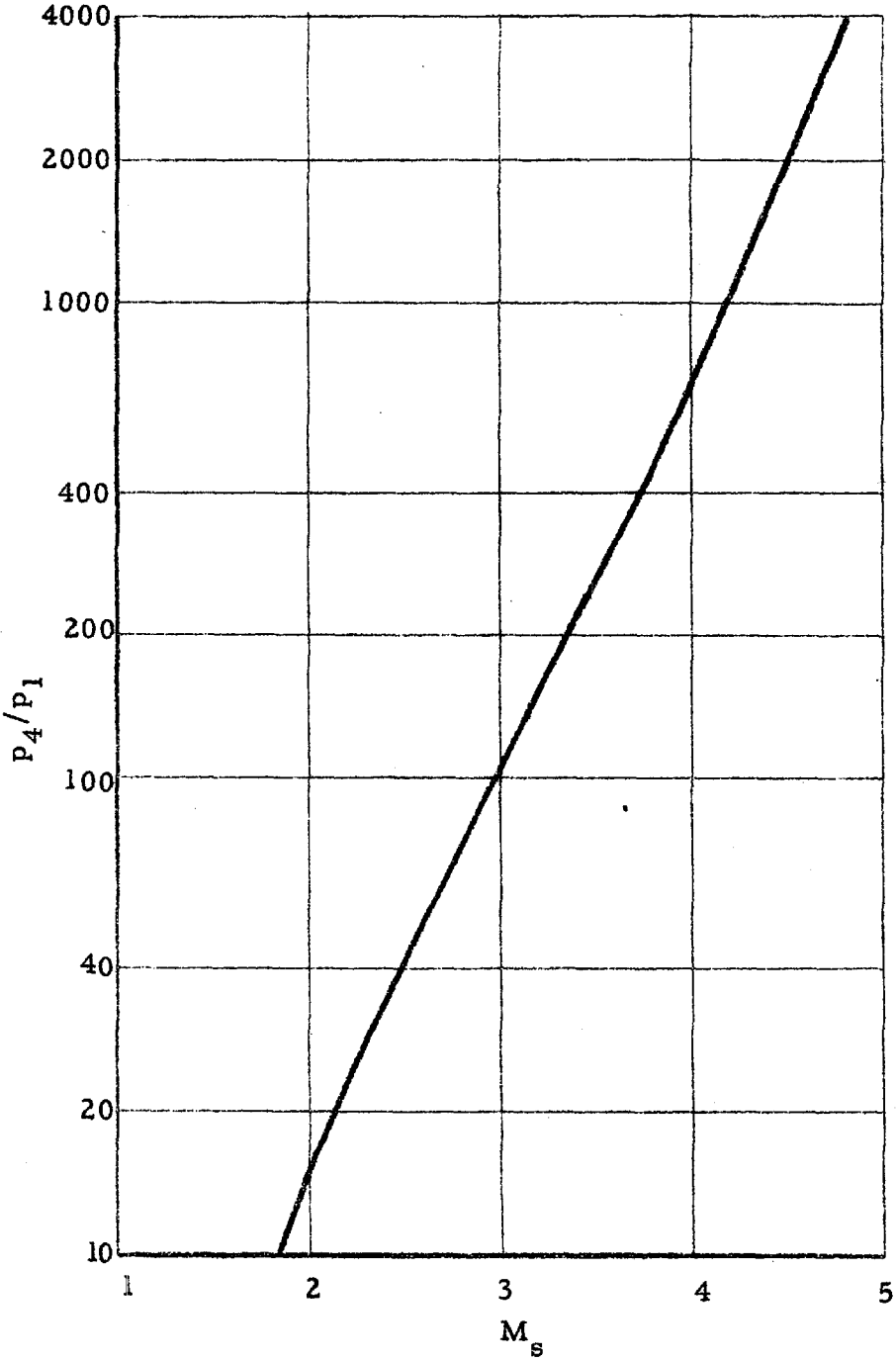

Fig. 36. Initial pressure ratio p_4/p_1 vs. initial shock Mach number for methane; equilibrium value of γ; $T_1 = 300^{\circ}K$ ($a_1 = 1558$ ft/sec).

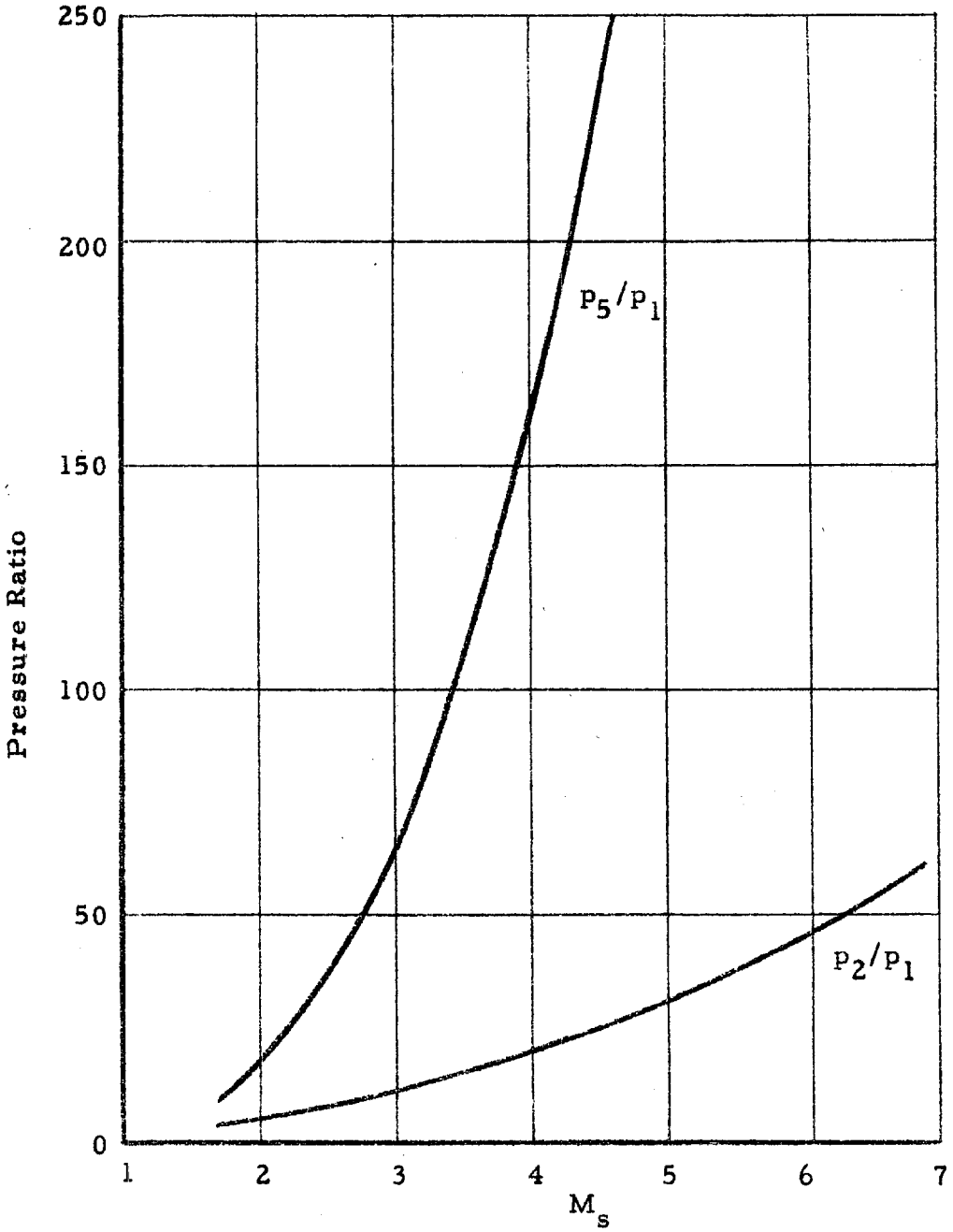

Fig. 37. Pressure ratios p_5/p_1 and p_2/p_1 vs. incident shock Mach number for methane; equilibrium value of γ; $T_1 = 300^{\circ}K$ ($a_1 = 1558$ ft/sec).

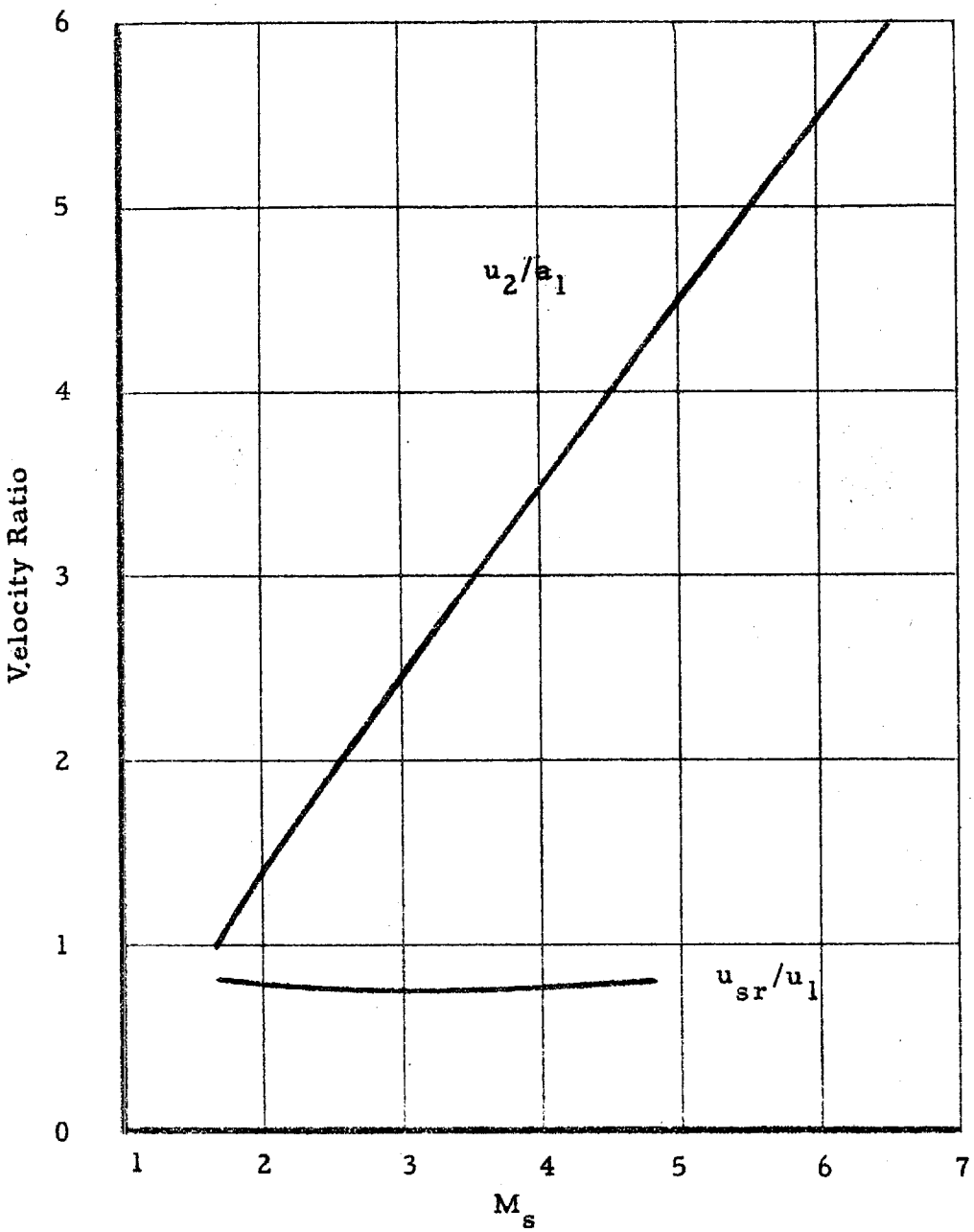

Fig. 38. Velocity ratios u_2/a_1 and u_{sr}/a_1 vs. incident shock Mach number for methane; equilibrium value of γ; $T_1 = 300^{\circ}K$ ($a_1 = 1558$ ft/sec).

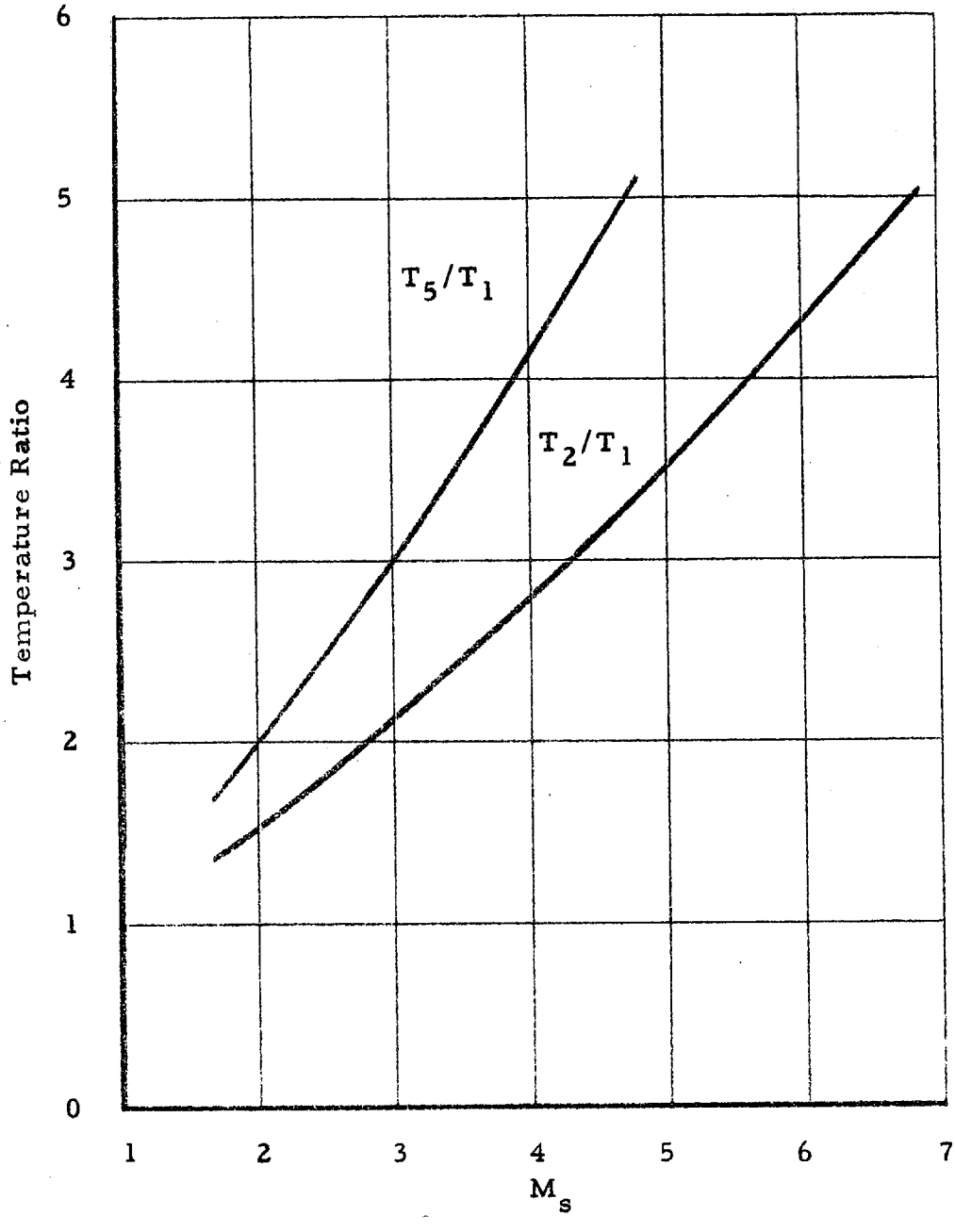

Fig. 39. Temperature ratios T_5/T_1 and T_2/T_1 vs. incident shock Mach number for methane; equilibrium value of γ; $T_1 = 300^{\circ}K$ ($a_1 = 1558$ ft/sec).

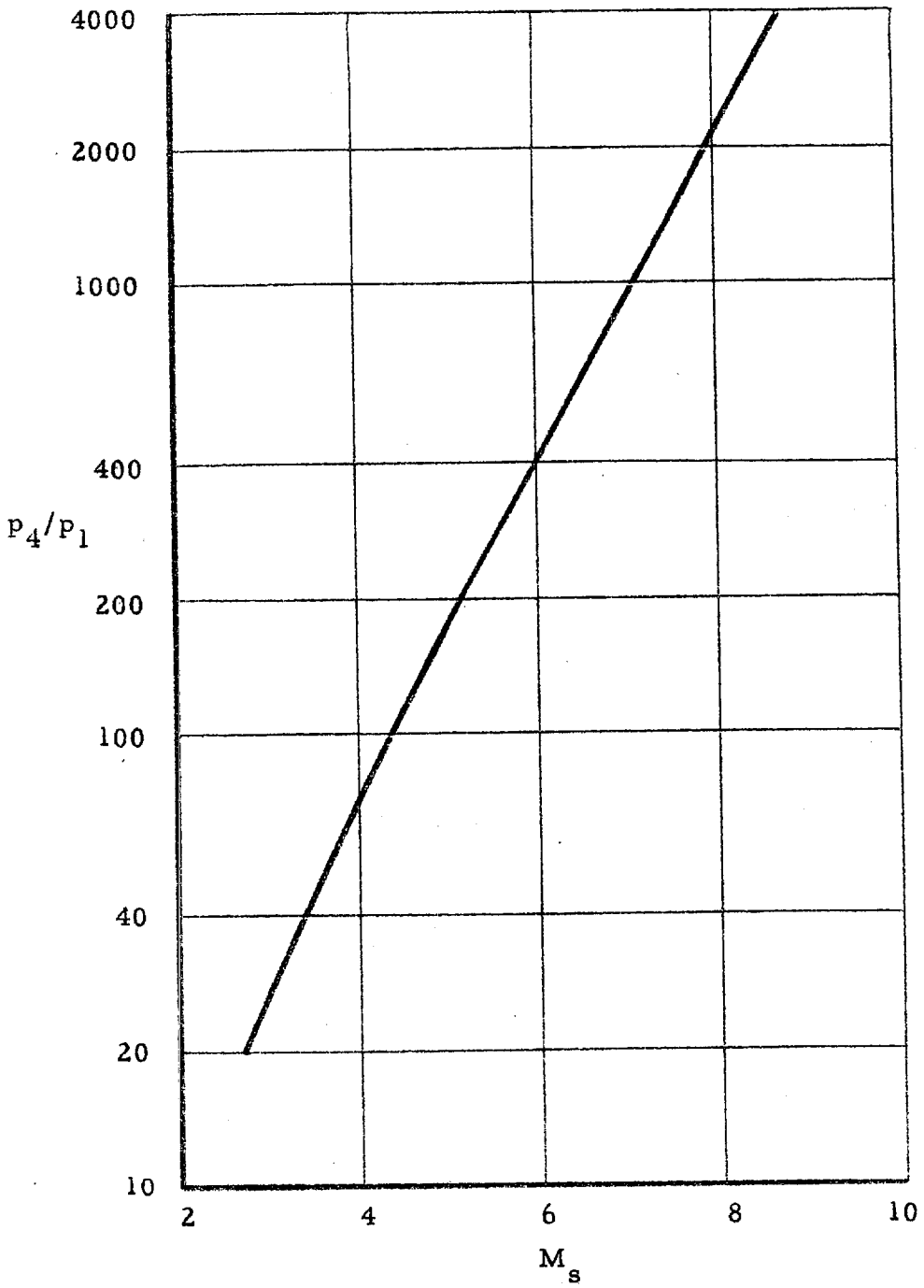

Fig.40. Pressure ratio p_4/p_1 vs. incident shock Mach number for benzene; equilibrium value of γ; $T_1 = 300^{\circ}K$ ($a_1 = 638$ ft/sec).

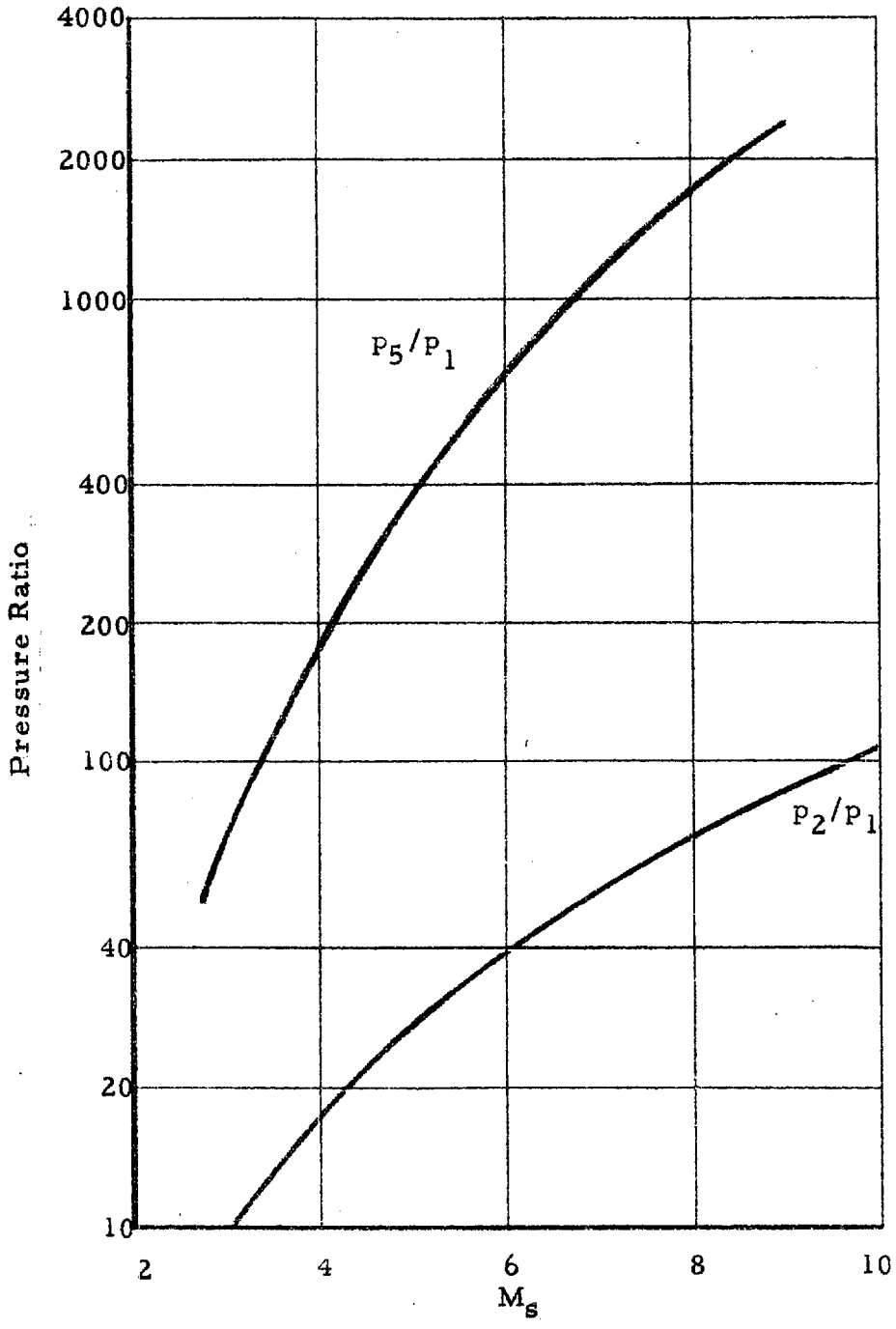

Fig. 41. Pressure ratios p_5/p_1 and p_2/p_1 vs. incident shock Mach number for benzene; equilibrium value of γ; $T_1 = 300^{\circ}K$ ($a_1 = 638$ ft/sec).

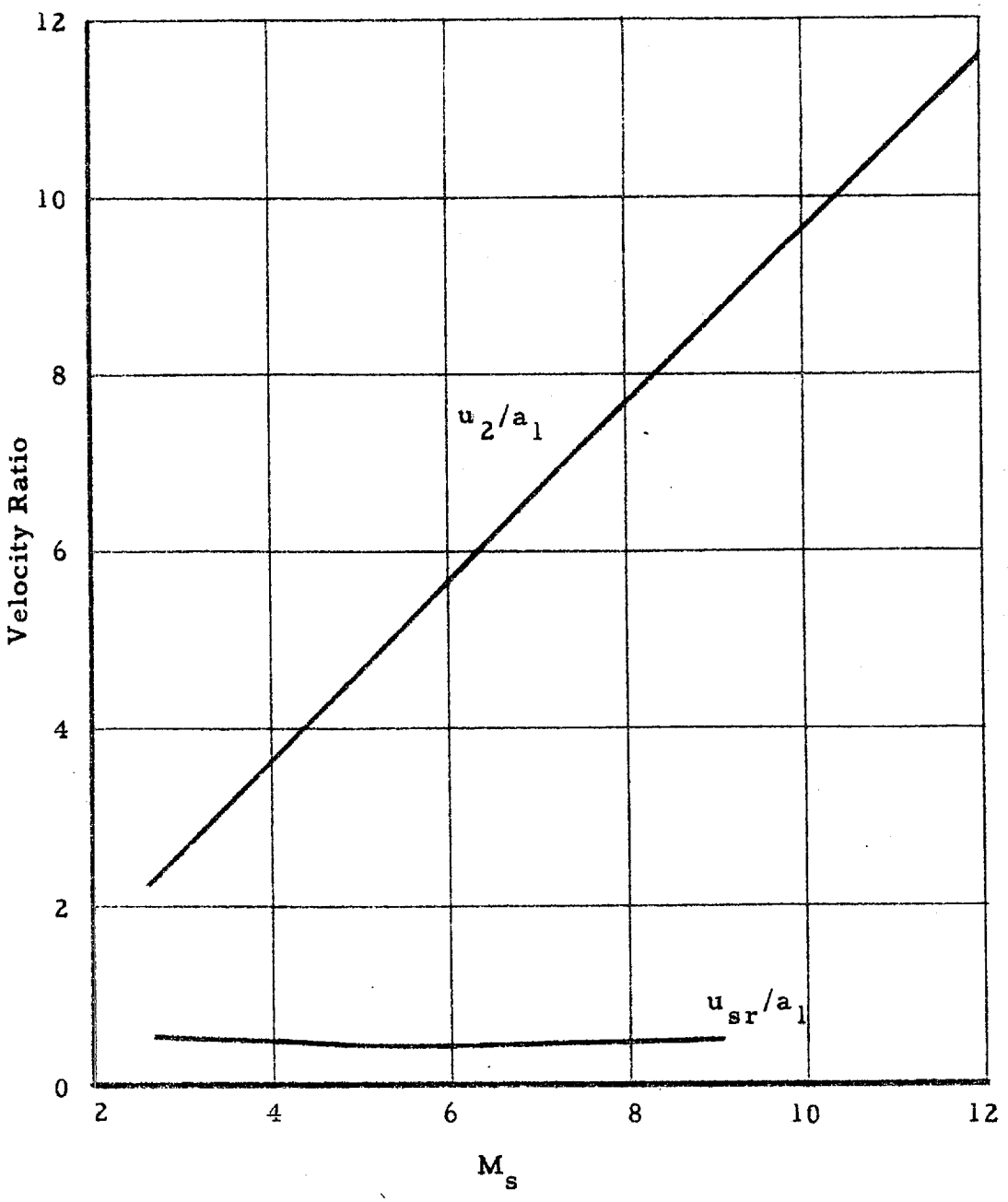

Fig. 42. Velocity ratios u_2/a_1 and u_{sr}/a_1 vs. incident shock Mach number for benzene; equilibrium value of γ; $T_1 = 300^{\circ}K$ ($a_1 = 638$ ft/sec).

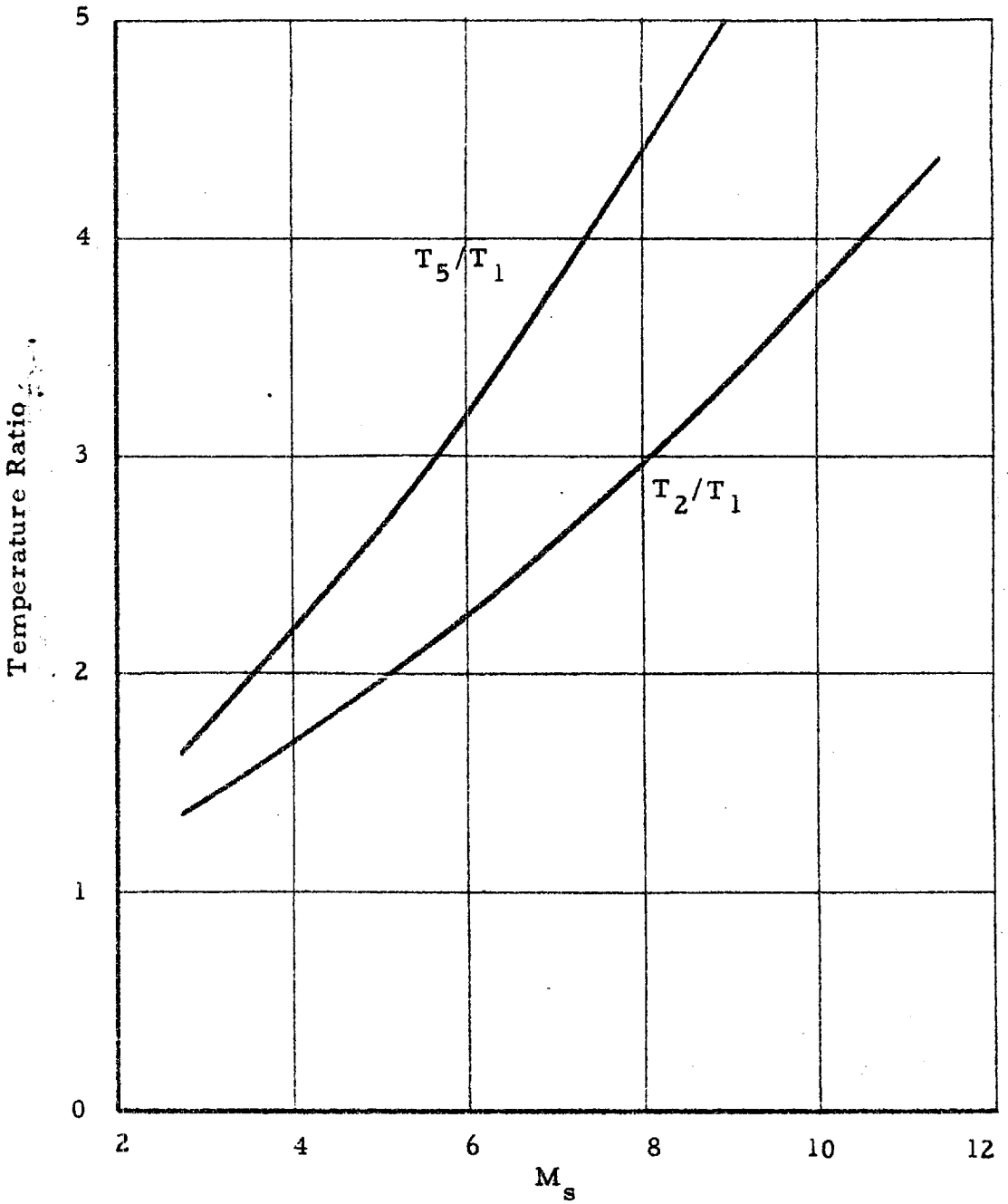

Fig. 43. Temperature ratios T_5/T_1 and T_2/T_1 vs. incident shock Mach number for benzene; equilibrium value of γ; $T_1 = 300^{\circ}K$ ($a_1 = 638$ ft/sec).

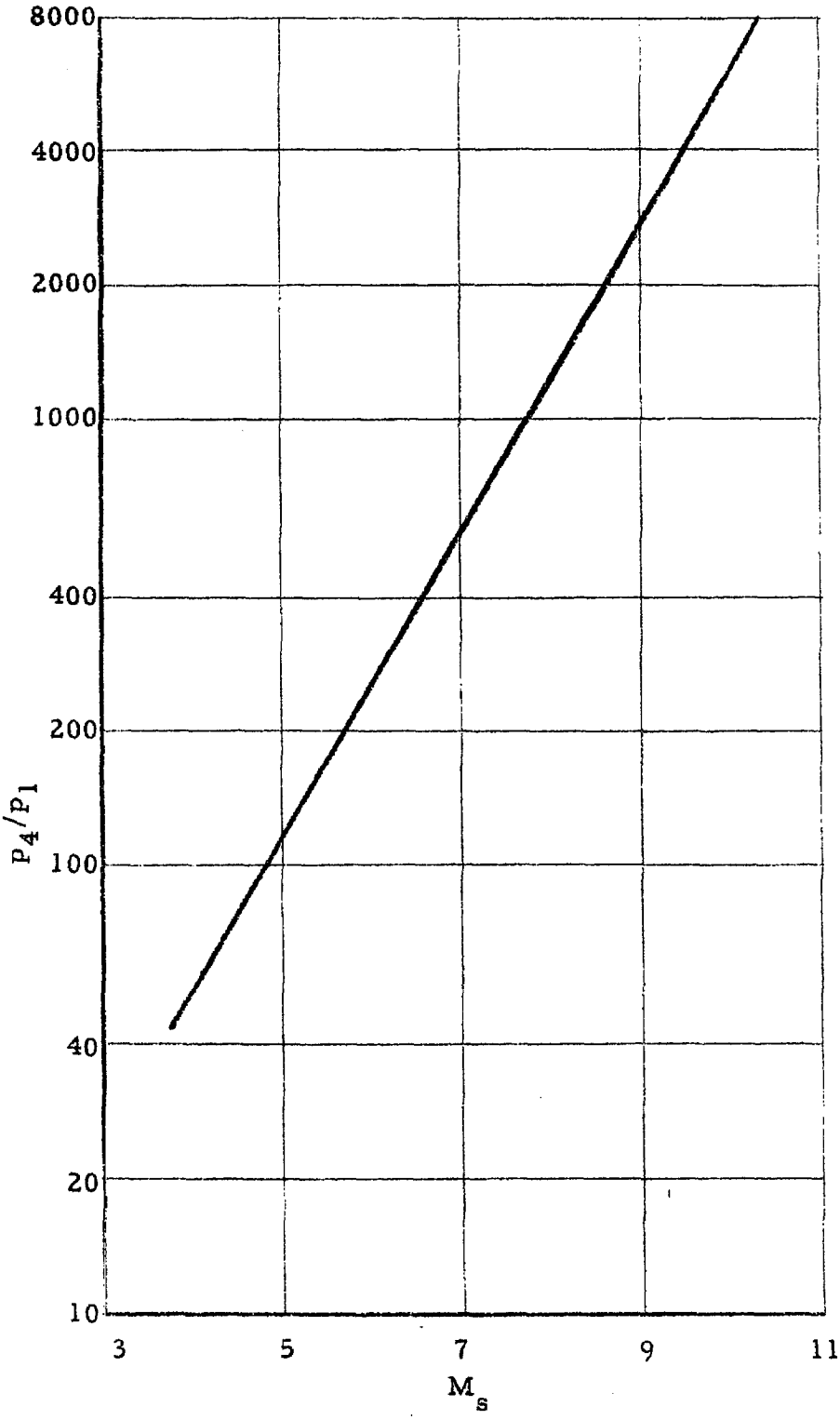

Fig. 44. Pressure ratio p_4/p_1 vs. incident shock Mach number for n-heptane; equilibrium value of γ; $T_1 = 300^{\circ}K$ ($a_1 = 565$ ft/sec).

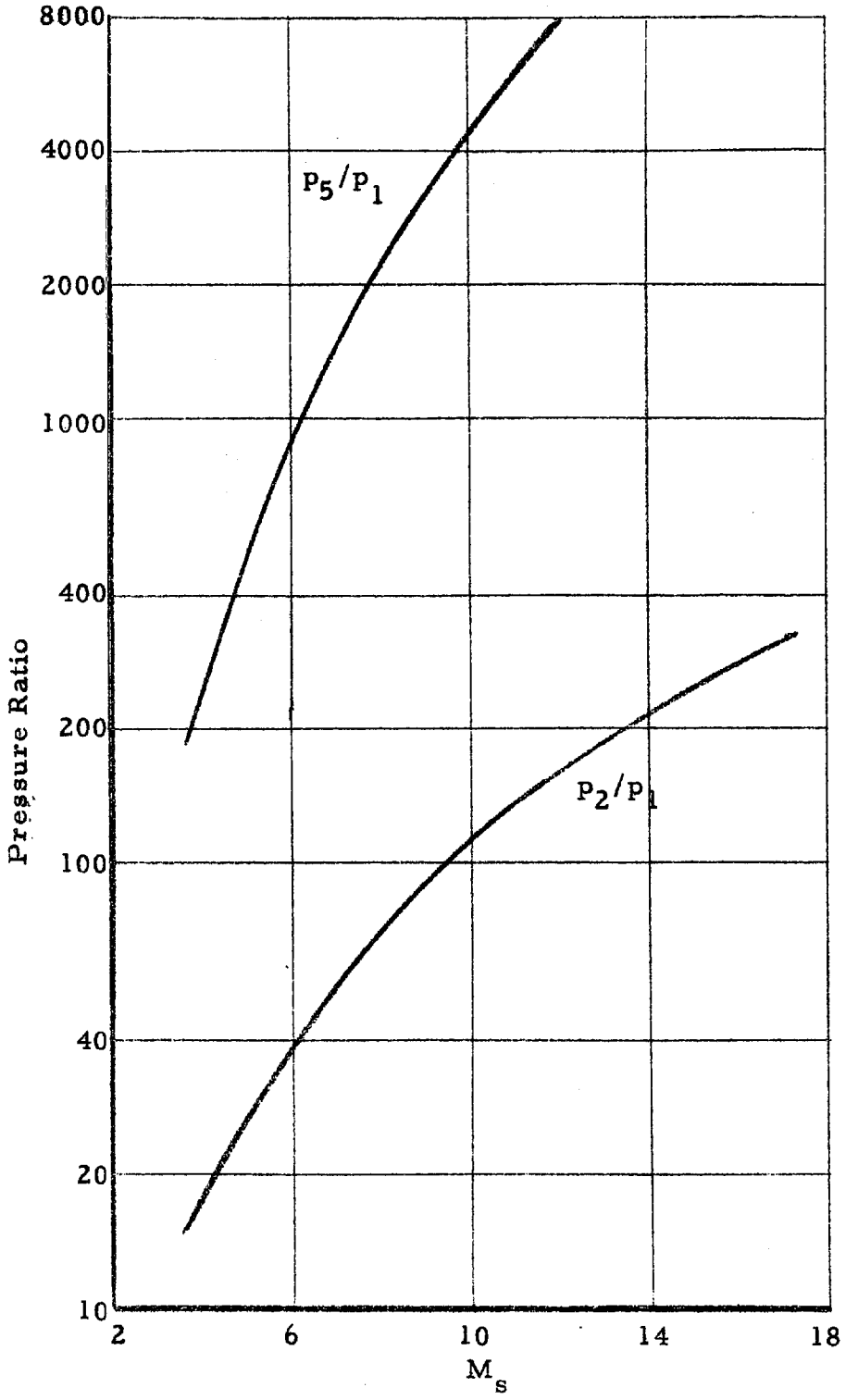

Fig. 45. Pressure ratios p_2/p_1 and p_5/p_1 vs. incident shock Mach number for n-heptane; equilibrium value of γ; $T_1 = 300^{\circ}K$ ($a_1 = 565$ ft/sec).

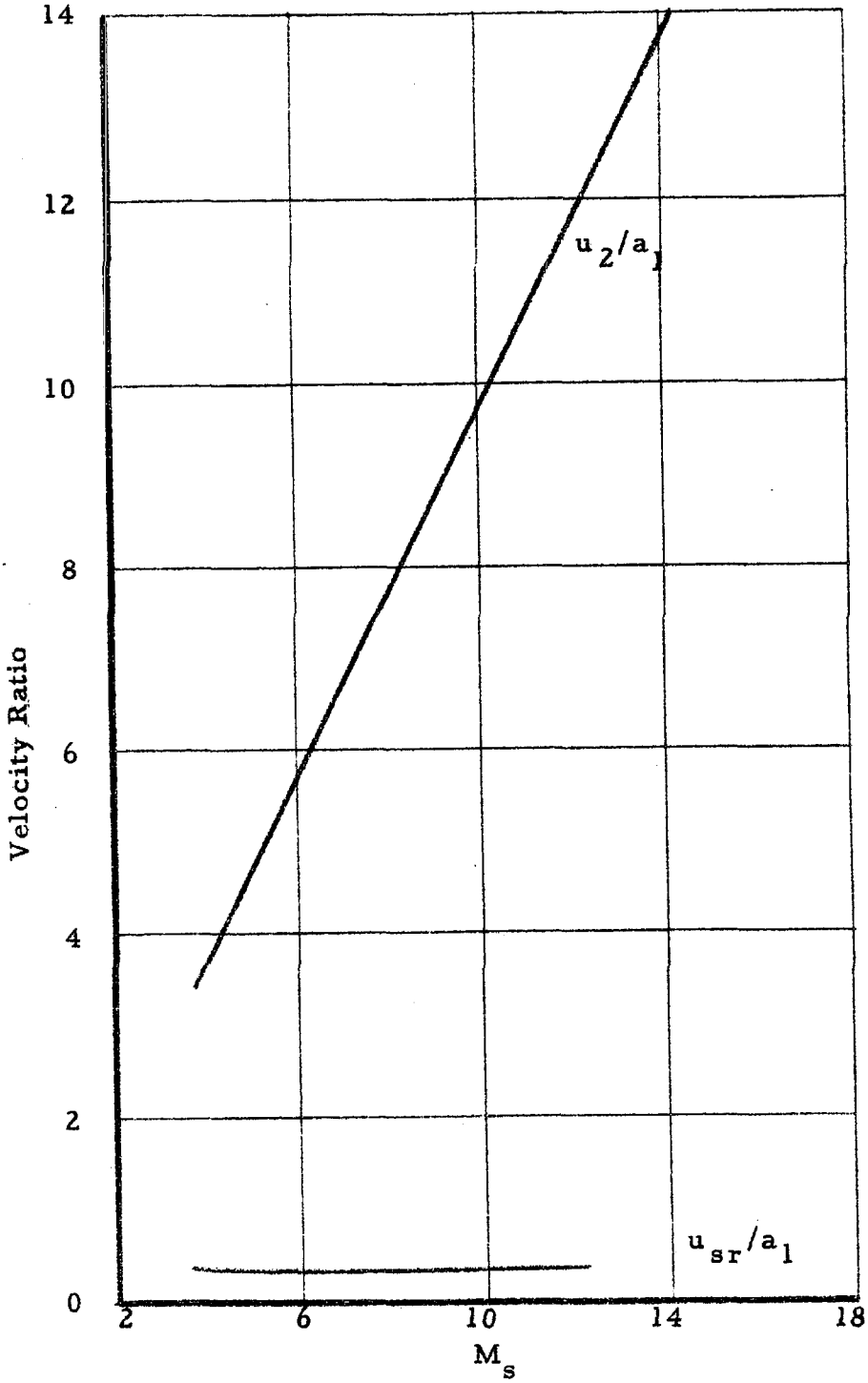

Fig. 46. Velocity ratios u_2/a_1 and u_{sr}/a_1 vs. incident shock Mach number for n-heptane; equilibrium value of γ; $T_1 = 300^{\circ}K$ ($a_1 = 565$ ft/sec).

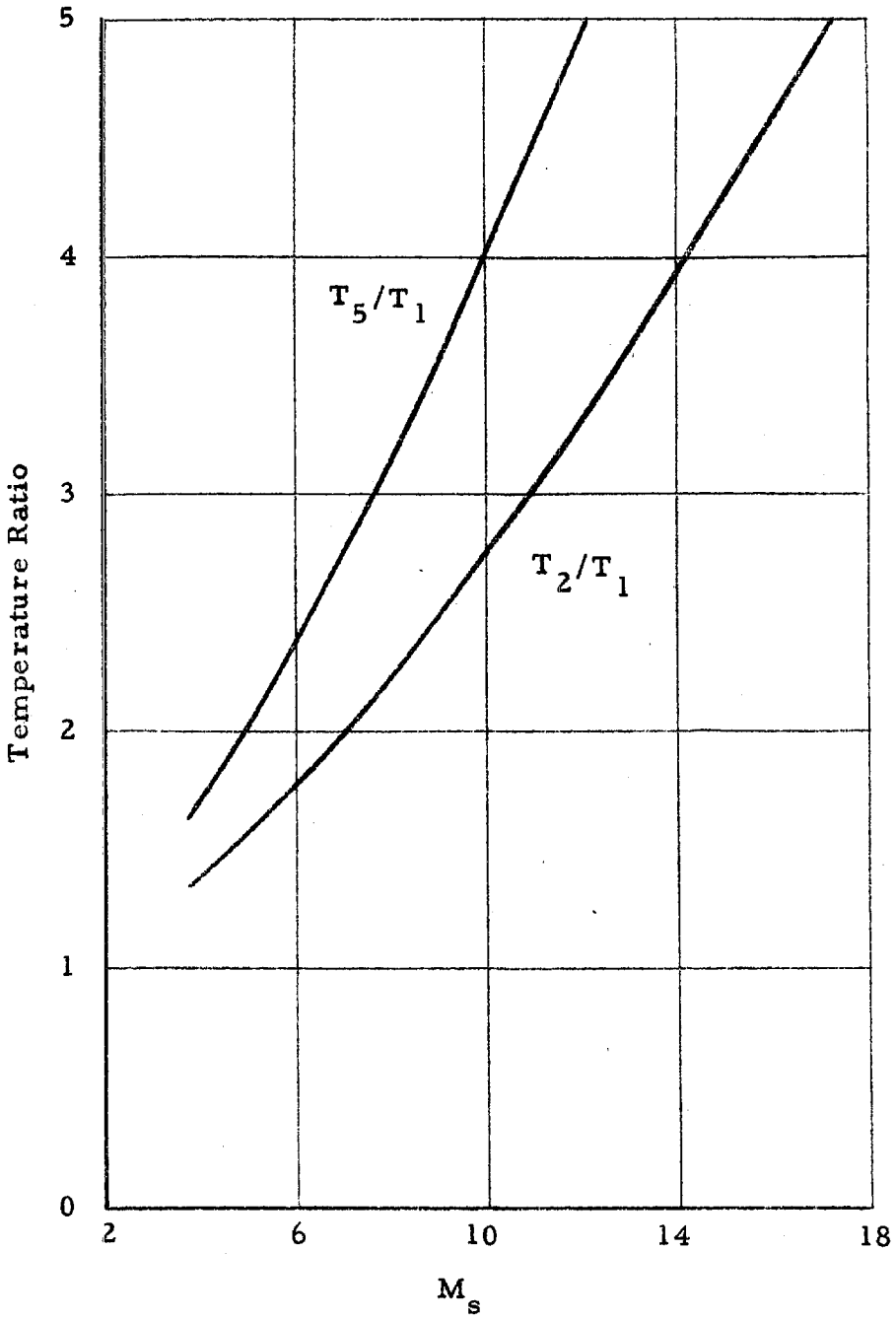

Fig. 47. Temperature ratios T_5/T_1 and T_2/T_1 vs. incident shock Mach number for n-heptane; equilibrium value of γ; $T_1 = 300^{\circ}K$ ($a_1 = 565$ ft/sec).

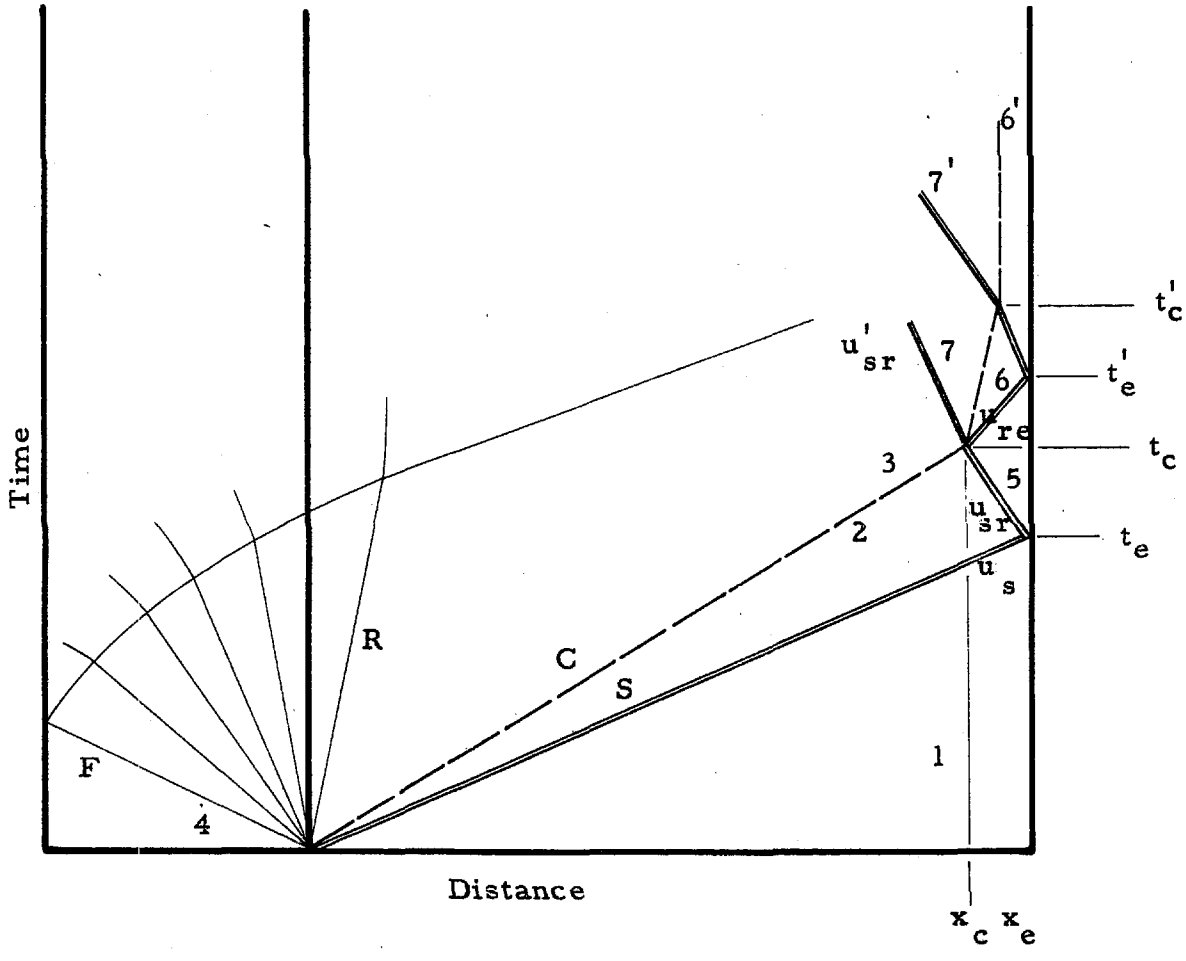

Fig. 48. A distance-time diagram showing a complex interaction of the reflected shock wave with the contact surface.

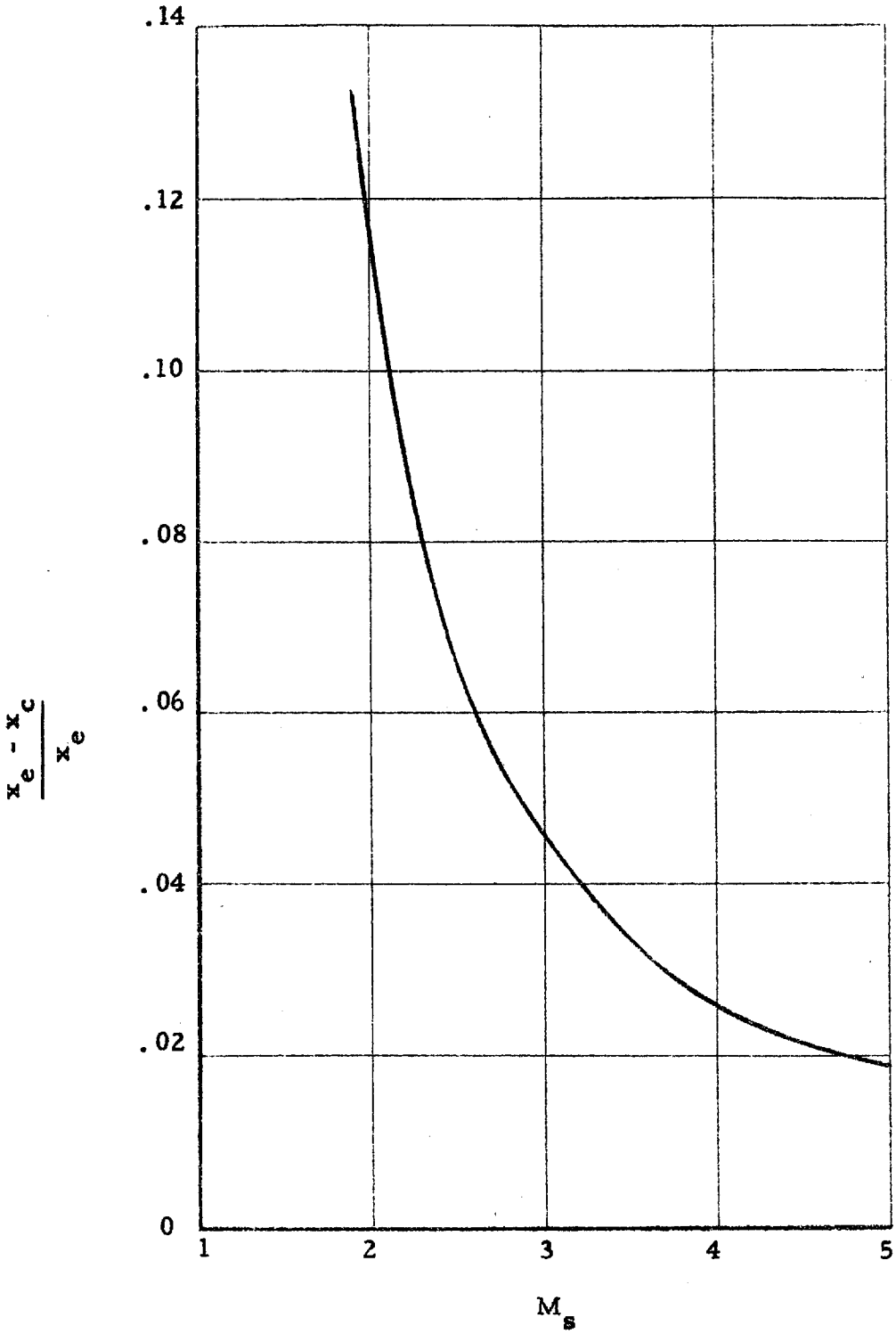

Fig. 49. The ratio $(x_e - x_c)/x_e$ vs. initial shock Mach number for acetylene; equilibrium value of γ; $T_1 = 300^{\circ}K$ ($a_1 = 1139$ ft/sec).

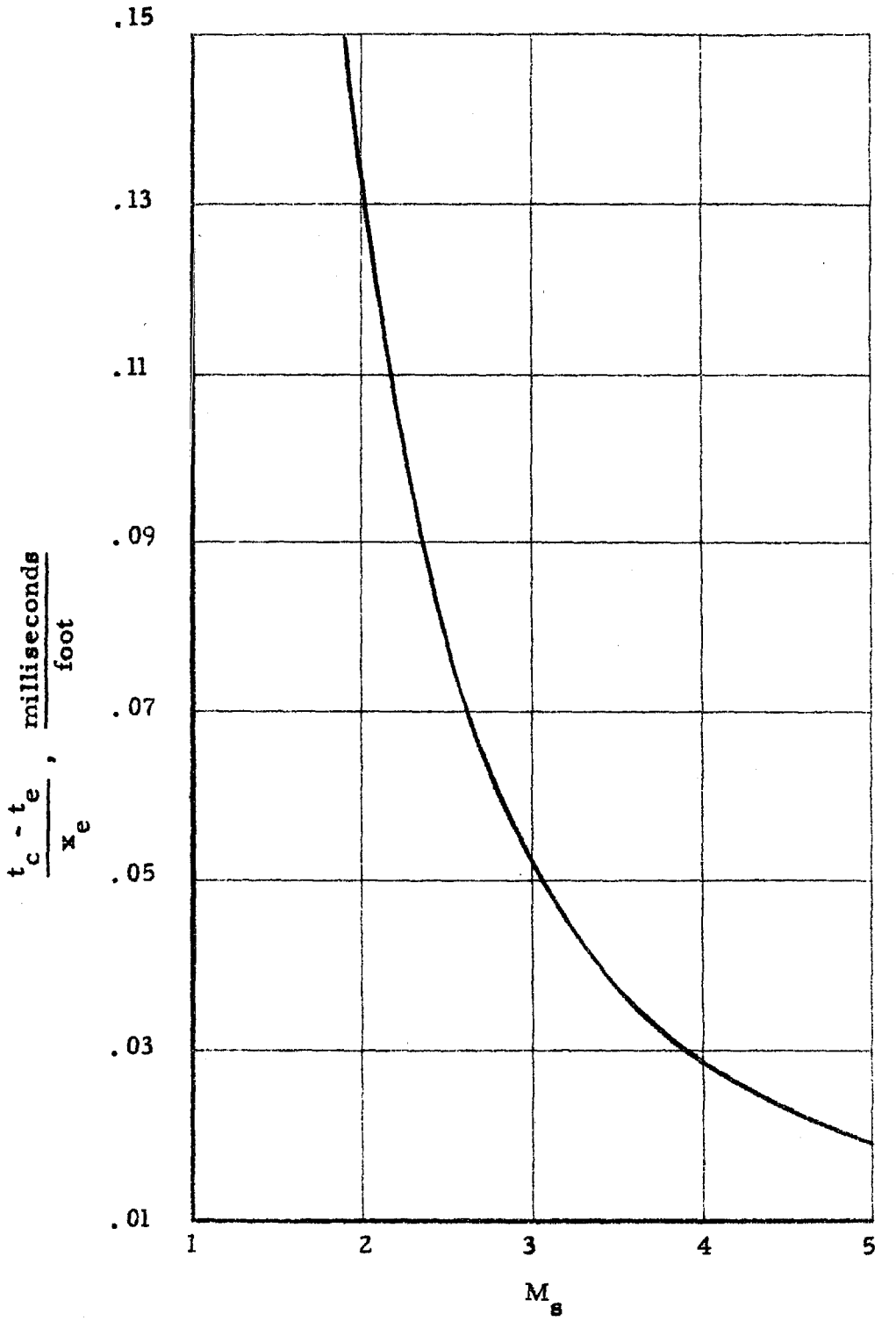

Fig. 50. The ratio $(t_c - t_e)/x_e$ vs. initial shock Mach number for acetylene; equilibrium value of γ; $T_1 = 300^\circ K$. ($a_1 = 1139$ ft/sec).

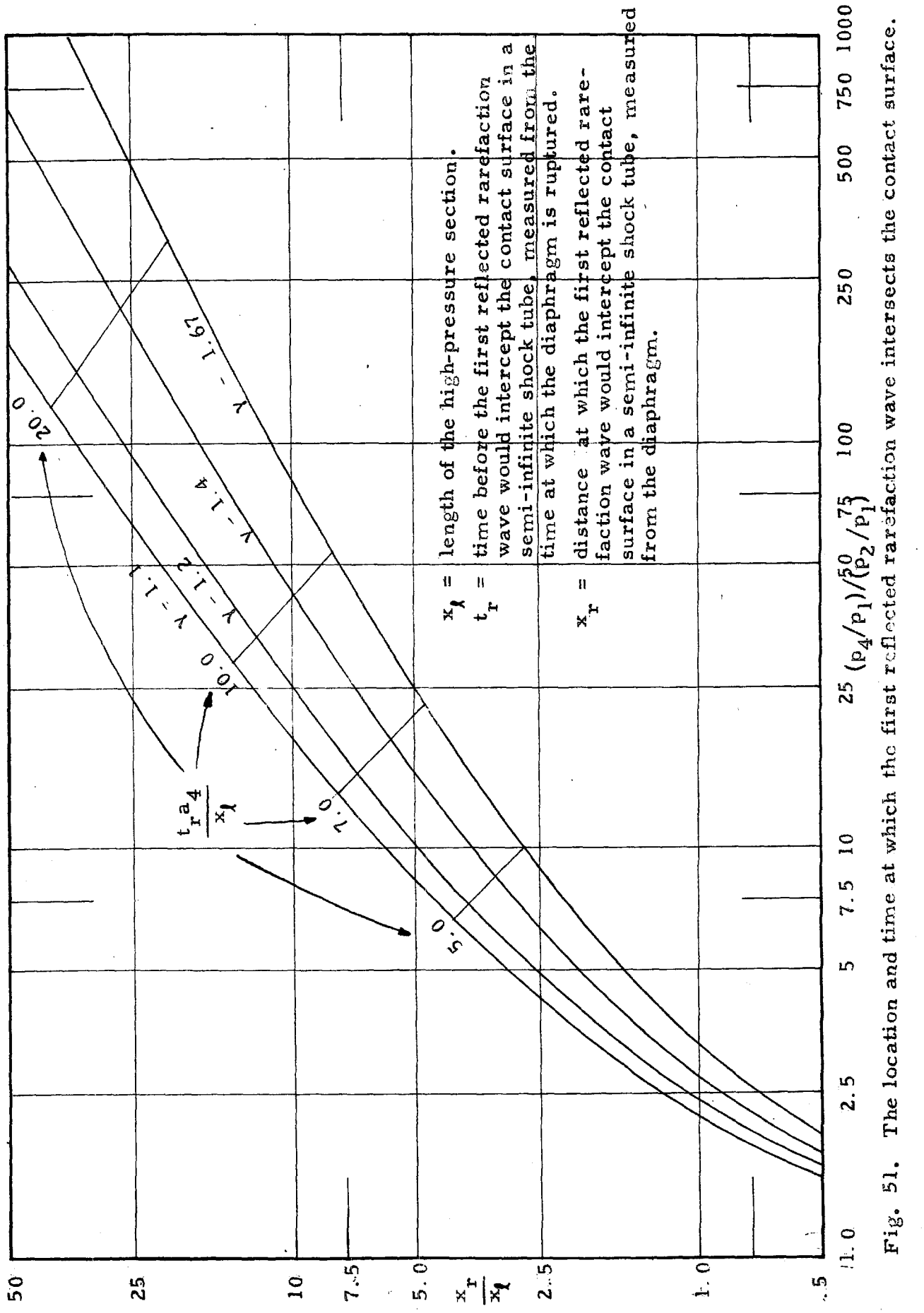

Fig. 51. The location and time at which the first reflected rarefaction wave intersects the contact surface.

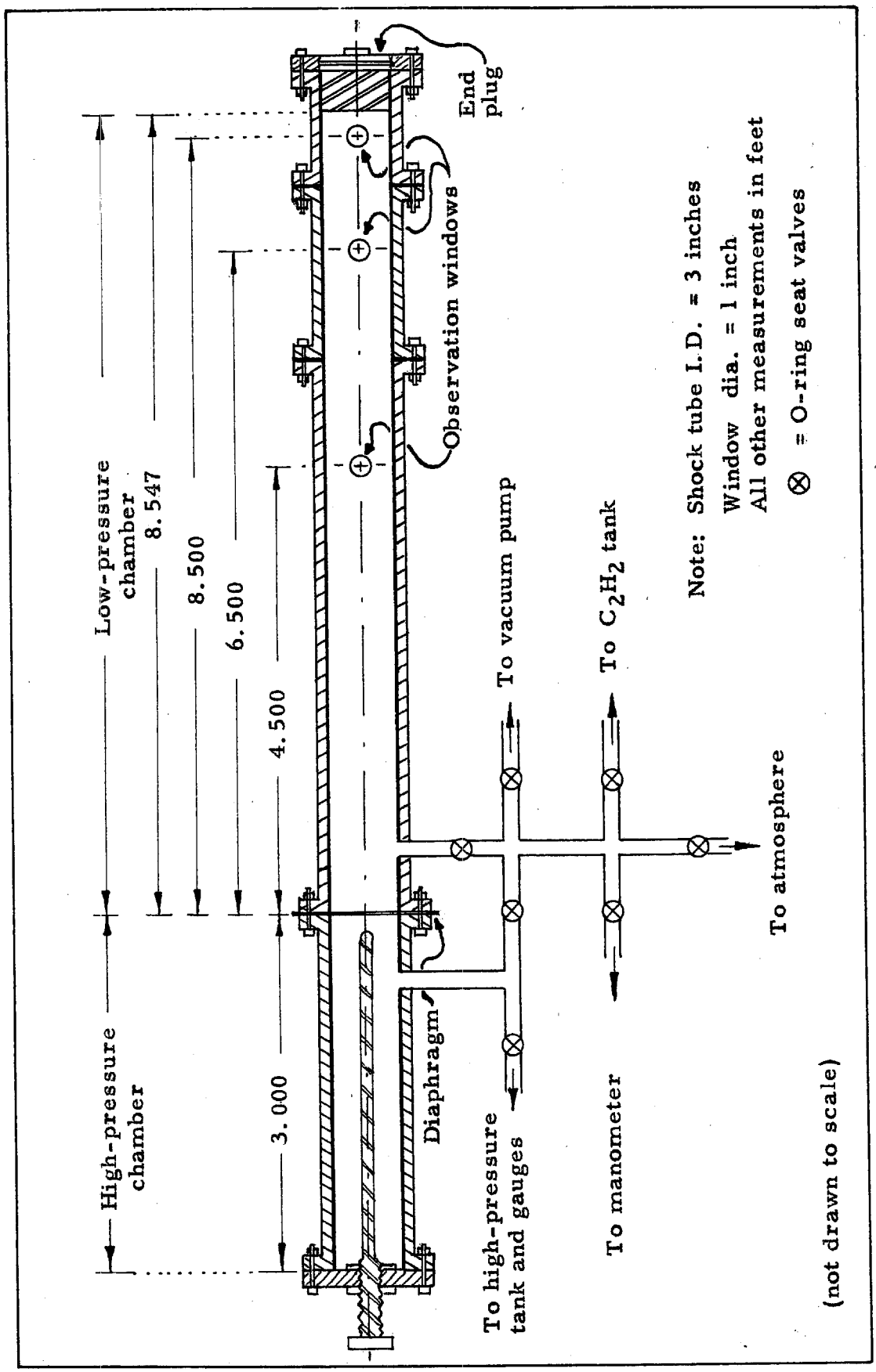

Fig. 52. Schematic diagram of the shock tube and gas supply manifold.

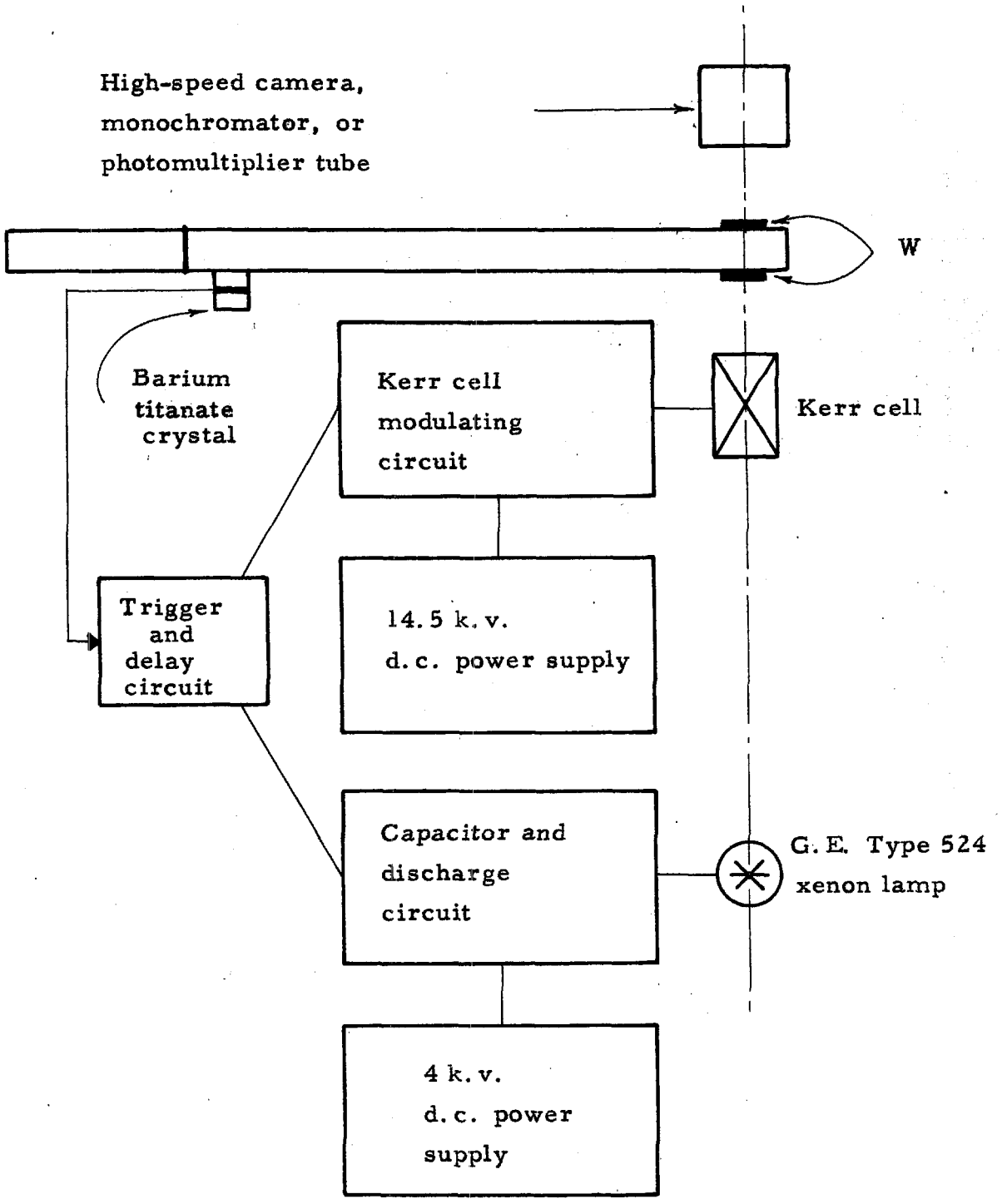

Fig. 53. Schematic diagram of the Kerr cell used to make simultaneous absorption and emission measurements behind shocks; W: window.

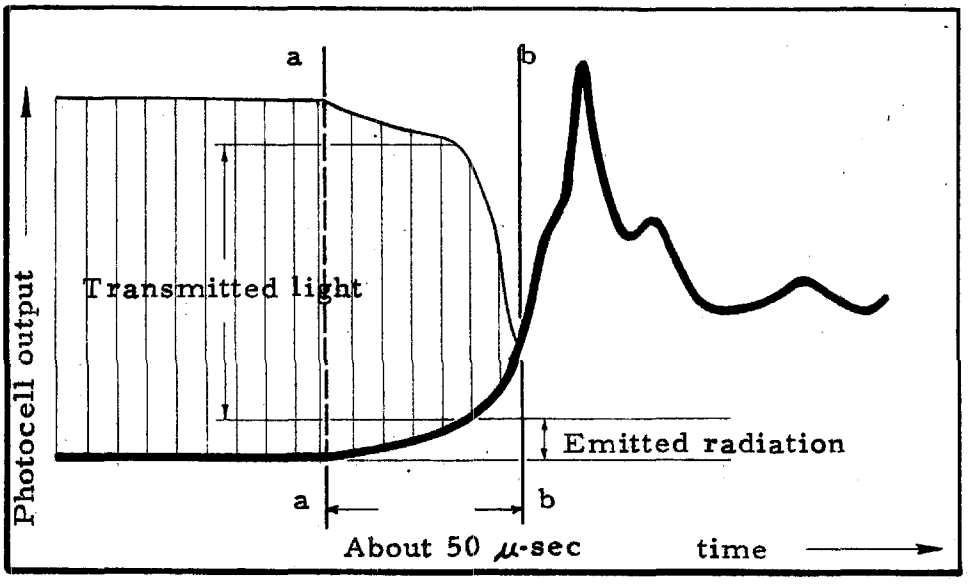

Fig. 54. The photocell output as a function of time at the onset of light emission when a Kerr cell is used to modulate the incident light (see fig. 53).

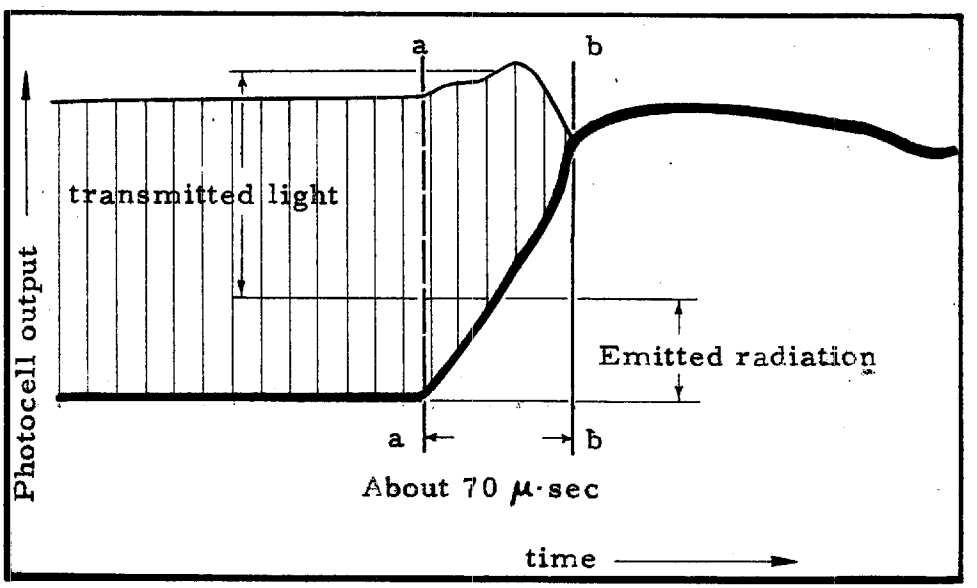

Fig. 55. The photocell output as a function of time at the onset of light emission when a Kerr cell is used to modulate the incident light (see fig. 53).

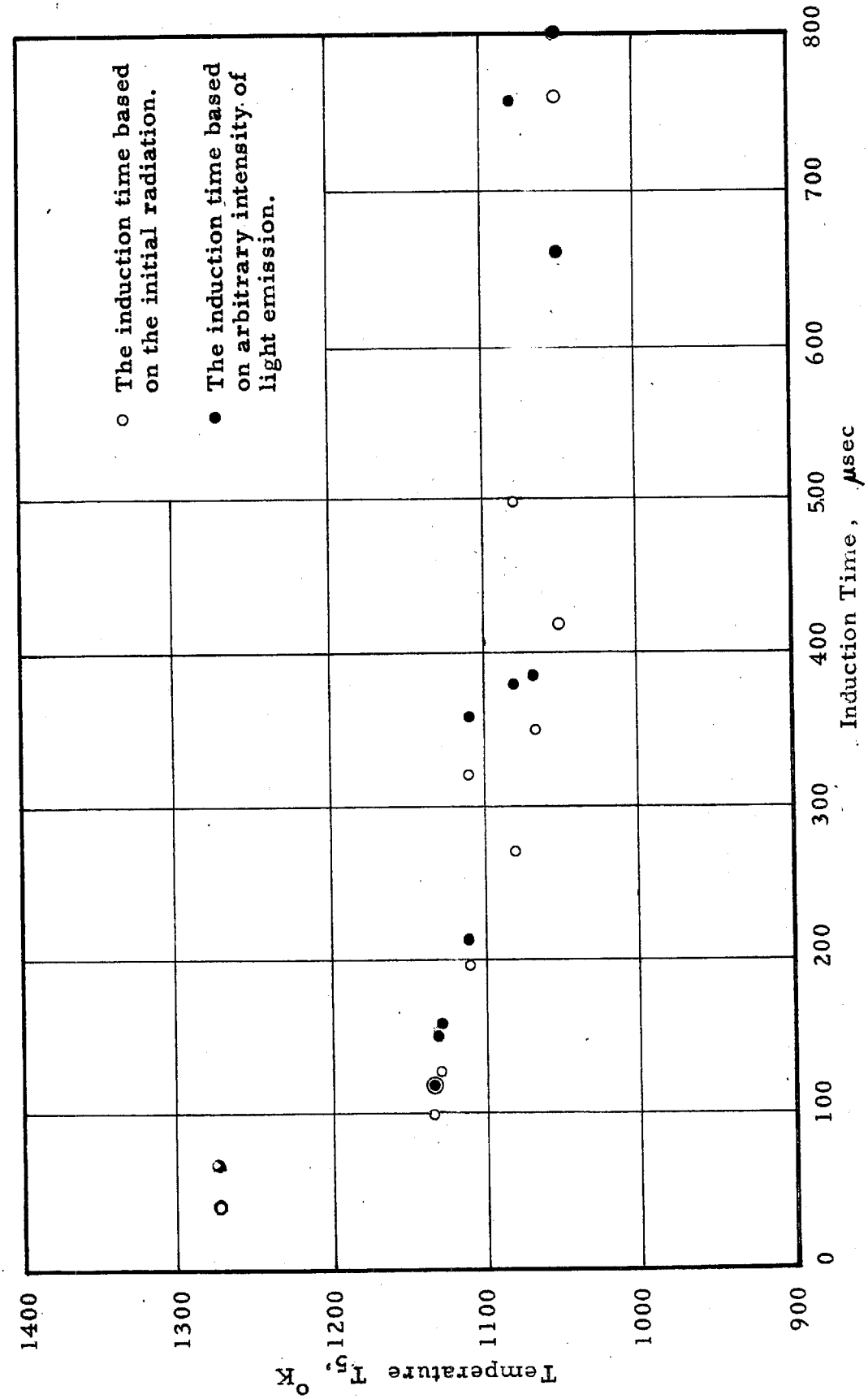

Fig. 56. The temperature T_5 versus the induction time before the onset of carbon formation.

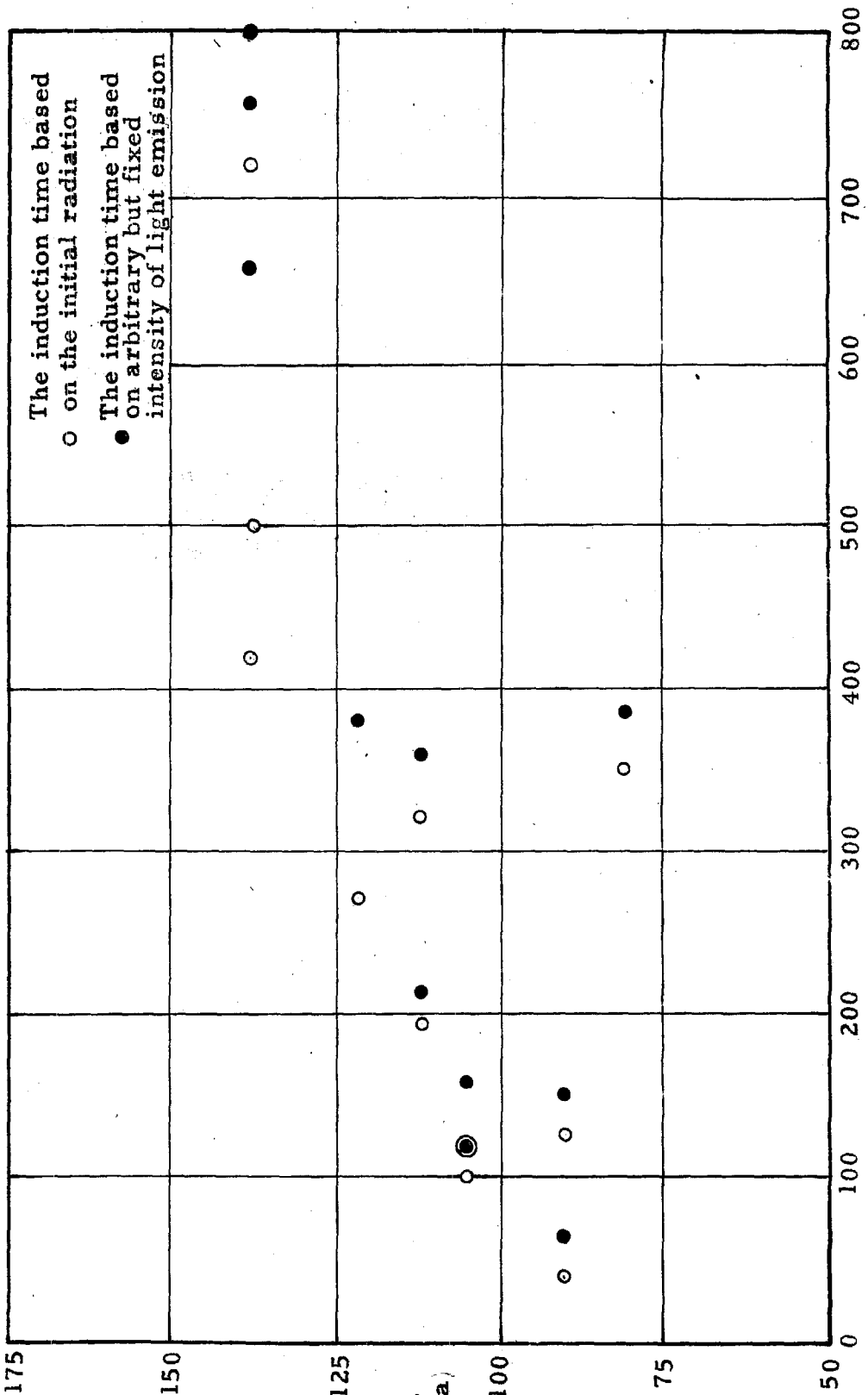

Fig. 57. The pressure P_5 versus the induction time before the onset of carbon formation.

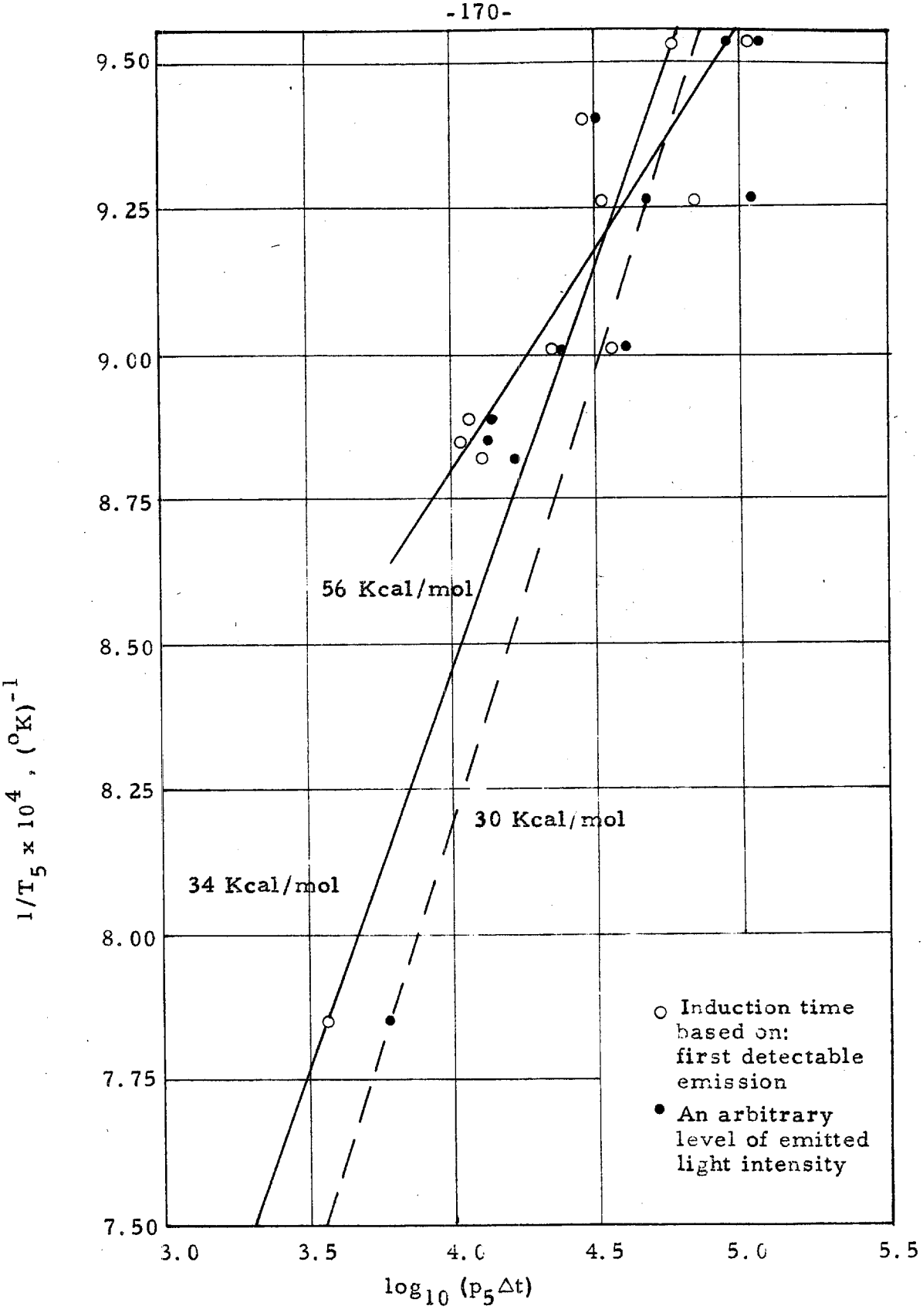

Fig. 58. Plot of $1/T_5$ versus $\log_{10}(p_5\Delta t)$. Data from figures 56 and 57.

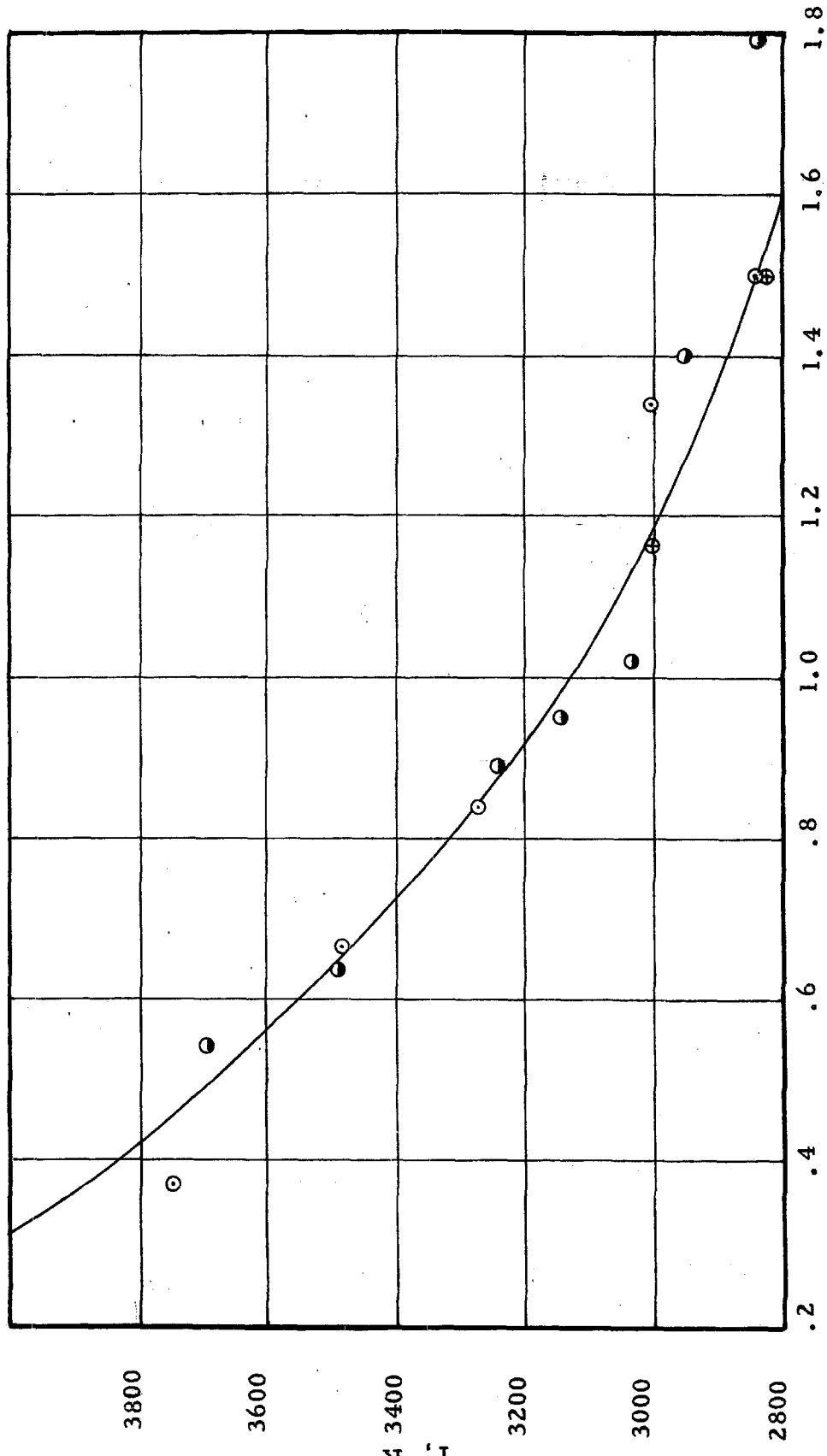

Fig. 59. The intensity ratio R(T) as a function of brightness temperature (calibration curve).

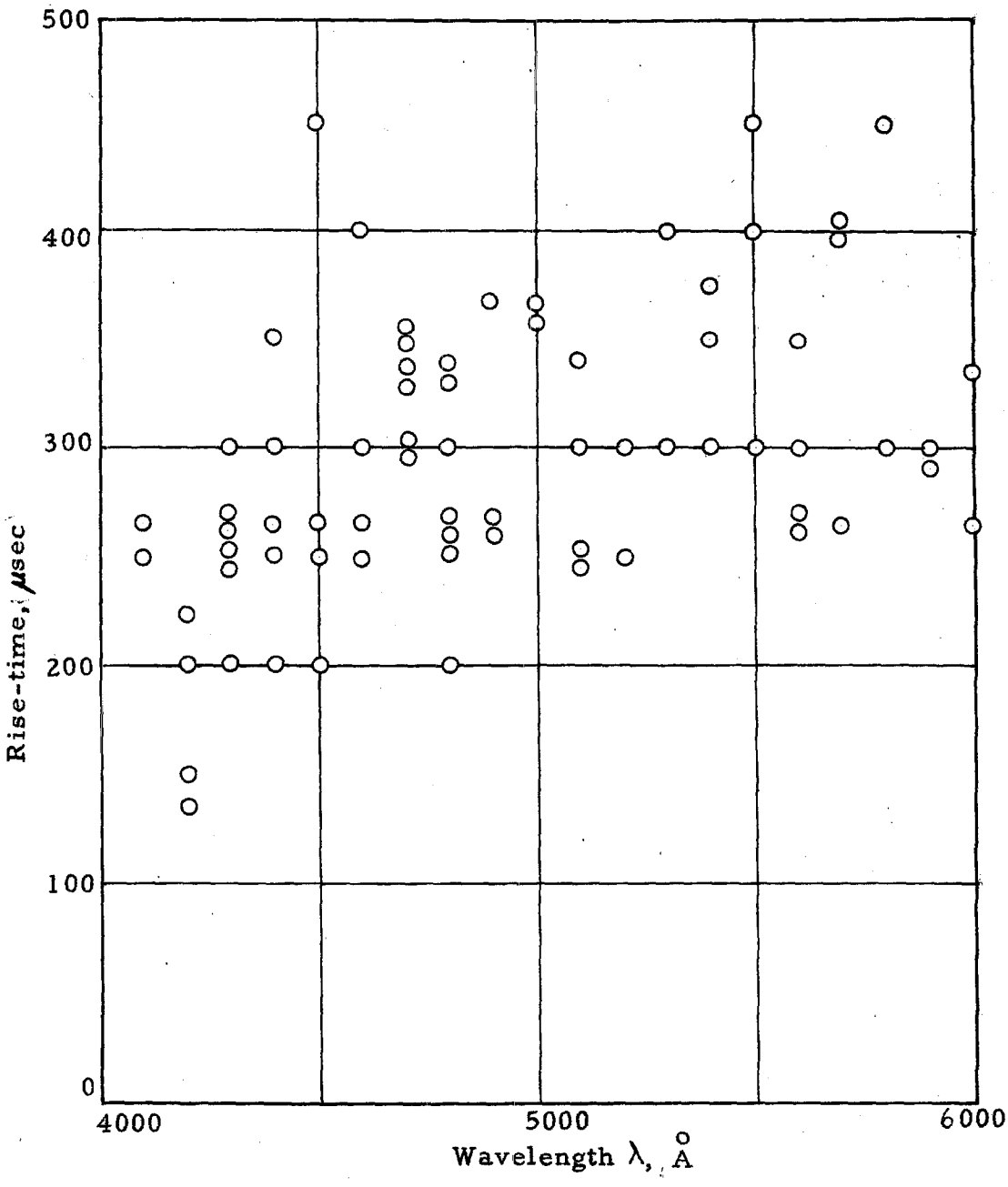

Fig. 60. The rise-time (as measured from the onset of emission until the time of peak intensity) of the radiation behind carbon-forming shocks versus wave length.

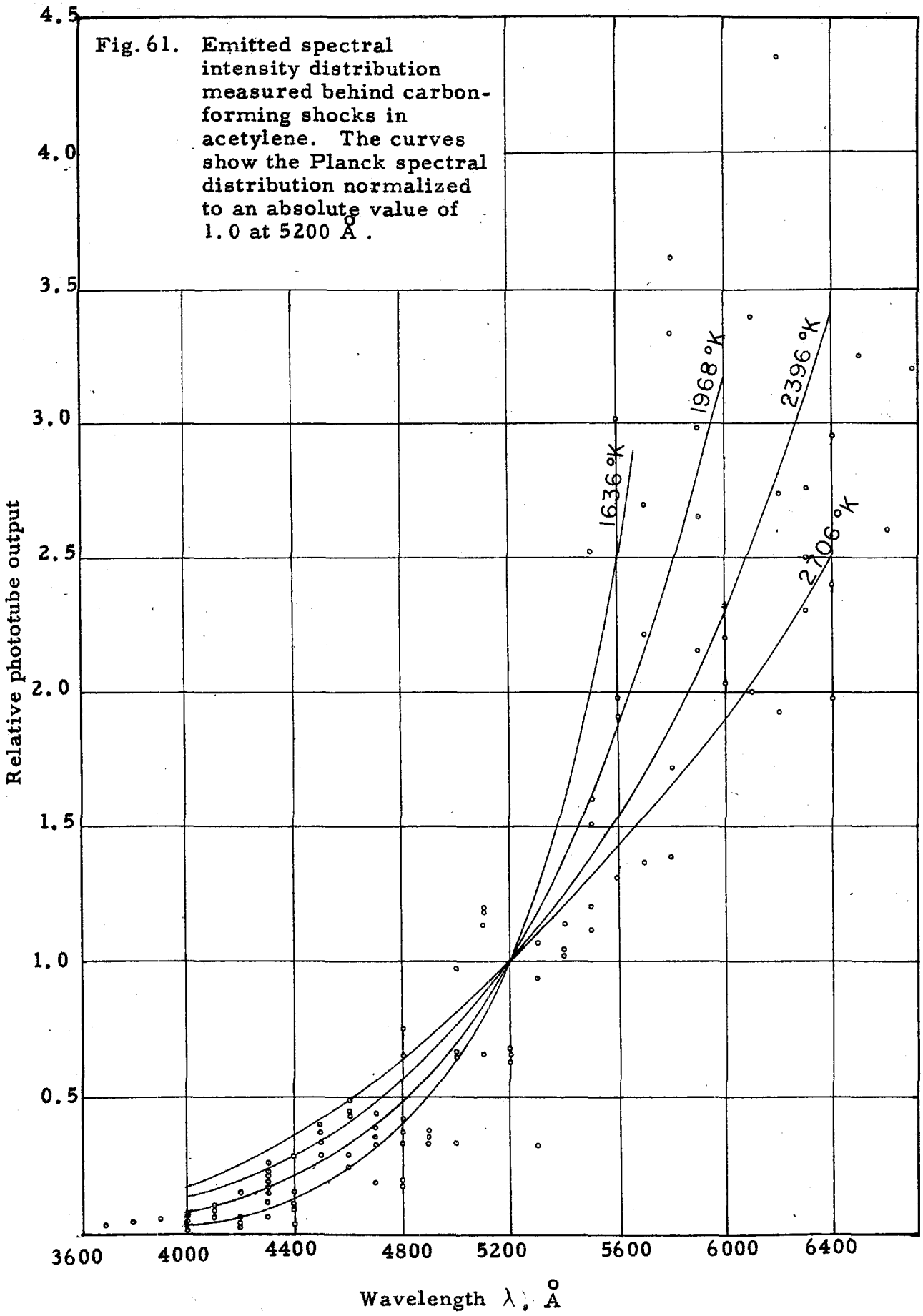

Fig. 61. Emitted spectral intensity distribution measured behind carbon-forming shocks in acetylene. The curves show the Planck spectral distribution normalized to an absolute value of 1.0 at 5200 Å.

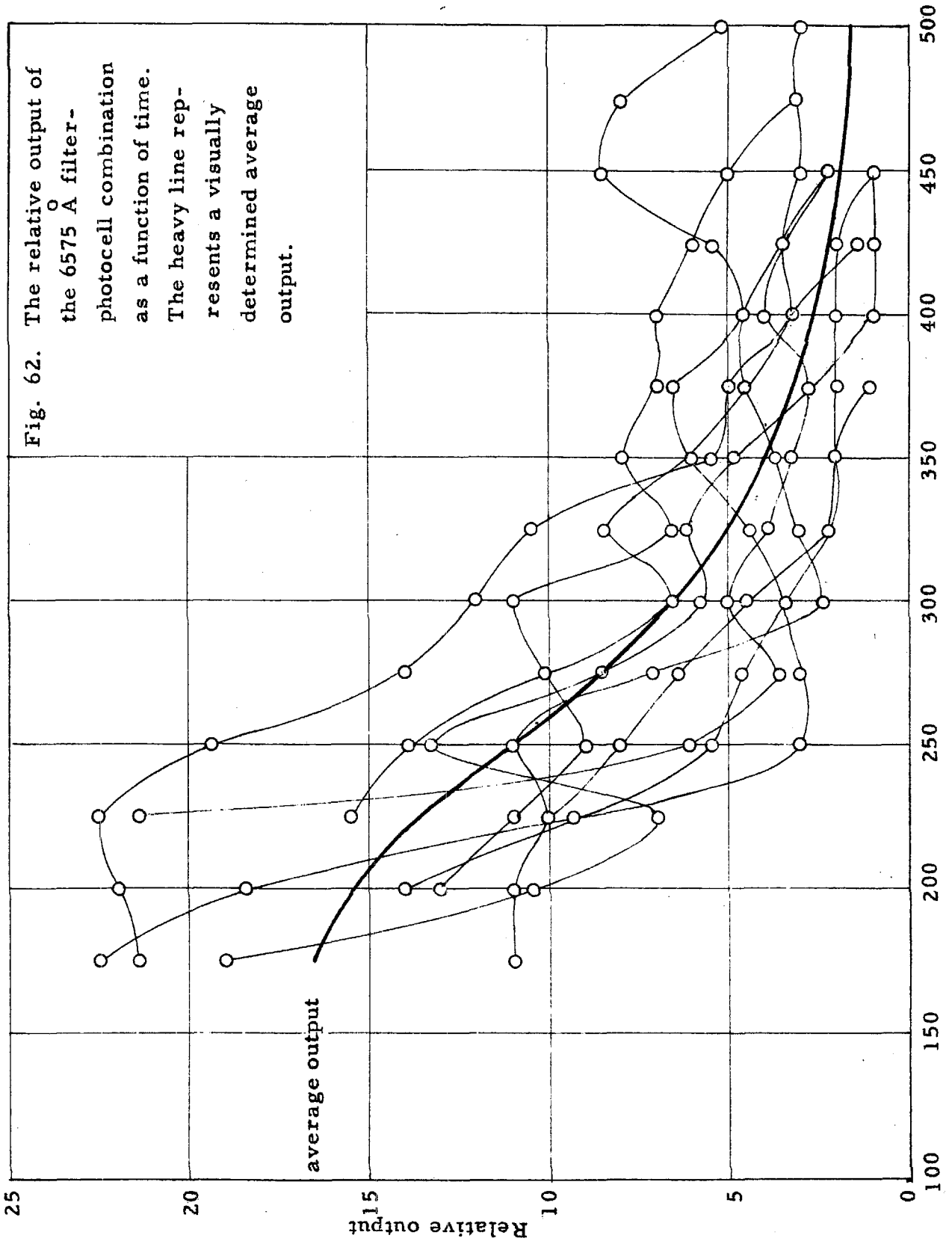

Fig. 62. The relative output of the 6575 Å filter-photocell combination as a function of time. The heavy line represents a visually determined average output.

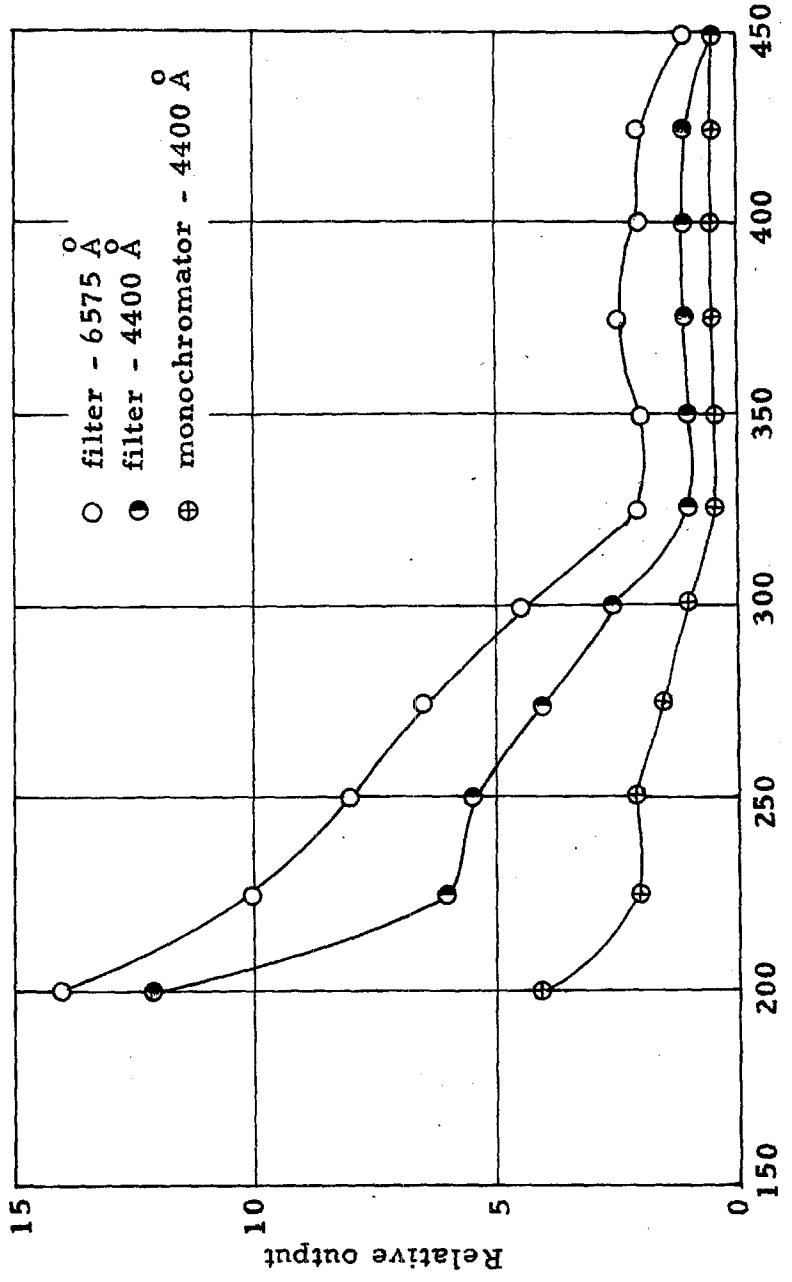

Fig. 63. The relative output of the two filter-photocell combinations and of the monochromator set at 4400 Å as a function of time (run A).

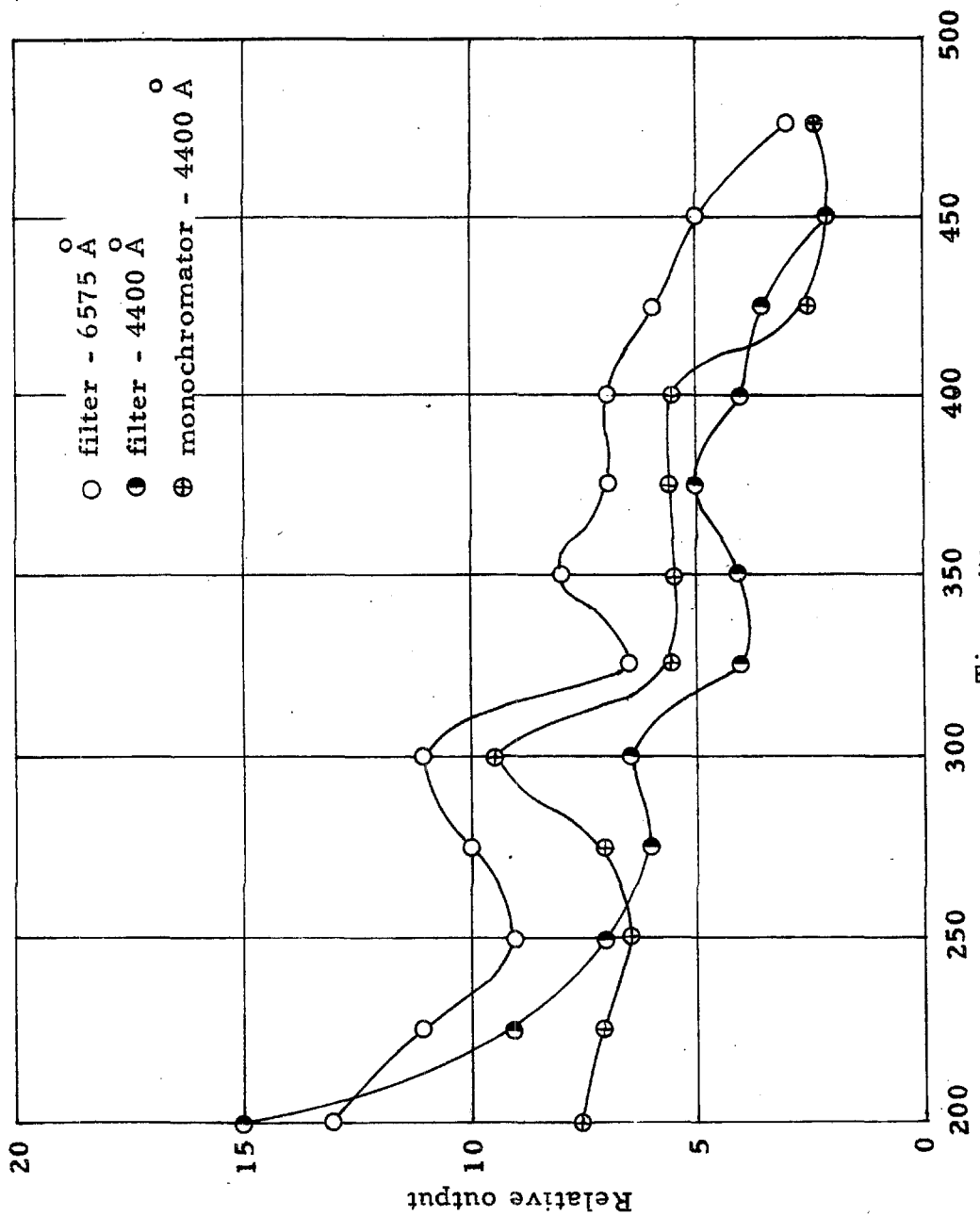

Fig. 64. The relative output of the two filter-photocell combinations and of the monochromator set at 4400 Å as a function of time (run C).

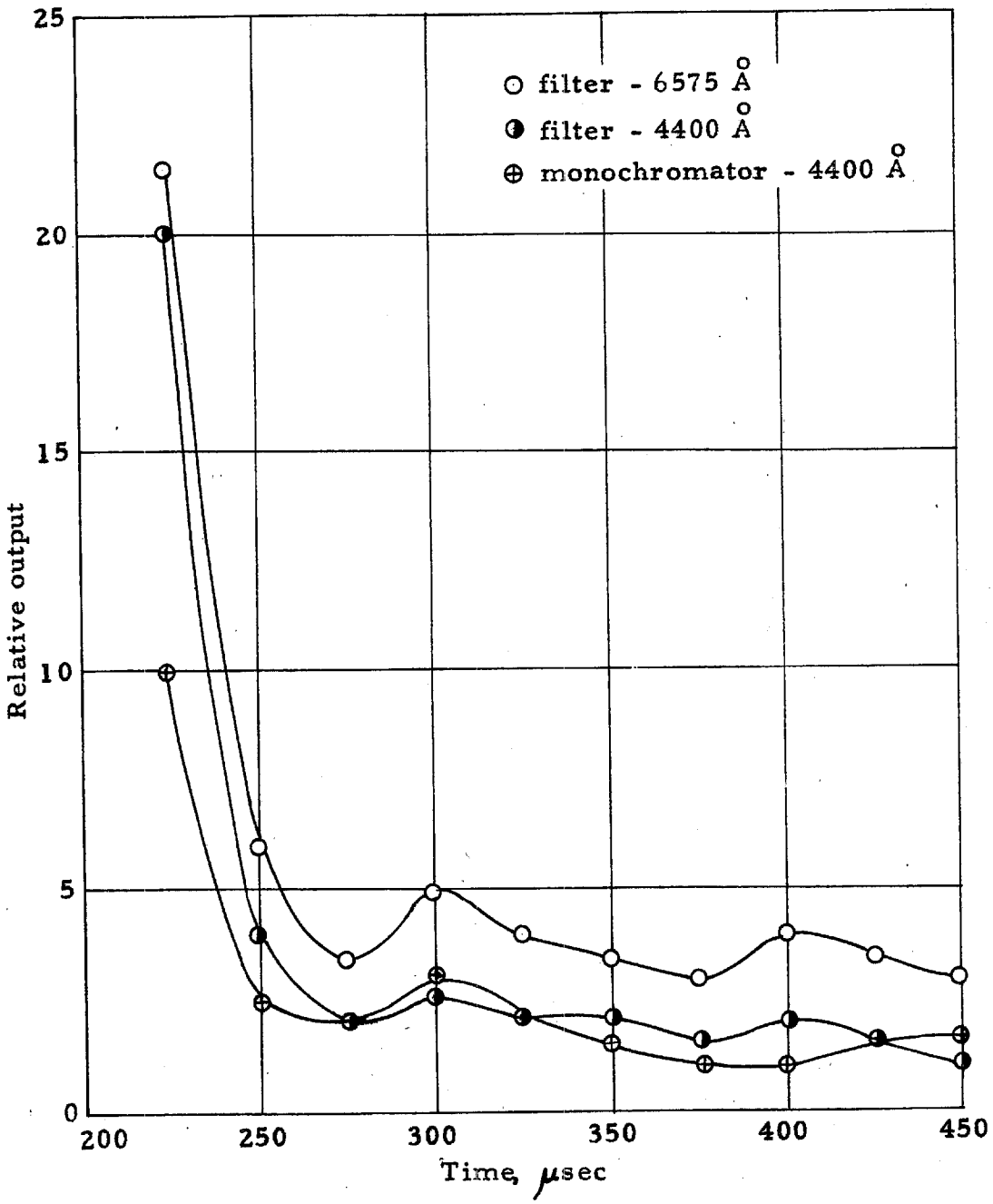

Fig. 65. The relative output of the two filter-photocell combinations and of the monochromator set at 4400 Å as a function of time (run B).

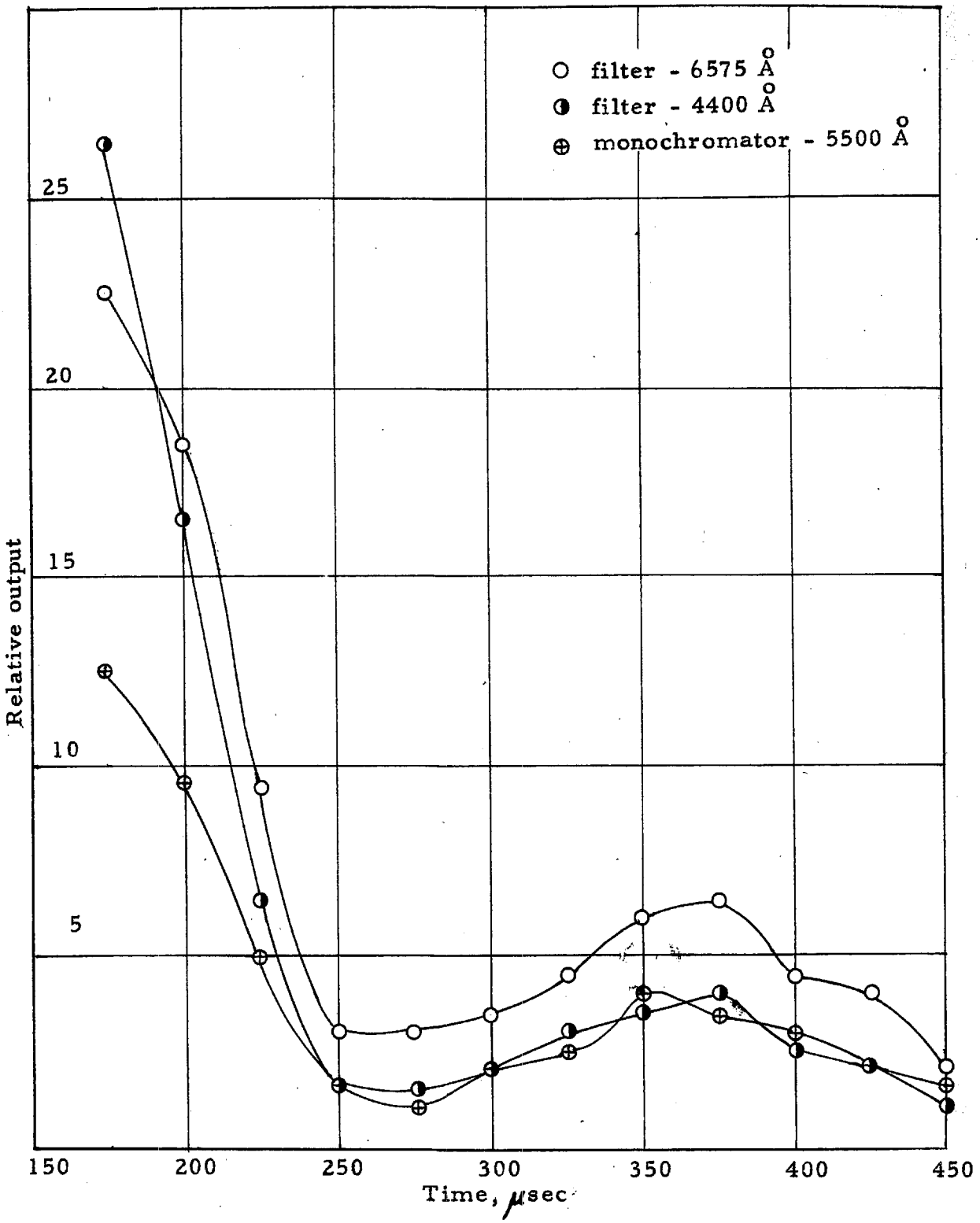

Fig. 66. The relative output of the two filter-photocell combinations - and of the monochromator set at 5500 Å as a function of time (run D).

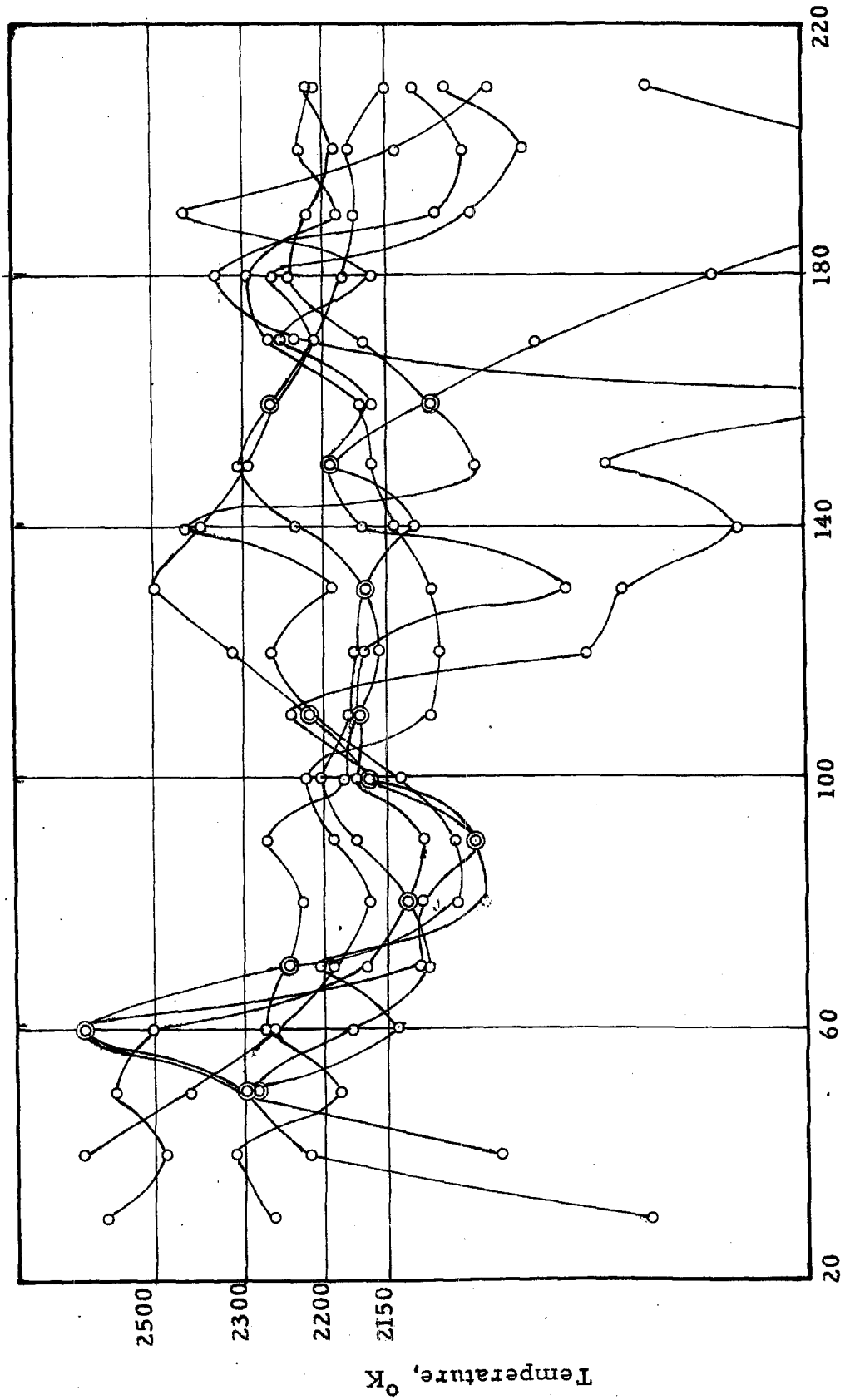

Fig. 67. True temperature versus time as determined by a two-color method in several experiments behind carbon-forming shocks (initial shock Mach number M_s = 4.2).

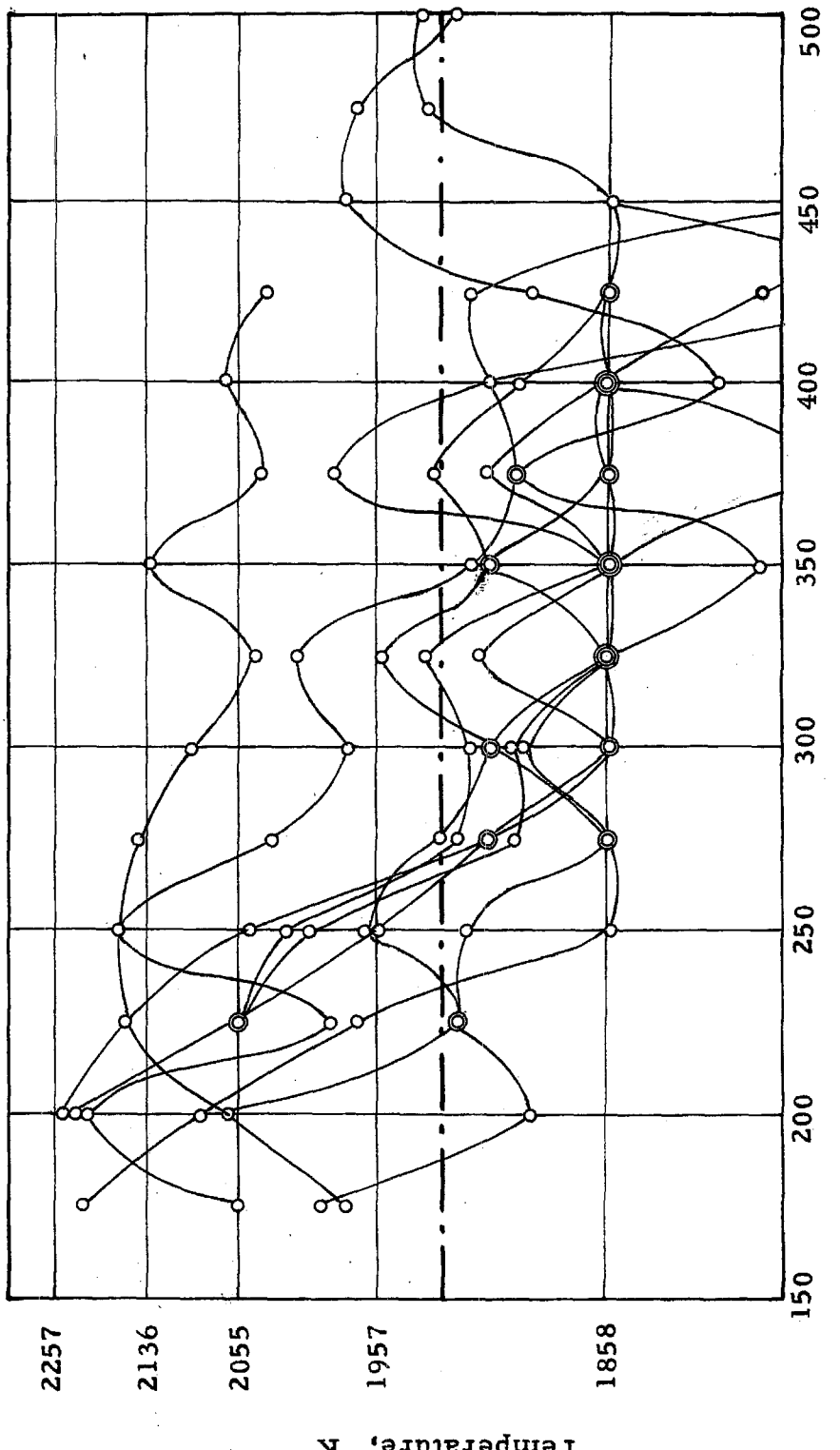

Fig. 68. Temperature versus time as determined by the two-color method in several experiments behind carbon-forming shocks (initial shock Mach number M_s = 4.2). The dashed line indicates the lower calibration limit.

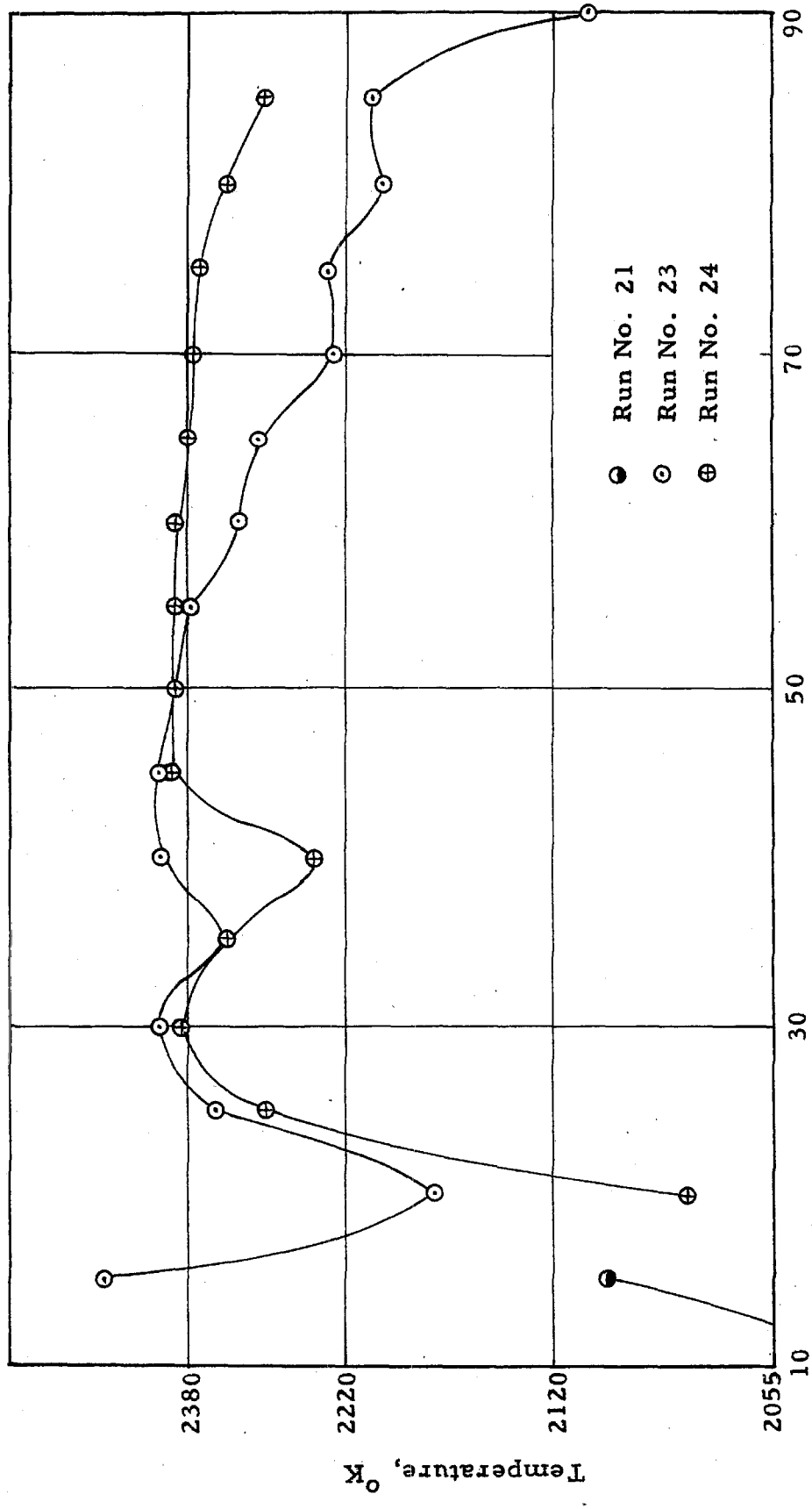

Fig. 69. Temperature versus time as determined by the two-color method behind a carbon-forming reflected shock (initial shock Mach number $M_s = 5.2$).

Fig. 70. High speed photograph of the onset of emission behind a carbon-forming shock (time increases to the left).

Fig. 71. Photograph of the last stages of emission behind a carbon-forming shock (time increases to the left; the time resolution is 13.7 μsec per inch).